NACA RM L9L28a

NACA

RESEARCH MEMORANDUM

AERODYNAMIC INVESTIGATION AT MACH NUMBER 1.92 OF A RECTANGULAR WING AND TAIL AND BODY CONFIGURATION AND ITS COMPONENTS

By Macon C. Ellis, Jr., and Carl E. Grigsby

Langley Aeronautical Laboratory
Langley Air Force Base, Va.

NATIONAL ADVISORY COMMITTEE
FOR AERONAUTICS

WASHINGTON
March 1, 1950

NACA RM L9L28a

NATIONAL ADVISORY COMMITTEE FOR AERONAUTICS

RESEARCH MEMORANDUM

AERODYNAMIC INVESTIGATION AT MACH NUMBER 1.92 OF A RECTANGULAR WING AND TAIL AND BODY CONFIGURATION AND ITS COMPONENTS

By Macon C. Ellis, Jr., and Carl E. Grigsby

SUMMARY

An investigation at Mach number 1.92 in the Langley 9-inch supersonic tunnel of a variable body-wing-tail configuration has been made in order to determine and to isolate the aerodynamic effects on each other of the components of the configuration. The body had a fineness ratio of 12.5 with a cylindrical midsection so that the aspect-ratio-4 rectangular wing could be located at three longitudinal positions along the body. The after portion of the body converged to the sting diameter. The variable-incidence-angle rectangular tail was of the same aspect ratio as the wing but one-fourth the wing area, and could be located at three vertical positions relative to the plane of the wing. The test data presented include lift, drag, and pitching-moment measurements through a range of angles of attack for all configurations of this model.

In the presentation of results from the tests, the basic lift, drag, and pitching-moment data for all the components and combinations of components are first discussed and, where possible, elemental comparisons with theory are made. Next, various factors affecting the longitudinal stability of each complete body-wing-tail configuration are isolated from the test results and discussed separately. These factors include the effect of the wing on the tail lift effectiveness, the effects of the body upwash and wing downwash on the pitching moment, and the effects on the pitching moment of tail center-of-pressure shift due to adding the wing. Finally, the pitching-moment-curve-slope variations with wing position and tail height for the complete configuration are discussed in terms of the combined effects of the various factors previously isolated.

INTRODUCTION

Prediction of the longitudinal stability characteristics of supersonic aircraft or missile configurations from either test data or theory for the components requires knowledge of the aerodynamic effects on each other of the various components when added together. It is thus desirable to know, for the usual configuration of body and tandem lifting surfaces, such effects as that of the body on the forward lifting surface and the body and forward surface on the tail surface. Important elements in these general considerations are the downwash due to the wing and the upwash due to the body and their consequent effects on the tail and wing and the longitudinal stability. Some of the theories based on the linearized equations of motion for the downwash field behind isolated wings are given in references 1 to 8 and computations for the upwash around slender bodies are given in reference 9. The experiments of reference 10 for a rectangular wing, reference 11 for a triangular wing, and reference 12 for a trapezoidal wing provide downwash measurements at supersonic speeds which are compared with the predictions of the linear theory. It is recognized and shown in the experiments of these references that the linear-theory downwash results must be altered to account for the effects of the displacement and distortion of the trailing vortex sheet.

The body-wing interference problem has been treated by means of inviscid linear theory in references 13 to 17. Some basic considerations and suggested approaches to the general problem are given in reference 18. The method of characteristics with suitable simplifying assumptions has been used to calculate certain body-wing interference problems in reference 19. General treatment of this problem is difficult, indeed, because of the great number of possible configurations. When a tail or wing is added to the body-wing configuration, general treatment becomes untractable and reliance must be made on experiments and theoretical study of component effects on each other. Another phase of the problem which has received recent theoretical attention is that of predicting the characteristics of a lifting surface in a nonuniform stream such as exists in the downwash field behind a lifting wing. Some of these results appear in references 20 and 21.

A large number of experiments to determine the aerodynamic characteristics of complete configurations at supersonic speeds have been made. Most of these experiments have been made on missiles and missile components and, in nearly every case, an attempt has been made to obtain from the data general interference effects among the configuration components. Also, some systematic tests of a series of components

and configurations have been made. From all these experiments many interference quantities of general interest have been obtained; however, the proportionate yield appears small, principally because of insufficient precision in the tests.

The purpose of the present investigation was to isolate, insofar as possible in terms of lift, drag, and pitching moment, the effects on each other of the components of a variable body–wing–tail configuration. The basic test model was made so that the rectangular wing could be located at three longitudinal positions along the body and the horizontal tail could be located at three vertical positions relative to the plane of the wing. The tests included three–component measurements on all possible elements and combinations of this basic model and were made at a Mach number of 1.92 in the Langley 9–inch supersonic tunnel.

In the presentation of results from the tests, the basic lift, drag, and pitching–moment data for all the components and combinations of components are first discussed and, where possible, elemental comparisons with theory made. Next, various factors affecting the longitudinal stability of each complete body–wing–tail configuration are isolated from the test results and discussed separately. These factors include the effect of the wing on the tail lift effectiveness, the effects of the body upwash and wing downwash on the pitching moment, and the effects on the pitching moment of tail center–of–pressure shift due to adding the wing. Finally, the pitching–moment–curve–slope variations with wing position and tail height for the complete configuration are discussed in terms of the combined effects of the various factors previously isolated. It will be obvious that the final longitudinal–stability changes with wing position and tail height are relatively small for the configuration of these tests; however, a rather detailed discussion is made for the sake of other cases where these combined effects may not be small.

SYMBOLS

A	aspect ratio $\left(b^2/S\right)$
α	angle of attack
$\alpha_{C_L=0}$	angle of zero lift
b	wing span
c	wing chord

C_D drag coefficient (D/qS)

C_L lift coefficient (L/qS)

$C_{L_\alpha} = \frac{dC_L}{d\alpha}$

$C_{L_{i_t}} = \frac{dC_L}{di_t}$

C_m pitching-moment coefficient, referred to theoretical flat-plate center of pressure of wing (M/qsc) (fig. 2)

C_m' pitching-moment coefficient calculated from measured incremental lift values assuming tail center of pressure at theoretical flat-plate location for isolated tail

$C_{m_\alpha} = \frac{dC_m}{d\alpha}$

$(C_m)_{\alpha=0}$ pitching-moment coefficient at $\alpha = 0$

ϵ downwash angle (positive downward)

ϵ_e average effective downwash angle from theory or force tests (fig. 18)

ϵ_w effective average downwash angle from force tests (equation (6))

ϵ_w' effective average downwash angle from force tests (equation (7))

η_t wing-wake parameter $\left(\frac{\left(C_{L_{i_t}}\right)_{BWT}}{\left(C_{L_{i_t}}\right)_{BT}}\right)$

h tail height (fig. 2)

i_t tail incidence angle

l tail length (fig. 2)

M	Mach number
q	dynamic pressure $\left(\rho V^2/2\right)$
ρ	stream density
R	Reynolds number $(\rho Vc/\mu)$
S	wing area

Subscripts:

B	model configuration of body and vertical tail
BT	model configuration of body, vertical tail, and horizontal tail
BW	model configuration of body, vertical tail, and wing
BWT	model configuration of body, vertical tail, wing, and horizontal tail
t	refers to horizontal tail
b	in presence of body
bw	in presence of body and wing
w	due to addition of wing
min	minimum

APPARATUS AND TEST PROCEDURE

Description of Tunnel

All tests were conducted in the Langley 9-inch supersonic tunnel which is a continuous-operation closed-circuit type in which the stream pressure, temperature, and humidity conditions can be controlled and regulated. Different test Mach numbers are provided by interchanging nozzle blocks which form test sections approximately 9 inches square. Throughout the present tests, the moisture content in the tunnel was kept sufficiently low so that the effects of condensation in the supersonic nozzle were negligible. Eleven fine-mesh turbulence-damping

screens are provided in the relatively large area settling chamber just ahead of the supersonic nozzle. A schlieren optical system is provided for qualitative visual flow observations.

Models and Test Setup

A drawing of the test setup in the tunnel is shown in figure 1 and details and dimensions of the model are shown in figure 2. The wing could be fixed at any one of three longitudinal locations along the fineness-ratio-12.5 body. A smooth plug was also available to make up the body for tests with no wing. The tail section was removable so that different tails could be provided and, as shown, three values of tail height were used in the tests. All surfaces had symmetrical circular-arc sections of 6-percent thickness ratio. Both wing and horizontal tail were of aspect ratio 4 and the tail area was one-fourth that of the wing. The vertical tail was provided solely for supporting the horizontal tail in positions above the body but was included on all model configurations. In order to complete the series, wing-alone tests were made in which the wing was mounted on a very slender sting in conjunction with a different movable windshield. The sting and windshield arrangement was similar to that used in the tests of reference 22. This arrangement is described in reference 22 and is shown to have small effect on the flow over the wings of those tests.

The present tests were divided into two series. The lift-strain-gage arrangement shown in figure 2 was that used in the first series of tests. In this arrangement, the lift gages were wired in such a way that the force normal to the beam was indicated directly and independently of longitudinal location. The moment was indicated independently on the other gage. Readings of both sets of gages were taken from Baldwin Southwark SR-4 strain indicators. In the second series of tests, the internal beam simply had two moment gages, and moment values at each station were taken independently. The use of the internal sting balance permitted evaluation of forces on the model only and excluded forces on the support sting. There did, however, exist the possibility of small forces acting on the inner portion of the body shell at the rear, these forces arising from flow through the small gap between the body and exposed sting at angles of attack. Also, there existed the possibility of effects on the flow over the rear portion of the body of disturbances due to the windshield being felt forward through the exposed-sting boundary layer. Both of these effects, however, are believed to be small in most of the data presented.

In addition to measurements of normal force and pitching moments by means of the strain gages, the sting was connected to external mechanical scales which measured the lift, pitching moment, and drag

of the model plus any forces on the sting. The lift and pitching-moment data from the external scales were observed to include large side forces on the spindle; hence, only the drag data from the external scales are presented or used herein, except that forces on the wing alone using a different sting and windshield arrangement were obtained from the external scales. A drag measurement was, of course, necessary in order to reduce the strain-gage normal-force values to lift values. Fortunately, the drag forces on the sting, which are included in the external scale measurement, are very small as was proved by auxiliary tests.

Angles of attack of the model were measured by means of a very narrow light beam reflected onto a scale from a small mirror embedded in the rear section of the body. In this way, true angles of attack of the model were indicated directly.

Test Procedure

Configurations.- Force measurements yielding lift, drag, and pitching moment were made over a range of angles of attack of about $\pm 6^{\circ}$ for all possible elements and combinations of the body, wing, and horizontal tail. Also, the tests included configurations having several tail incidence angles for each of the three horizontal tails. In addition, a test of the wing on a very slender sting was made at two values of Reynolds number - one value the same as that for the configuration tests, and the other value one-half this value to approximate the isolated-tail characteristics.

Test series.- The data presented were obtained from tests divided into two series. In the first series of tests, measurements of lift, drag, and moment for all configurations were made. Subsequent analysis of the data, however, revealed that errors had been made in initially referencing the model angle of attack with respect to the stream direction. These errors appeared random and indicated errors in absolute angle of attack relative to the stream of as much as 0.5°. The data further indicated that errors, though much smaller than the angle-of-attack referencing errors, had also been made in the tail-incidence-angle measurements. In a given run of this series, however, model angles of attack relative to each other were within $\pm 0.01^{\circ}$; thus, lift- and moment-curve-slope values were still acceptable. It was concluded that the errors arose from the methods of mechanical measurements used. As a consequence of these errors, a second complete series of tests was made.

The purpose of the second series of tests was to position the curves of lift, pitching moment, and drag with respect to the angle of attack as precisely as possible. If the errors in the first series had been

confined to angle-of-attack reference, it would have been sufficient to establish the angle of zero lift as a function of tail incidence angle. Since the tail incidence angles were also in doubt, it became necessary to establish some value of moment coefficient as a function of tail incidence angle. Once these variations were established, the lift and drag curves could be shifted along the angle-of-attack scale and the moment curves could be shifted along the angle-of-attack and moment scales to positions corresponding to the original measured values of tail incidence angle. The only assumption involved in this procedure is that the shapes of the curves do not change in being shifted from a position corresponding to that for the true tail incidence angle to the position for the measured tail incidence angle. Analysis of the data showed that this assumption was valid for the small differences in tail incidence angle. In this second test series, the angle of zero lift and the pitching-moment coefficient at zero angle of attack as functions of the tail incidence angle were accurately established for each configuration by running the model through only the necessary small range of angles of attack. Different measuring procedures were adopted so as to increase the accuracy of the angle-of-attack reference and the tail-incidence measurements. In the second test series, the internal beam with only two simple moment gages was employed.

Precision of Data

The precision of the data has been evaluated by estimating the uncertainties in each item involved in a given quantity and combining these errors by the method which follows from the theory of least squares. (See reference 23.) The final values thus obtained for the uncertainties in the quantities involved in the present tests are summarized in table I and a discussion of the various factors affecting each of these quantities is given in appendix A. For those cases in which the precision varies with lift coefficient, values are given for lift coefficients corresponding approximately to the limit of linearity of the lift and moment curves as well as for zero lift. The uncertainties continue to increase beyond the linear range.

RESULTS AND DISCUSSION

The basic data are presented in the form of lift, pitching-moment, and drag coefficients, and the coefficients for all configurations are based on the total wing area. Pitching-moment coefficients are based on the wing chord and are referred to the theoretical center of pressure of the wing (0.486c) as calculated from the linear theory for a flat plate at the test Mach number. For the configurations without the wing,

the pitching-moment coefficients given in the graphs are referred to the point corresponding to the aerodynamic center of the wing in the most forward position $\left(\frac{l}{c} = 3.34\right)$. The Reynolds number was 0.4×10^6 based on the wing chord or 2.8×10^6 based on the body length for all the tests except as noted.

Lift Results

The lift results for all the configurations are presented in figures 3 and 4. As mentioned earlier in the section on test series, the data from the first test series have been shifted along the angle-of-attack scales so that the angles of zero lift correspond to the correct value as determined in the second test series. These data from the first series are indicated by the larger test-point symbols. The smaller symbols represent data from the second test series and cover a much smaller angle-of-attack range in most cases. Although the data for the BWT and BT configurations in the second test series were obtained at values of i_t different from those of the first series, the data have been shifted along the angle-of-attack scale so that they coincide with the data for the nearest i_t values from the first series. This procedure aided in the accurate determination of lift-curve slopes and was considered justified since the difference in i_t values between the two test series was small and the curves were linear in the small angle-of-attack range of the second test series.

In the following sections on the lift results, discussion will be made of relatively small variations in lift-curve-slope values and small departures from linearity of the individual lift curves. Although small percentagewise, the variations in lift-curve slopes lead to significant changes in quantities such as the downwash due to adding the wing which will be subsequently obtained from formulas involving differences between slope values. Since these formulas involve linear slope values and are sensitive to small differences in these values, it is of significance also to point out, for each configuration, the limits of linearity of the lift curves so that the range of applicability of quantities subsequently obtained by the linear formulas can be qualified by reference to these limits of linearity defined here.

BWT configurations.- Lift curves for all the BWT configurations are shown in figures 3(a) to 3(i). In general, it appears that the linear range of lift variation with angle of attack is roughly $\pm 2^\circ$ about the angle of zero lift, with the exception that the results for the tail at $\frac{h}{c} = 0.35$ show a tendency for the linear range to be reduced as the

incidence angle increases. Values of lift-curve slope taken from the linear range of the data are given in table II. The most significant trend of the values of lift-curve slope is the increase as the tail arm is shortened. For the two lower tails, the small increase in lift-curve slope as the tail arm is shortened is probably due to decreasing wing downwash as expected from theory. For the case of the highest tail where the wing downwash is expected to be small, there appears no significant effect of wing position on lift-curve slope. The most significant changes in lift-curve slope with tail incidence angle are seen for the case of $\frac{h}{c} = 0.35$. This increase is due to changes in the flow in the region between the tail and the body and will be discussed subsequently.

BT and B configurations.- Lift curves for all the BT configurations are shown in figures 3(j) to 3(l). In general, the linear range of angle of attack is greater than for any of the other configurations. One significant departure from linearity appears for the case of the tail for $\frac{h}{c} = 0.35$ at $i_t = 7.79^\circ$ in the angle range from about -5° to 1°. The values of lift-curve slope for all the BT configurations are the same within a maximum variation of 7 percent. The fact that the tail for $\frac{h}{c} = 0$ has a lift-curve slope equivalent to that for the two higher tails, in spite of the fact that over 20 percent of its area is submerged within the body, is due to the greater upwash at the body meridian plane.

Results for the B configuration (no wing or horizontal tail) shown in figure 3(m) indicate a linear range of about $\pm 3^\circ$.

BW and W configurations.- The last of the lift results for the BW and W configurations are shown in figure 4. The B and W results are included on each graph for comparison. The values given in table II indicate the lift-curve slope of the BW configuration to increase slightly as the wing moves rearward along the body. The range of linearity for both the BW and W configurations appears to be about $\pm 2^\circ$ about the angle of zero lift.

Comparison of wing and body lift results with theory.- Comparison of the experimental lift-curve-slope value $\left((C_{L_\alpha})_W = 0.0365\right)$ for the wing alone with the theoretical value from the linearized theory for a flat plate indicates that 93 percent of the theoretical lift has been realized. The theoretical value of $C_{L_\alpha} = 0.0392$ is computed for a flat-plate rectangular wing of aspect ratio 4 at $M = 1.92$, with no second-order corrections for thickness effects.

For the case of the body lift, a rough theoretical estimate of its lift may be simply obtained provided the body is considered sufficiently slender. From Munk's airship theory, the lift-curve slope of a very slender arbitrary body is given as $C_{L_\alpha} = 2$ where α is in radians and C_L is based on the base area of the body. In discussing the theoretical lift of the body from this simple concept, several facts are important, namely, that, if the body closes so as to terminate in a point, the total lift at an angle of attack is zero. If the initially ogival nose is followed by a cylindrical section, the lift on the cylindrical portion of the body is zero. One other important fact is that the forward portion of the body that increases in area rearward carries positive lift and the rearward converging portion of the body carries negative lift. Thus, for a body which has a rear section that converges (boat-tailing), any separation at angles of attack tends to reduce the negative lift, thereby increasing the total lift. If the lift-curve slope of the present body is calculated as previously outlined based on the base area and converted to the model wing area, a value of C_L per degree of 0.0011 is obtained. This value is seen to be only one-half of the experimental value given in table II. Since a large part of the body length rearward of the nose section is cylindrical, it might be expected that the theoretical situation would be more closely represented by ignoring the rear converging section and basing the lift on the cross-sectional area of the cylindrical portion. Such a value is double that obtained by considering the negative lift of the rear portion and is about identical with the experimental value. It thus appears that if these simple concepts may be considered applicable, the negative lift over the rear portion of the body is essentially wiped out by separation.

Combining the lift-curve-slope values for the body and wing tested separately gives $C_{L_\alpha} = 0.0387$, which value is seen to be lower than any of those for the body and wing in combination. This is probably due largely to the increase in lift of the wing in the upwash region created by the body. Beskin, in reference 9, has carried out, by means of linearized theory, calculations for the lateral upwash distribution in the meridian plane of a body made up of a slender ogive followed by a cylinder. His results show that as the cylindrical portion of the body is approached the upwash distribution out from the body in the meridian plane follows very closely that for an infinite cylinder; that is, $\epsilon = -\frac{R^2}{r^2}$ where r is the distance out from the body and R is the radius of the body. By use of strip theory along the wing for the present configuration, an average effective upwash along the span of 0.05α is obtained. It is then assumed that the lift of the exposed wing in the presence of the body would be increased by 5 percent. By using the experimental value obtained for the wing alone and assuming further

that the unit lift of the buried section of the wing is equal to the average unit lift of the wing alone, the estimated lift increment of the wing added to the body would be

$$\Delta\left(C_{L_\alpha}\right)_W = (0.86)(1.05)\left(C_{L_\alpha}\right)_W + (0.14)\left(C_{L_\alpha}\right)_W = 0.0380$$

The experimental values for the wing-lift increment, $\left(C_{L_\alpha}\right)_{BW} - \left(C_{L_\alpha}\right)_B$, vary from 0.0378 to 0.0383 as the wing moves back along the body. The apparent check of the experimental values with the above estimate is no doubt fortuitous, since the assumptions, especially that of lift carry-over, may not be justified. In light of computations made in reference 24 for a similar configuration using Ferrari's body-wing interference theory, however, there is reason to believe that the effect of the wing on the body is such that the lift of the buried portion of the wing tends to be preserved. Results from these computations in reference 24 show that the lift of the wing first increases, then falls off as the body is approached, and that the effect of the wing on the body is to increase the body lift; in fact, the greatest portion of the lift on the body due to the wing appears downstream of the wing-trailing-edge Mach plane and body intersection. The effect of the rearward shift of the carry-over wing-lift increment will be more apparent in the moment results.

Variation of $\alpha_{C_L=0}$ with tail incidence.- Variations in the angle of zero lift with tail incidence obtained in the second test series are shown in figure 5 for the BT configurations and in figure 6 for the BWT configurations. The results in figure 5 for the BT configurations show that for $i_t = 0^\circ$, $\alpha_{C_L=0}$ is nearly 0.9° for the $\frac{h}{c} = 0.35$ case and about 0.3° for the $\frac{h}{c} = 0.70$ case. This result undoubtedly arises from a downflow at the tail due to the flow field induced by the converging body, although the displacement of $\alpha_{C_L=0}$ at $i_t = 0^\circ$ for the intermediate tail is also influenced, as will be shown subsequently, by a different flow field which is created between the tail and the body. The much smaller displacement at $i_t = 0^\circ$ for the lower tail is probably associated with the influence of the vertical tail.

The lower slope, $\frac{d\alpha_{C_L=0}}{di_t}$, for the $\frac{h}{c} = 0$ tail is due to the fact that the lift-curve slope of this tail obtained by varying i_t is appreciably less than the incremental lift-curve slope obtained by varying the angle of attack of the body and tail. This lower slope is as might be expected since a relatively large fraction of the total tail area is buried in the body.

The displacement of $\alpha_{C_L=0}$ for $i_t = 0^\circ$ is still apparent for the BWT configurations as shown in figure 6, although the values of displacement are lower because of the lift of the wing. No significant effect of wing longitudinal position is noted except for the case of $\frac{h}{c} = 0.70$ where moving the wing rearward is seen to shift the angles of zero lift to slightly more positive values.

Moment Results

The moment results for all the configurations are presented in figures 7 and 8. For each configuration, the pitching-moment-coefficient values from the first test series (larger symbols) have been shifted along the angle-of-attack scale by the same corresponding increment as was required to make the angles of zero lift correct for the original i_t measurements. If the original i_t measurements had been correct, this shift in angle of attack for the moment values would have been sufficient; however, measurements in the second test series of the moment coefficient at 0° angle of attack showed that the angle shift was not sufficient, thus positively indicating errors in the original i_t measurements. The moment-coefficient values were therefore also shifted along the moment scale by a constant increment for each configuration so that the moment coefficient at 0° angle of attack corresponded with the value as determined in the second test series. As for the lift results, the results from the second test series (smaller symbols) were shifted along the angle-of-attack scale so that the curves occupied the position corresponding to the original i_t values.

Since the moment- and lift-curve slopes were unaffected by small changes in incidence angle, an equation giving the error in the original i_t measurements can be set up by using results obtained in both test series. Calculations using this equation were made for most of the configurations with the tail, and the results for each setting were seen to scatter rather widely because of the sensitivity of the equation to

small changes in some of the terms. It was thus believed that it would be more satisfactory to present the data as corresponding to the original tail-angle measurements rather than attempt to correct the i_t values only approximately.

BWT configurations.- Pitching-moment curves for all the BWT configurations are given in figures 7(a) to 7(i). It may be seen that the scatter of the moment data is generally greater than the scatter of lift data. Also, the trends of the scatter can be seen to follow generally the trends of uncertainty as given in table I. It thus appears most probable that variations in the last digit of the values shown for the pitching-moment-curve slopes in table II may not be significant for some cases. Furthermore, since the uncertainty of moment values increases with lift or angle of attack, the range of linearity of the curves is not readily determinable. It is generally observed, however, that the changes in slope of the moment curves coincide with changes in slope of the lift curves; thus, the linear range of angle of attack of the moment curves appears approximately the same as that for the lift curves.

The effects of changes in downwash with wing position are not obvious from the moment-curve slopes given in table II because of the changing tail arm. It is apparent, however, that the effects of variations in the tail incidence angles on the moment-curve slopes for the two higher tails are greater than the effects on the lift-curve-slope values. As mentioned for the lift results, these effects are probably due to changes in the flow between the tail and the body.

BT and B configurations.- Moment curves for all the BT configurations are shown in figures 7(j) to 7(l). The differences in magnitude between the BT moment-curve-slope values and the corresponding values for the BWT configurations are due both to the effect of the wing on the body and the effect of the wing on the tail. The effects of incidence angle for the two higher tails are seen to be of the same magnitude as for the BWT configurations.

From the values of $\left(C_{M_\alpha}\right)_B$ and $\left(C_{L_\alpha}\right)_B$ given in table II, it appears that the center of pressure of the body lies about at the nose. This indicates that most of the lift is carried on the nose section but that some negative lift over the rear section of the body is still present. This result is not necessarily contradictory to the deduction from the lift results that the negative lift over the rear portion of the body is wiped out by separation, since even the small negative lift at the rear of the body can have an appreciable influence on the body center of pressure.

BW and W configurations.– The moment data for the BW and W configurations are given in figures 8(a) to 8(d). The moment-curve-slope results qualitatively bear out the statement made in regard to the lift that the lift "carry over" of the wing is, as predicted by calculations based on Ferrari's work, shifted rearward relative to the center of lift of the wing alone. This may be seen by comparing the values of the moment-curve slope for the wing alone with the incremental value for the wing on the body. The incremental moment-curve slope contribution of the wing $\left(\left(C_{m_\alpha}\right)_{BW} - \left(C_{m_\alpha}\right)_B\right)$ is, from table II, for l/c values of 3.34, 2.74, and 2.14, respectively, $\Delta\left(C_{m_\alpha}\right)_W = 0.0009$, 0.0008, and 0.0004. Since $\left(C_{m_\alpha}\right)_W = 0.0055$ and the lift increment of the wing on the body is greater than the lift of the wing alone, it is clear that for all wing positions the effective center of the incremental wing lift is considerably farther rearward than the center of lift of the wing alone.

Variation of $\left(C_m\right)_{\alpha=0}$ with tail incidence.– The parameter $\left(C_m\right)_{\alpha=0}$ was selected for determination in the second test series since values of this parameter were always in the linear range of the lift and moment curves and the moment curves from the first test series could thus be correctly positioned. The variations in $\left(C_m\right)_{\alpha=0}$ with i_t are given in figure 9 for the BT configurations and in figure 10 for the BWT configurations. The slopes of these curves are given in table III. The positive moment at $i_t = 0^\circ$ arises from the down load at the tail shown in the lift results. The same trends with tail height as for the lift are indicated, that is, the largest displacement of $\left(C_m\right)_{\alpha=0}$ at $i_t = 0^\circ$ occurs for the intermediate tail, decreasing for the highest and lowest tails. The magnitude of $\left(C_m\right)_{\alpha=0}$ at $i_t = 0^\circ$ appears essentially unchanged by adding the wing except for the intermediate tail for which case the displacement is a function of wing position. This variation with wing position is indicated to be due to the influence of the flow field from the wing on the flow around the tail, since the displacements for the other two tail positions are unchanged by addition of the wing.

Drag Results

The drag data from the first test series for all configurations are given in figures 11 to 14. No drag data are presented for the second test series. As for the lift, the drag values have been shifted along the angle-of-attack scale by the same increment as was required to make the angles of zero lift correct for the tail incidence angles shown. It

is obvious that the value of minimum drag is a function of tail incidence, but since the errors in tail incidence were small, the corresponding drag errors would also be small and the nature of the drag rise should not be significantly affected. It should be mentioned that the low Reynolds number of the tests tends to lessen the significance of the absolute values of the drag coefficients.

Drag of wing on sting.- The drag data obtained from tests of the wing on the slender sting are presented in figures 11(d), 12(d), and 13(d). Also included in figure 11(d) are results for a test Reynolds number approximately one-half the value for all other tests presented. Evidence that the boundary-layer flow over the wing is almost wholly laminar can be seen by calculation of the incremental pressure and viscous drags. The following table shows a breakdown of the drag increments at 0° angle of attack:

Test Reynolds number	Experimental C_D total	Calculated C_D pressure (Reference 25)	C_D total - C_D pressure	C_D friction for laminar flow, $\frac{2.654}{\sqrt{R}}$
395,000	0.0162	0.0118	0.0044	0.0042
202,000	.0174	.0118	.0056	.0059

The close agreement between the friction drag increment from the tests and the calculated friction drag increment, together with schlieren studies which showed very small separation, suggest that at 0° angle of attack the boundary-layer flow over the wing is essentially laminar.

It is apparent in figure 11(d) that the rate of drag rise with angle of attack is lowest for the lower Reynolds number results. For this case, the drag rise is as predicted by assuming the resultant force on the wing to be normal to the chord line. For the higher Reynolds number case, the drag rise is higher. The lift- and moment-curve slopes were indicated to be unchanged by the variation in Reynolds number, thus the reason for the increase in the rate of drag rise for the higher Reynolds number case is not clear but may be associated with an increase with angle of attack of the viscous chordwise force.

Drag increments due to adding wing and tail.- The increments in drag due to adding the wing to the B and BT configurations for various incidence angles were compared at the angle of attack for minimum drag of each BWT configuration. These increments were then referred to the drag of the wing alone (wing on sting) at the same angle of attack and compared

with each other. This comparison is shown in table IV in terms of the ratio of wing drag increment to the drag of the wing alone. It is indicated from this comparison that the increase in drag increment above that for the wing alone is primarily due to adding the wing to the body and that only secondary changes arise from the effect of the wing in changing the flow at the tail. Comparisons at higher and lower angles of attack within the range of the tests showed that the value of both of these ratios generally tended to approach 1 as the angle of attack was increased or decreased with respect to that for minimum drag. This latter result is associated mostly with the fact that the configurations with the wing have higher drag rises with angle of attack than do the B and BT configurations. The large increase in the wing drag increment when added to the body as compared with the drag of wing alone may be associated with a change from laminar to turbulent flow over the rear portion of the body when the wing is added. This possibility is suggested by the decrease in wing drag increment as the wing is moved rearward.

A similar comparison was also made between the drag increments of the tail in the presence and not in the presence of the wing. For the reference drag, that is, the drag of the tail alone, the one-half Reynolds number wing-alone test values of drag coefficient were quartered since the tail area is one-fourth that of the wing and the coefficients are all based on the wing area. This comparison showed the same general results as did the comparison for adding the wing, that is, the effect of adding the wing on the drag increment due to the tail was small. The most significant result of the tail-drag-increment study was the observation that the drag increments of the two highest tails at the highest incidence angles approached values 2.3 to 2.8 times the drag of the tail alone. Drag increments for the lowest tail and the higher tails at lower incidence angles varied between 0.8 and 1.3 times the drag of the tail alone.

Factors Affecting Pitching Moment of BWT Configurations

In the following sections, the data just presented will be used to isolate various factors which affect the pitching moment of each BWT configuration. These factors include the effects of the wing on tail effectiveness, the effects of body upwash and wing downwash on the tail, and the effects of the wing on the tail center of pressure. Lastly, the pitching-moment variations with tail height and wing position of the BWT configuration will be discussed in terms of the combined effects of the various factors. The procedure used to obtain the body upwash and effective average wing downwash at the tail is given in appendix B which also includes a general discussion of the limitations of various procedures for reducing force data from tests of variable tail-incidence configurations to effective average downwash angle at the tail.

Wing-Wake Effects on Tail Effectiveness

It would be expected that, if effects of the wing friction wake on the tail lift or moment exist, variations in these effects would occur as the tail moves vertically with respect to the friction wake and its boundaries. From the present tests, detailed examination of the data failed to reveal any change from linearity in the lift or moment curves for the angles of attack corresponding to those at which the tail might be expected to pass through the friction wake. It was concluded, therefore, that if any such effects were present, they were small and the precision of the measurements was insufficient to show them. The linear results shown in table III, however, indicate significant effects on the tail effectiveness due to adding the wing, η_t, thus suggesting that the effects arise from the wing wake as a whole and are not confined to the vicinity of the friction wake. The values of dC_L/di_t given in table III were obtained by multiplying the average lift-curve-slope value throughout the i_t range for each tail from table II by the $\frac{d\alpha_{C_L=0}}{di_t}$ values from figures 5 and 6. The values of dC_m/di_t given in table III were taken directly from figures 9 and 10.

The values of wing-wake parameter η_t given in figure 15 were obtained from the linear results of table III. It should be noted, in observing the variations shown in figure 15, that small changes in the slope values result in changes in η_t which are a large fraction of the η_t values shown. For instance, if it is assumed that the lift-curve-slope values are within ±0.0002 and the $\frac{d\alpha_{C_L=0}}{di_t}$ values within ±0.002, then from the method of least squares, the maximum probable errors in η_t vary from about ±0.03 for the lowest tail to ±0.02 for the highest tail. With these possible variations in mind, the results of figure 15 indicate that the lift effectiveness of the tail is unchanged due to adding the wing for the two higher tails but is increased for the lower tail. This result is that for the average effectiveness of the tail throughout the i_t range; however, if the individual lift-curve-slope values of table I are used in computing η_t, it is indicated that, for the two highest tails, the lift effectiveness of the tail tends to be reduced due to adding the wing as the incidence angle increases, although the differences from the average values are

not appreciably more than the probable deviation estimated previously. The wing longitudinal position relative to the tail does not appear to have a significant effect on η_t.

Using moment instead of lift results for the wake parameter, the same trends with vertical-tail location are seen, but the absolute values of η_t are reduced, indicating that an effect of the wing is to move the tail center of pressure forward.

Downwash Results

Theoretical considerations.- The theoretical downwash distribution behind the wing as obtained from reference 1 is given in figures 16 and 17. The linearized theory of reference 1 is for isolated wings and computations of downwash values are presented therein only in the plane of the wing from the trailing edge to infinity and for vertical distances above and below the plane of the wing at infinity $\left(\frac{l}{c} = \infty\right)$. These downwash distributions at the tail are given mainly for the purpose of showing trends and the order of magnitude of the angle gradients across the tail. The magnitude of the values at infinity is too large, as can be seen from the comparison of figure 16(a). From calculations for finite tail distances not given herein, however, it appears that the trends with tail height of the values shown at infinity are correct. Computations of the downwash values at the test longitudinal tail locations above the plane of the wing were not carried out since the effort required did not appear justified in yielding a comparison with the present results which represent integrated effects. Also, since the test angle-of-attack range was small and only linear results were considered, no considerations of the distortion of the downwash field due to displacement of the trailing vortex sheet were made. Reference 10 shows these effects to be small for small angles of attack and within spanwise distances such as that covered by the tail of the present tests.

Effective downwash angles from test results.- The effective downwash angles as obtained from the test results are given in figure 18. The theoretical downwash values from figures 16 and 17 averaged across the tail span are given in figure 18(a) for comparison with the test values calculated from equation (6) in appendix B using lift results. Since the method used for reducing the data to average downwash assumes linear characteristics of the various configurations, and since the variations of lift-curve slope with i_t are small, average values of the lift-curve slope throughout the i_t range of each configuration from table II were used in obtaining the results shown in figure 18.

First, it is seen that a large upwash due to the flow field about the body occurs at the $\frac{h}{c} = 0$ tail on the meridian plane through the body. This large upwash is as expected, and the average value roughly checks that obtained considering the body ahead of the tail to be an infinite cylinder. As the tail is raised above the body, the upwash falls off to nearly zero at the highest tail location. Addition of the wing creates downwash for all cases; however, for the two lower tails, the resultant is still upwash. Comparison of the effective downwash due to the wing with the theoretical values for $\frac{h}{c} = 0$ shows decreasing downwash as predicted by theory as the tail arm is shortened, but consistently greater downwash at $\frac{h}{c} = 0$ than the average theoretical values. Examination of the effects on the $\frac{d\epsilon_w}{d\alpha}$ values of changes in the quantities used in equation (6) shows, for instance, that if η_t were equal to 1, the $\frac{d\epsilon_w}{d\alpha}$ values for the $\frac{h}{c} = 0$ tail would be 0.08, 0.03, and −0.02 for $\frac{l}{c} = 3.34$, 2.74, and 2.14, respectively. These values are seen to be less than the average theoretical values, thus suggesting that the differences between the preceding values assuming $\eta_t = 1.0$ and the theoretical values are due both to the effects of the mutual interference between the flow due to the wing and that due to the body and the effects on the integrated force on the tail of the nonuniform flow across the tail. This suggestion assumes that the theoretical downwash for the isolated wing would be realized. The results of reference 10 indicate that for the regions occupied by the tail in the present tests, the theoretical values for the isolated wing should be closely approached. The trend with increasing tail height is decreasing downwash as shown by both the theory and the experiments. The hump in the curves at the $\frac{h}{c} = 0.35$ tail height is probably associated with the different effects of the flow due to the wing at angles of attack on the asymmetrical flow around this tail. Positive qualitative indication of this effect on the flow about the tail was gained from schlieren photographs which are discussed in the next section.

Downwash values computed using pitching-moment-curve slopes instead of lift-curve slopes in equation (6) are given in figure 18(b). The moment-curve-slope values used are, as for the lift, average values throughout the i_t range from table II. It is seen that, although the trends are generally the same as those obtained using lift results, the magnitude of the values is appreciably different. Some of these differences are probably due to the lesser accuracy of the moment results

as seen by the scatter of C_{m_α} values in table II. The largest part of the differences in magnitude, however, is due primarily to the shifts in center of pressure of the tail caused by addition of the wing. These results illustrate the necessity of using lift instead of moment results in the procedure used herein in order to obtain effective average downwash values closer to the physical values.

Comparison of the downwash values obtained from equation (7) in appendix B and shown in figures 18(c) and 18(d) with values from figures 18(a) and 18(b) show the large differences which result from ignoring the body upwash and wing effects on the tail effectiveness. Comparison between the downwash values in figures 18(a) and 18(c) for the $\frac{h}{c} = 0$ tail, shows that the differences in the wing-wake parameter from unity, and the effects of the large body upwash have combined to greatly reduce the values calculated by equation (7) below those calculated by equation (6). The downwash values for the two higher tails are underestimated using equation (6) by a factor approximately equal to $1 - \frac{d\epsilon_b}{d\alpha}$, since the wing-wake parameter was about unity as shown in figure 15. A roughly similar comparison may be obtained between the downwash values of figures 18(b) and 18(d), although the comparison is further complicated by the shifts in center of pressure of the tail.

Schlieren Photographs

In order to provide an indication of the location and relative intensity of the various disturbances due to the flow about the models, systematic schlieren photographs were made. These are shown for one value of the tail incidence angle for each BWT configuration in figures 19, 20, and 21. Dashed Mach lines from the wing tips enclosing the two-dimensional flow or zero-downwash region behind an isolated wing are shown in each plan view.

An interesting observation is afforded by the shock waves, seen in the photographs, emanating from the region between the $\frac{h}{c} = 0.35$ tail and the upper surface of the body. In the plan views of figures 19, 20, and 21, for the $\frac{h}{c} = 0$ and $\frac{h}{c} = 0.70$ tails, a single shock crossing each tail semispan trailing edge inboard from the tip can be traced in a nearly straight line to the leading edge of the vertical tail. For the $\frac{h}{c} = 0.35$ tail, however, two distinct shocks intersecting the

horizontal-tail trailing edge are seen in the plan views. The most inboard of these two shocks can be traced to the vertical-tail leading edge, but tracing the outboard shock forward suggests that a strong, detached shock exists ahead of the vertical tail between the horizontal tail and the body. It is thus indicated that a relatively large region of subsonic flow exists beneath the $\frac{h}{c} = 0.35$ tail, and it is probable that the flow is locally "choked" in the region bounded by the side of the vertical tail, the lower inboard surface of the horizontal tail, and the upper surface of the body. This mixed flow undoubtedly influences the flow at the tail which led to the negative lift due to the tail for zero angle of attack and zero incidence angle shown in figures 5 and 6.

In the curves of figure 18(a) showing the variation in effective downwash angle with tail height, a "hump" is indicated at the $\frac{h}{c} = 0.35$ tail location. This hump indicates that the wing has affected this mixed-flow region to a greater extent than it has affected the flow about the body and tail for the other two tail positions. In other words, for the lowest and highest tails, it appears that the flow due to the wing is more nearly superimposed upon the flow due to the body at the tail without mutual interference than is the case for the intermediate tail. In an effort to furnish some quantitative information from schlieren photographs on the validity of this deduction, plan-view schlieren photographs were made of the $\frac{h}{c} = 0.35$ BT and BWT configurations with the tail set at various incidence angles. The quantity selected for measurement was the distance between the vertical-tail shocks at the horizontal-tail trailing edge. First, it was observed that the distance between the legs of the inboard shock (originating at the leading edge of the vertical tail above the horizontal tail) varied only slightly with angle of attack and to a somewhat greater extent with tail incidence angle. Little change in these distances was noted when the wing was added. For the outboard shock (originating ahead of the vertical tail beneath the horizontal tail), the measurements showed a large, but smooth (nearly linear) increase in the distance as either the incidence angle or the angle of attack was increased. The effect of adding the wing was to increase the distance between the shock legs for negative angles of attack and to approach no change in the distance at some positive angle of attack. Thus taking these variations in the location of the limit of the disturbance to the flow beneath the tail as indicative of variations in the flow itself in this region, the schlieren observations clearly showed an appreciable effect on the local flow at the tail due to adding the wing.

Collected Pitching-Moment Results

The variation in pitching-moment-curve slope with tail height for the BT and BWT configurations is given in figure 22. Average values of the moment-curve slopes throughout the i_t range from table I are shown, although there appears to be a significant effect of i_t for the $\frac{h}{c} = 0.35$ tail. The significant pitching-moment trends with tail height and wing position are not changed, however, by using averages; also, it seems logical in observing general trends to omit consideration of the $\frac{h}{c} = 0.35$ tail as an unusual or peculiar case. In order to isolate the effect of the wing on the tail contribution to the moment, the effect of the wing on the body is taken out of the moment curves for the BWT configuration and shown as the dashed curves in figure 22. The effect on the tail due to adding the wing is thus the difference between the dashed curves and the BT curves. In order to show the shifts in tail center of pressure as the wing is added and as the wing and tail positions are changed, the incremental moment-curve slopes due to the measured incremental tail lifts have been calculated (assuming the tail center of pressure at the theoretical flat-plate location) and compared in figure 23 with the measured moment-curve slopes. In order to regard the relative differences between the calculated and measured moment-curve slopes in figure 23 as due to tail center-of-pressure shift, the contribution of the tail-drag increment to C_{m_α} must be shown to be small. The contribution of the tail drag change with angle of attack is in the stabilizing direction in every case, and calculations showed the contribution to be almost linear in the test angle-of-attack range. The bracketing values of this contribution for the lowest tail and largest tail volume and highest tail and smallest tail volume were found to be $\Delta C_{m_\alpha} = -0.0002$ and -0.0004, respectively. These values were calculated for the average i_t value and are considered to be small.

In discussing the effects of the various factors on C_{m_α}, it is realized that some of the changes in C_{m_α} would be of small consequence from a practical viewpoint. The discussion is thus primarily made for the sake of other cases where the same factors may be of different magnitudes and combine to produce much larger changes in static longitudinal stability. Such a case might be provided by the present configurations at a lower Mach number.

For the BT configuration in figure 22, disregarding the $\frac{h}{c} = 0.35$ tail, the effect of raising the tail is to move the moment-curve slopes

in a destabilizing direction. Comparing the differences between the measured and calculated moment-curve slopes in figure 23 indicates that this trend is due to a forward movement in center of pressure as the tail is raised to the highest position, since from table II, the lift increments of the two tails are about equal. Incidentally, the center of pressure of the lowest tail appears about at the assumed location.

From figure 22, the effect of adding the wing to each of the BT configurations is to reduce or not change the static stability margin in every case, which trend is in the direction of that to be expected from consideration of only the downwash due to the wing. For the lowest and highest tails, the effect on C_{m_α} due to adding the wing decreases as the tail arm decreases, as would be expected from the trend of $d\epsilon/d\alpha$. For the shortest-tail-arm case, the effect of the wing on the tail contribution to C_{m_α} appears about zero for both tails; however, the reason for this result can be shown to be different for the two cases. First, from figure 23 for $\frac{l}{c} = 2.14$, comparison of the relative difference between the calculated and measured C_{m_α} values for these two tails indicates no center-of-pressure shift as the tail is moved from $\frac{h}{c} = 0$ to $\frac{h}{c} = 0.70$ (for these two cases, it appears that the tail center of pressure is coincidentally at the assumed location). Thus, from the previous discussion of downwash and wing-wake effects on tail effectiveness, it is indicated that for the lower tail, the increase in tail effectiveness due to adding the wing offsets the destabilizing effect of the positive $d\epsilon/d\alpha$ value, whereas for the higher tail, $d\epsilon/d\alpha$ is nearly zero and the tail effectiveness is unchanged by addition of the wing.

For the BWT configurations, figure 23 shows that for the $\frac{l}{c} = 3.34$ case, addition of the wing produces a shift in tail center of pressure about the same for both the lowest and highest tails; thus the trend of no significant change with tail height (again disregarding the intermediate tail) arises from compensating effects of the wing downwash and wing effects on tail effectiveness. For the $\frac{l}{c} = 2.74$ case, it appears from figure 23 that addition of the wing has produced a forward shift in center of pressure of the lowest tail relative to the highest tail. It also appears, for this tail arm, that addition of the wing to the low tail configuration produces a greater shift in tail center of pressure than addition of the wing to the high tail configuration. The trend of increasing static margin as the tail is raised for the $\frac{l}{c} = 2.74$ case is

thus indicated to be due primarily to a rearward movement in the tail center of pressure. For the $\frac{l}{c} = 2.14$ case, no shift in tail center of pressure with tail height is involved; thus as compared with the $\frac{l}{c} = 3.34$ case where also no corresponding tail center-of-pressure shift was involved, the change in trend with increasing tail height to decreasing static margin arises from the fact that while the wing downwash decreases as the wing moves rearward, the increased tail effectiveness due to the wing remains unchanged.

CONCLUSIONS

An investigation at Mach number 1.92 in the Langley 9-inch supersonic tunnel of a variable body-wing-tail configuration has been made in order to determine and to isolate the basic aerodynamic effects on each other of the components of the configuration. The body had a fineness ratio of 12.5 with a cylindrical midsection so that the aspect-ratio-4 rectangular wing could be located at three longitudinal positions along the body. The after portion of the body converged to the sting diameter. The variable-incidence-angle rectangular tail was of the same aspect ratio as the wing, but one-fourth the wing area, and could be located at three vertical positions relative to the plane of the wing. The results of the investigation within the range of the linear variations of lift and moment with angle of attack indicated the following conclusions:

1. The lift- and moment-curve slopes of the body alone were approximately in agreement with values obtained from Munk's simple body theory considering only the positive lift on the ogival nose.

2. The lift-curve slope of the wing alone was 93 percent of the linear-theory value and the center of pressure was 0.15 chord ahead of the theoretical location.

3. The increased lift increment of the wing when added to the body was about the same as calculated from simple body upwash considerations, but the lift carry-over of the wing is located aft the wing trailing edge on the body as predicted by calculations based on Ferrari's body-wing interference work.

4. When the wing was added to the body, a large incremental drag above the drag of the wing alone occurred. This drag increment was believed to be associated with a change in the boundary-layer flow over the body rearward of the wing from laminar to turbulent, since the drag increment decreased as the wing was moved back along the body.

5. The effect of adding the wing on the drag increment due to the tail was small, except for the two higher tail positions at the highest test incidence angles.

6. The effect on the lift effectiveness of the tail due to varying tail incidence, $\frac{dC_L}{di_t}$, of adding the wing was to increase the value for the lower tail position and not to change the value for the two higher tail positions. The corresponding changes in moment effectiveness, $\frac{dC_m}{di_t}$, indicated a forward shift in the tail center of pressure due to adding the wing for all tail positions.

7. The average effective values of wing downwash, $d\epsilon/d\alpha$, at the tail obtained from the component force tests were greater than the average values across the tail calculated from linear theory. These differences are attributed to the wing-wake effects on tail effectiveness, the effects of mutual interference between the flow due to the wing and that due to the body, and the effects on the integrated force on the tail of the nonuniform flow across the tail.

8. Various factors influencing the static longitudinal stability of each complete configuration were isolated and shown to combine in different fashions for the various configurations so as to produce C_{m_α} variations with tail height and wing position which were significantly different from those to be expected from considerations of only the wing downwash.

9. For the intermediate vertical location of the tail, a mixed or locally choked flow was found to exist in the region bounded by the lower surface of the horizontal tail, the side of the vertical tail, and the upper portion of the body surface. This asymmetrical flow was shown to be influenced to a greater extent by addition of the wing than was the flow at the highest and lowest tail locations.

Langley Aeronautical Laboratory
National Advisory Committee for Aeronautics
Langley Air Force Base, Va.

APPENDIX A

DISCUSSION OF FACTORS AFFECTING UNCERTAINTY OF TEST QUANTITIES

A discussion is given in the following paragraphs of the various factors contributing to the final total uncertainty of each of the test quantities listed in table I.

Strain-gage measurements.- In the strain-gage measurements, two factors have affected the accuracy of the final values, namely, random shifts in the zero readings during each test run and uncertainties in calibrations. Variations in the zero shifts were the largest factor contributing to the uncertainties of both lift and moment and constitute the greater part of the values of uncertainty shown in the table for $C_L = 0$. These zero shifts were random and were not due to temperature effects since the gages were accurately temperature compensated. It is seen in the table that as the center of lift moves rearward, (l/c decreases) even for the case of zero lift in the first test series, the uncertainty of C_m decreases. This change in the precision for a given deviation from the mean of the zero readings arises from the conversion of the moment value from the point of measurement to the given reference point. As the transfer distance or the magnitude of the lift increases, the contribution of the lift error to the final moment value is increased.

The strain-gage beams used in the first test series were bench-calibrated before the tests and calibrated in the tunnel with the model in place a number of times during the tests. From a total of nine such calibrations, the maximum probable deviation of any calibration about a mean was found to be ±0.6 percent for the lift gages and ±0.4 percent for the moment gage. Estimates of errors entering into the computation of lift and moment coefficients other than the calibration errors showed their effects to be small as compared with the calibration errors. Thus the increase in uncertainty with increase in lift coefficient shown in the table is primarily due to the calibration errors.

For the second test series, the random shifts in zero readings were much smaller, and no significant changes in calibration of the two gages were observed, thus no estimate of the uncertainties is shown for the approximate end of the linear range of the lift and moment curves. The reversal of the trend in the variation of the uncertainty for C_m as the tail arm is changed is due to the fact that the moment is indicated

on two gages instead of one as for the first test series. The precision of the moment readings is thus a function of the location and magnitude of the normal force relative to both gages.

Pressure measurements.- All pressure measurements were taken directly from a vertical mercury-filled manometer where a reading accuracy of ±0.01 inch of mercury was obtained. The effect of this possible reading error on dynamic-pressure values was negligible. In computing the final drag results using the external balance readings, a measurement of the pressure in the box enclosing the support spindle and balance system was necessary. The difference between this box pressure and stream pressure constitutes a pressure force acting on the spindle cross-sectional area. This pressure force could be evaluated within ±10 percent, and since the correction was never greater than 5 percent of the total drag, the maximum uncertainty in C_D from this source is about ±0.0001.

Stream conditions.- Detailed stream surveys throughout the tunnel test section have indicated the variation in Mach number to be no more than ±0.01 about the mean value of 1.92, and the stream-static-pressure variation no more than $\pm 1\frac{1}{2}$ percent about the mean. Less detailed flow-angle measurements indicate negligible flow deviations. It should be mentioned in this regard that the model was mounted in the test section so that the wing leading and trailing edges were parallel to the tunnel side walls. Thus with changes in angle of attack, the model should encounter smaller changes in the stream angle and stream pressure gradients than if mounted with the wing leading and trailing edges parallel to the two-dimensional nozzle surfaces. In any case, the effects on the data of those small variations in stream conditions are not known, but it is believed that they are very small.

Angle-of-attack and tail-incidence-angle measurements.- Angles of attack of the model indicated by a light beam reflected from a small mirror in the model could be visually read to an accuracy of ±0.01°. Likewise, the model could be reset relative to the side walls and the air stream upon each installation within ±0.01°. Tail-incidence-angle measurements were made by taking the averages of a large number of angle measurements made at several spanwise stations at each tail setting. The most probable deviation from a mean for these measurements for each tail setting was ±0.03°.

Mechanical-scale measurements.- Although the lift, moment, and drag forces indicated by the mechanical scales were recorded for all the tests, the only scale lift and moment results finally considered were those obtained for the wing-alone tests, using a different sting and windshield

arrangement. In regard to the drag data which were taken directly from the scale measurements for all configurations, auxiliary tests showed only negligible effects on the drag of the flow over the spindle and in the windshield slot region. The total uncertainty in the drag-coefficient values is thus made up of the uncertainty in scale readings and the uncertainty in the buoyancy-force correction already discussed.

APPENDIX B

DISCUSSION OF PROCEDURES FOR REDUCING FORCE DATA FROM COMPONENT TESTS OF VARIABLE-TAIL-INCIDENCE CONFIGURATIONS TO EFFECTIVE DOWNWASH ANGLES AT THE TAIL

There appear several possible procedures for reducing force data from tests of complete variable-tail-incidence configurations and their components to effective, average downwash angles at the tail, each procedure involving different assumptions or, conversely, each procedure yielding different effective downwash angles. All the procedures involve either lift or moment measurements and consequently yield downwash angles which are integrated or average values across the tail. Thus, strictly speaking, the results for even the best procedures include in the downwash-angle values the effects on the forces on the tail of changes in stream pressure and Mach number due to the wing and the effect on the forces of the nonuniform flow field ahead of the tail.

The usual technique which has been employed extensively in the past in subsonic wind-tunnel tests involves the measurements of the variation of moment coefficient with angle of attack for the configuration without the tail (BW), and the measurement of the same variation for the complete configuration with the tail (BWT), with the tail set at several values of incidence angle. It is then assumed that when the moments of the BW and BWT configurations are equal, the tail does not contribute to the moment and the average flow angle across the tail plane is zero. The average flow angle at the tail is then obtained as the algebraic sum of the angle of attack and the angle of incidence at the angle of attack for equal moments.

The principal assumptions involved in this procedure are: (1) only a change in average flow angle affects a change in moment, hence only a change in tail lift contributes to the moment; (2) the influence of the tail on the body moment is small. The first of these restrictions may be of consequence in cases where the tail drag contributes to the moment, such as for a configuration in which the tail location is displaced vertically from the moment reference. Also, changes in the stream conditions at the tail due to the wing can change the lift-curve slope of the tail. The second restriction is probably of small consequence for the usual configuration in which the tail is at the rear of the body. This procedure, in which tests of only the BW and BWT configurations are made, yields only the absolute average flow angle at the tail due to the induced flow field about the body and wing, not the average downwash due

to the wing. In order to obtain the effect of adding the wing, the same procedure must be followed for the configurations without the wing, that is, tests of the B and BT configurations with various incidence angles must be made. These latter tests give the average flow at the tail due to the induced flow field about the body. At each corresponding angle of attack, the difference between the average downwash values obtained in the presence of the body and wing and those obtained in the presence of the body is thus the effect of adding the wing. This final value is still not the true downwash due to the wing within the limitations mentioned in the first paragraph, since the flows due to the wing and body are superimposed upon each other and the effects of their mutual interference are included in the results.

Lift instead of moment results could be used in the foregoing procedure. The moment increments due to the tail, however, are usually much larger than the lift increment, so that use of moment values leads to more accurate results. Since this procedure is a "null" one, the shifts in center of pressure of the tail are not involved in the average downwash values and there appears little choice between lift and moment values except that of accuracy unless the tail drag contribution to the moment is appreciable, in which case use of the lift results would eliminate the errors arising therefrom.

The procedure used to obtain downwash values in the present report is essentially the same as that just described with additional restrictions as to linearity of the lift or moment variations. Also, the results were computed from test values rather than by "crossing curves." In the present procedure the use of lift instead of moment values is necessary in order to avoid the inclusion in the average downwash angles of the effects of tail center-of-pressure shift due to adding the wing.

For the complete configuration of BWT where the variation of tail lift with incidence angle is linear and not a function of α, the lift is summed as

$$C_{L_{BWT}} = C_{L_{BW}} + \left(C_{L_{i_t}}\right)_{BWT} \left(\alpha + i_t - \epsilon_{bw}\right)$$

and

$$\epsilon_{bw} = \alpha + i_t - \frac{C_{L_{BWT}} - C_{L_{BW}}}{\left(C_{L_{i_t}}\right)_{BWT}} \qquad (1)$$

For the BT configuration, the lift is summed similarly and

$$\epsilon_b = \alpha + i_t - \frac{C_{L_{BT}} - C_{L_B}}{\left(C_{L_{i_t}}\right)_{BT}} \tag{2}$$

The difference between these values is the effect of adding the wing

$$\epsilon_w = \epsilon_{bw} - \epsilon_b \tag{3}$$

If the variations of lift with angle of attack of the B, BT, BW, and BWT configurations are also linear and the BT and BWT configuration slopes are not functions of the tail incidence angle, then equations (1), (2), and (3) may be written as

$$\frac{d\epsilon_{bw}}{d\alpha} = 1 - \frac{\left(C_{L_\alpha}\right)_{BWT} - \left(C_{L_\alpha}\right)_{BW}}{\left(C_{L_{i_t}}\right)_{BWT}} \tag{4}$$

$$\frac{d\epsilon_b}{d\alpha} = 1 - \frac{\left(C_{L_\alpha}\right)_{BT} - \left(C_{L_\alpha}\right)_{B}}{\left(C_{L_{i_t}}\right)_{BT}} \tag{5}$$

and

$$\frac{d\epsilon_w}{d\alpha} = \frac{d\epsilon_{bw}}{d\alpha} - \frac{d\epsilon_b}{d\alpha} \tag{6}$$

A procedure which is even more restricted than that outlined above, but which is sometimes used, excludes the wing–wake effects on the

lift-curve slope of the tail and ignores the effects of body upwash. In this restricted procedure the lift is summed as follows:

$$C_{L_{BWT}} = C_{L_{BW}} + \left(\left(C_{L_\alpha} \right)_{BT} - \left(C_{L_\alpha} \right)_B \right) (\alpha - \epsilon)$$

where

$$\frac{d\epsilon_w'}{d\alpha} = 1 - \frac{\left(C_{L_\alpha} \right)_{BWT} - \left(C_{L_\alpha} \right)_{BW}}{\left(C_{L_\alpha} \right)_{BT} - \left(C_{L_\alpha} \right)_B} \tag{7}$$

The limitations of equation (7) in yielding a variation of effective average downwash angle with angle of attack are best illustrated by putting equation (6) in a form comparable with equation (7).

Equation (6) may be written as

$$\frac{d\epsilon_w}{d\alpha} = \left(1 - \frac{d\epsilon_b}{d\alpha} \right) \left(1 - \frac{\left(C_{L_\alpha} \right)_{BWT} - \left(C_{L_\alpha} \right)_{BW}}{\left(C_{L_\alpha} \right)_{BT} - \left(C_{L_\alpha} \right)_B} \frac{1}{\eta_t} \right)$$

Comparison of the above equation with equation (7) shows that for equality, both the factors $1 - \frac{d\epsilon_b}{d\alpha}$ and η_t must equal one. Thus equation (7) obviously ignores the effects of body upwash and the effects of the wing wake on the tail effectiveness.

REFERENCES

1. Lagerstrom, P. A., and Graham, Martha E.: Downwash and Sidewash Induced by Three-Dimensional Lifting Wings in Supersonic Flow. Rep. No. SM-13007, Douglas Aircraft Co., Inc., April 14, 1947.

2. Lagerstrom, P. A., and Graham, Martha E.: Methods for Calculating the Flow in the Trefftz-Plane behind Supersonic Wings. Rep. No. SM-13288, Douglas Aircraft Co., Inc., July 28, 1948.

3. Heaslet, Max A., and Lomax, Harvard: The Calculation of Downwash behind Supersonic Wings with an Application to Triangular Plan Forms. NACA TN 1620, 1948.

4. Nielsen, Jack N., and Perkins, Edward W.: Charts for the Conical Part of the Downwash Field of Swept Wings at Supersonic Speeds. NACA TN 1780, 1948.

5. Ward, G. N.: Calculation of Downwash behind a Supersonic Wing. The Aeronautical Quarterly, vol. I, pt. I, May 1949, pp. 35-38.

6. Robinson, A., and Hunter-Tod, J. H.: Bound and Trailing Vortices in the Linearised Theory of Supersonic Flow, and the Downwash in the Wake of a Delta Wing. Rep. No. 10, College of Aero. (Cranfield), Oct. 1947.

7. Lomax, Harvard, and Sluder, Loma: Downwash in the Vertical and Horizontal Planes of Symmetry behind a Triangular Wing in Supersonic Flow. NACA TN 1803, 1949.

8. Mirels, Harold, and Haefeli, Rudolph C.: Line-Vortex Theory for Calculation of Supersonic Downwash. NACA TN 1925, 1949.

9. Beskin, L.: Determination of Upwash around a Body of Revolution at Supersonic Velocities. CVAC-DEVF Memo BB-6, APL/JHU-CM-251, The Johns Hopkins Univ., Appl. Phys. Lab., May 27, 1946.

10. Perkins, Edward W., and Canning, Thomas N.: Investigation of Downwash and Wake Characteristics at a Mach number of 1.53. I - Rectangular Wing. NACA RM A8L16, 1949.

11. Perkins, Edward W., and Canning, Thomas N.: Investigation of Downwash and Wake Characteristics at a Mach number of 1.53. II - Triangular Wing. NACA RM A9D20, 1949.

12. Cummings, J. L., Mirels, H., and Baughman, L. E.: Downwash in Vortex Region behind Trapezoidal-Wing Tip at Mach Number 1.91. NACA RM E9H15, 1949.

13. Ferrari, Carlo: Interference between Wing and Body at Supersonic Speeds - Theory and Numerical Application. Jour. Aero. Sci., vol. 15, no. 6, June 1948, pp. 317-336.

14. Ferrari, Carlo: Interference between Wing and Body at Supersonic Speeds - Note on Wind-Tunnel Results and Addendum to Calculations. Jour. Aero. Sci., vol. 16, no. 9, Sept. 1949, pp. 542-546.

15. Spreiter, John R.: Aerodynamic Properties of Slender Wing-Body Combinations at Subsonic, Transonic, and Supersonic Speeds. NACA TN 1662, 1948.

16. Browne, S. H., Friedman, L., and Hodes, I.: A Wing-Body Problem in a Supersonic Conical Flow. Jour. Aero. Sci., vol. 15, no. 8, Aug. 1948, pp. 443-452.

17. Spreiter, John R.: Aerodynamic Properties of Cruciform-Wing and Body Combinations at Subsonic, Transonic, and Supersonic Speeds. NACA TN 1897, 1949.

18. Lagerstrom, P. A., and Van Dyke, M. D.: General Considerations about Planar and Non-Planar Lifting Systems. Rep. No. SM-13432, Douglas Aircraft Co., Inc., June 1949.

19. Ferrari, Carlo: Interference between Wing and Body at Supersonic Speeds - Analysis by the Method of Characteristics. Jour. Aero. Sci., vol. 16, no. 7, July 1949, pp. 411-434.

20. Mirels, Harold: Theoretical Method for Solution of Aerodynamic Forces on Thin Wings in Nonuniform Supersonic Stream with an Application to Tail Surfaces. NACA TN 1736, 1948.

21. Graham, Martha E.: Some Linearized Computations of Supersonic Wing-Tail Interference. Rep. No. SM-13430, Douglas Aircraft Co., Inc., Dec. 23, 1948.

22. Love, Eugene S.: Investigations at Supersonic Speeds of 22 Triangular Wings Representing Two Airfoil Sections for Each of 11 Apex Angles. NACA RM L9D07, 1949.

23. Michels, Walter C.: Advanced Electrical Measurements. Second ed., D. Van Nostrand Co., Inc., 1941.

24. Cramer, R. H.: Some Theoretical and Experimental Results for Wing–Body Interference at Supersonic Velocities. Paper presented in the Bumblebee Aerodynamics Symposium. APL/JHU TG–10–4, The Johns Hopkins Univ., Appl. Phys. Lab., Nov. 4–5, 1948, pp. 267–276 and Supp. TG–10–4B.

25. Harmon, Sidney M.: Theoretical Supersonic Wave Drag of Untapered Sweptback and Rectangular Wings at Zero Lift. NACA TN 1449, 1947.

TABLE I.- SUMMARY OF TOTAL UNCERTAINTY OF TEST QUANTITIES

Test series	Quantity	Configuration	Uncertainty for $C_L = 0$	Uncertainty at approximate end of linearity
First	C_L	BWT BW BT B	±0.0010	±0.0011 ±0.0011 ±0.0010 ±0.0010
First	C_m for $\frac{l}{c} = 3.34$	BWT BW BT B	±0.0033	±0.0034 ±0.0041 ±0.0035 ±0.0034
First	C_m for $\frac{l}{c} = 2.14$	BWT BW	±0.0021	±0.0022 ±0.0029
Second	C_L	All	±0.0004	-------
Second	C_m for $\frac{l}{c} = 3.34$	All	±0.0010	-------
Second	C_m for $\frac{l}{c} = 2.14$	All	±0.0012	-------
First	C_D (scales)	All	±0.0003	-------
	C_L (scales) C_m (scales)	W W	±0.0001 ±0.0006	------- -------
All	Angle of attack	All	±0.01°	-------
All	Tail incidence angle	BWT BT	±0.03°	-------
All	Stream Mach number	All	±0.01	-------
All	Stream pressure	All	±1½ percent	-------

TABLE II.- SUMMARY OF EXPERIMENTAL LIFT- AND PITCHING-MOMENT-CURVE SLOPES

Tail position, h/c	i_t (deg)	C_{L_α} for $\frac{l}{c}$ =			C_{m_α} for $\frac{l}{c}$ =			C_{L_α}	C_{m_α} referenced for $\frac{l}{c}$ =		
		3.34	2.74	2.14	3.34	2.74	2.14		3.34	2.74	2.14
		BWT						BT			
0	-0.43	0.0480	0.0487	0.0491	-0.0167	-0.0123	-0.0084	0.0107	-0.0214	-0.0150	-0.0086
0	5.00	.0480	.0486	.0491	-.0167	-.0119	-.0076	.0107	-.0216	-.0152	-.0088
.35	.81	.0478	.0480	.0484	-.0143	-.0132	-.0042	.0103	-.0194	-.0132	-.0070
.35	4.18	.0476	.0481	.0486	-.0156	-.0118	-.0057	.0111	-.0218	-.0151	-.0084
.35	7.79	.0484	.0490	.0491	-.0170	-.0137	-.0064	.0112	-.0222	-.0155	-.0088
.70	-0.68	.0480	.0486	.0486	-.0175	-.0130	-.0072	.0102	-.0194	-.0133	-.0072
.70	2.36	.0481	.0490	.0485	-.0158	-.0130	-.0069	.0108	-.0209	-.0144	-.0079
.70	5.56	.0482	.0488	.0491	-.0182	-.0144	-.0082	.0114	-.0214	-.0146	-.0078
.70	9.43	.0482	.0488	.0482	-------	-------	-------	------	-------	-------	-------
No horizontal tail		BW						B			
		.0400	.0403	.0405	.0080	.0092	.0101	.0022	.0071	.0084	.0097
Isolated wing		W									
		.0365			.0055						

TABLE III.- LIFT-CURVE AND MOMENT-CURVE SLOPES DUE TO VARYING i_t

h/c	$\frac{l}{c}$ = 3.34		$\frac{l}{c}$ = 2.74		$\frac{l}{c}$ = 2.14		No wing			
	$\frac{dC_L}{di_t}$	$\frac{dC_m}{di_t}$	$\frac{dC_L}{di_t}$	$\frac{dC_m}{di_t}$	$\frac{dC_L}{di_t}$	$\frac{dC_m}{di_t}$	$\frac{dC_L}{di_t}$	$\frac{dC_m}{di_t}$ referenced for $\frac{l}{c}$ =		
								3.34	2.74	2.14
0	0.0063	-0.0210	0.0064	-0.0172	0.0064	-0.0134	0.0060	-0.0204	-0.0166	-0.0130
.35	.0079	-.0260	.0079	-.0212	.0080	-.0164	.0078	-.0272	-.0223	-.0174
.70	.0086	-.0276	.0085	-.0227	.0082	-.0168	.0085	-.0290	-.0236	-.0177

TABLE IV.- COMPARISON OF INCREMENTAL DRAG OF WING ADDED TO B AND BT CONFIGURATIONS

[Each drag increment obtained for angle of attack at which minimum drag occurs for corresponding BWT configurations.]

h/c	i_t (deg)	$\frac{l}{c} = 3.34$		$\frac{l}{c} = 2.74$		$\frac{l}{c} = 2.14$	
		$\frac{C_{D_{BW}} - C_{D_B}}{C_{D_W}}$	$\frac{C_{D_{BWT}} - C_{D_{BT}}}{C_{D_W}}$	$\frac{C_{D_{BW}} - C_{D_B}}{C_{D_W}}$	$\frac{C_{D_{BWT}} - C_{D_{BT}}}{C_{D_W}}$	$\frac{C_{D_{BW}} - C_{D_B}}{C_{D_W}}$	$\frac{C_{D_{BWT}} - C_{D_{BT}}}{C_{D_W}}$
0	-0.43	1.30	1.29	1.26	1.26	1.18	1.16
	5.00	1.25	1.25	1.22	1.20	1.14	1.13
.35	.81	1.29	1.28	1.26	1.28	1.18	1.19
	4.18	1.25	1.21	1.22	1.19	1.14	1.09
	7.79	1.24	1.28	1.20	1.27	1.10	1.16
.70	-.68	1.29	1.34	1.26	1.29	1.18	1.19
	2.36	1.27	1.30	1.24	1.23	1.16	1.16
	9.43	1.20	1.22	1.19	1.18	1.09	1.01

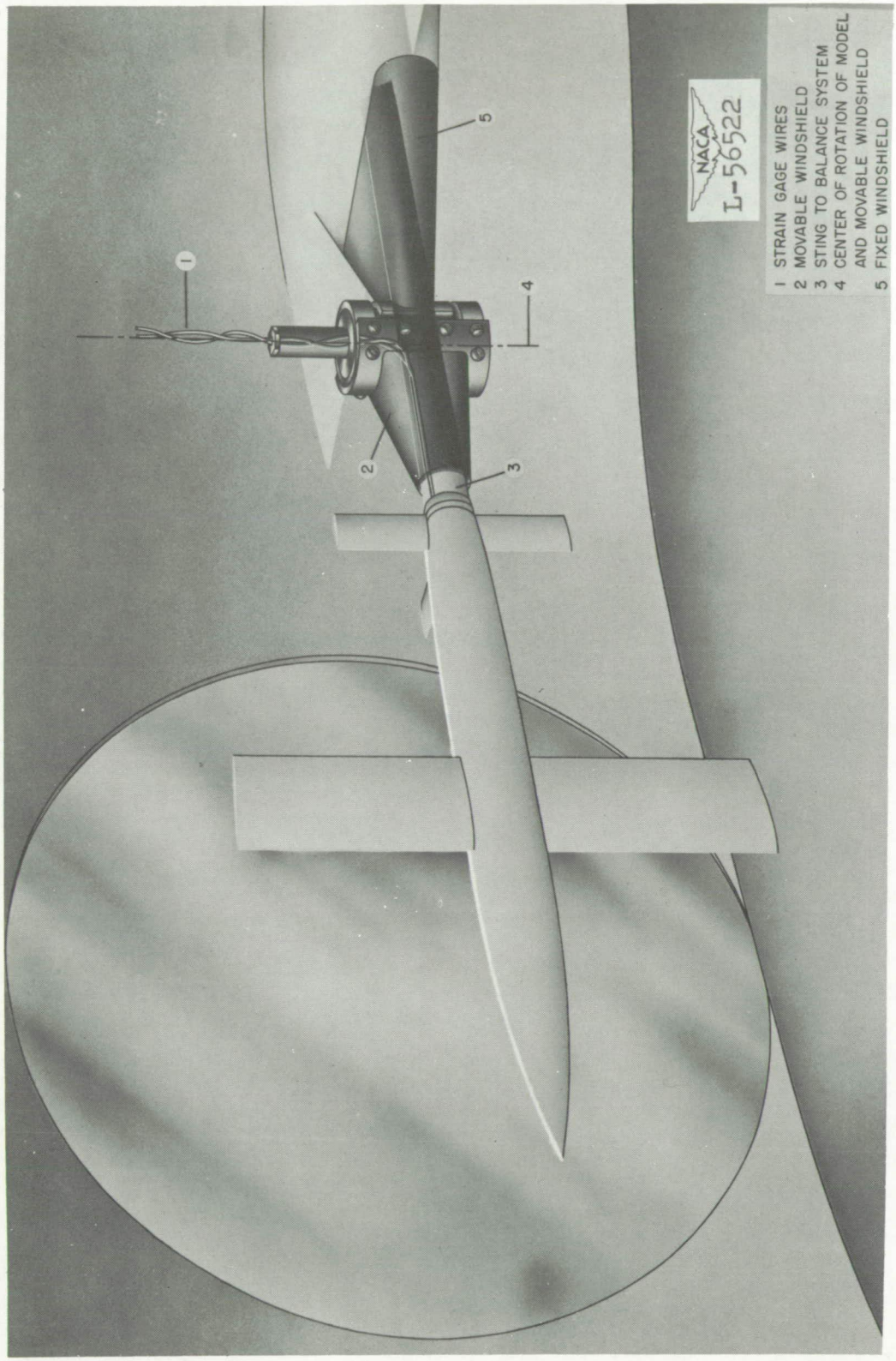


Figure 1.- Drawing of test setup in tunnel.

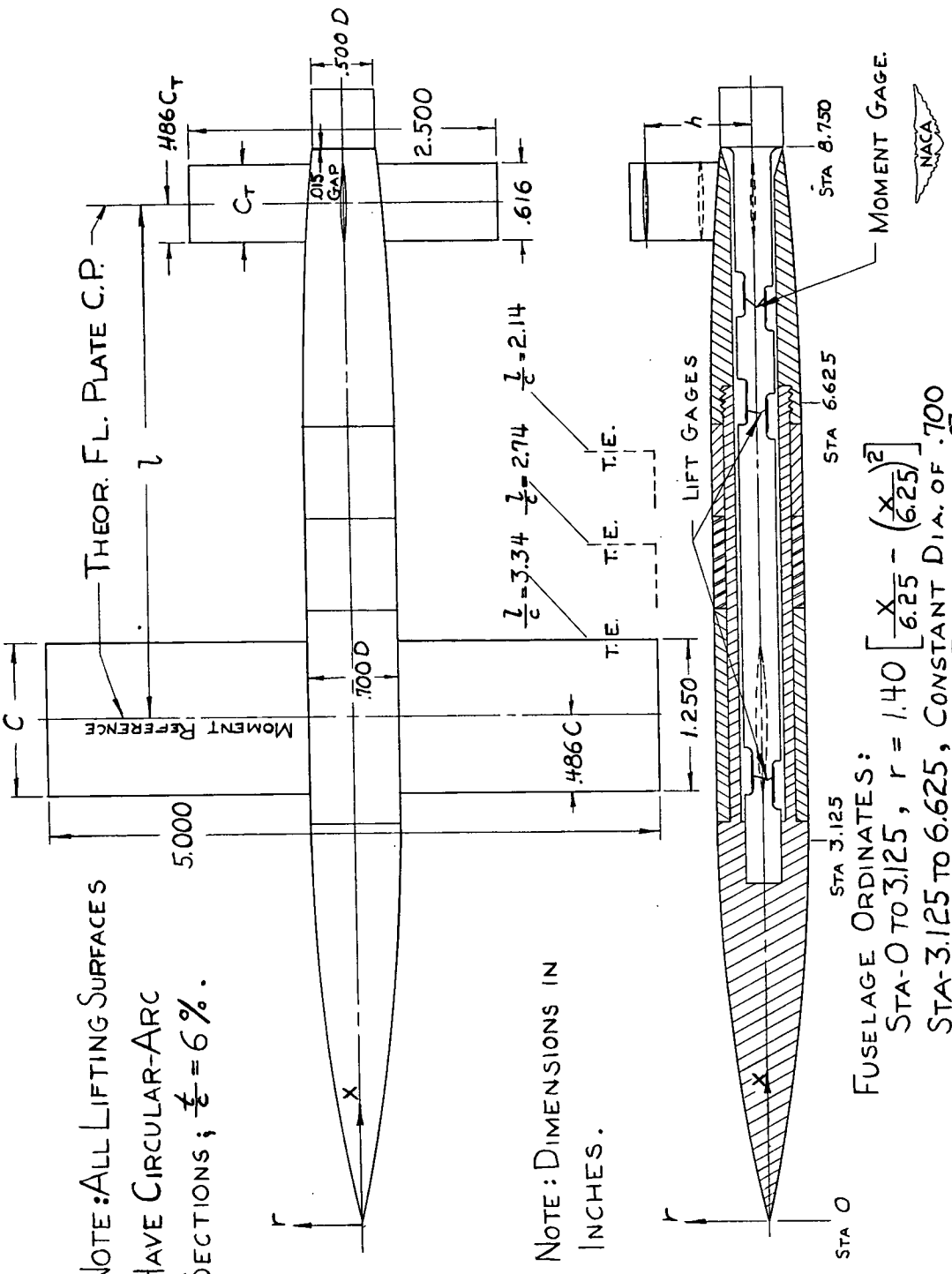
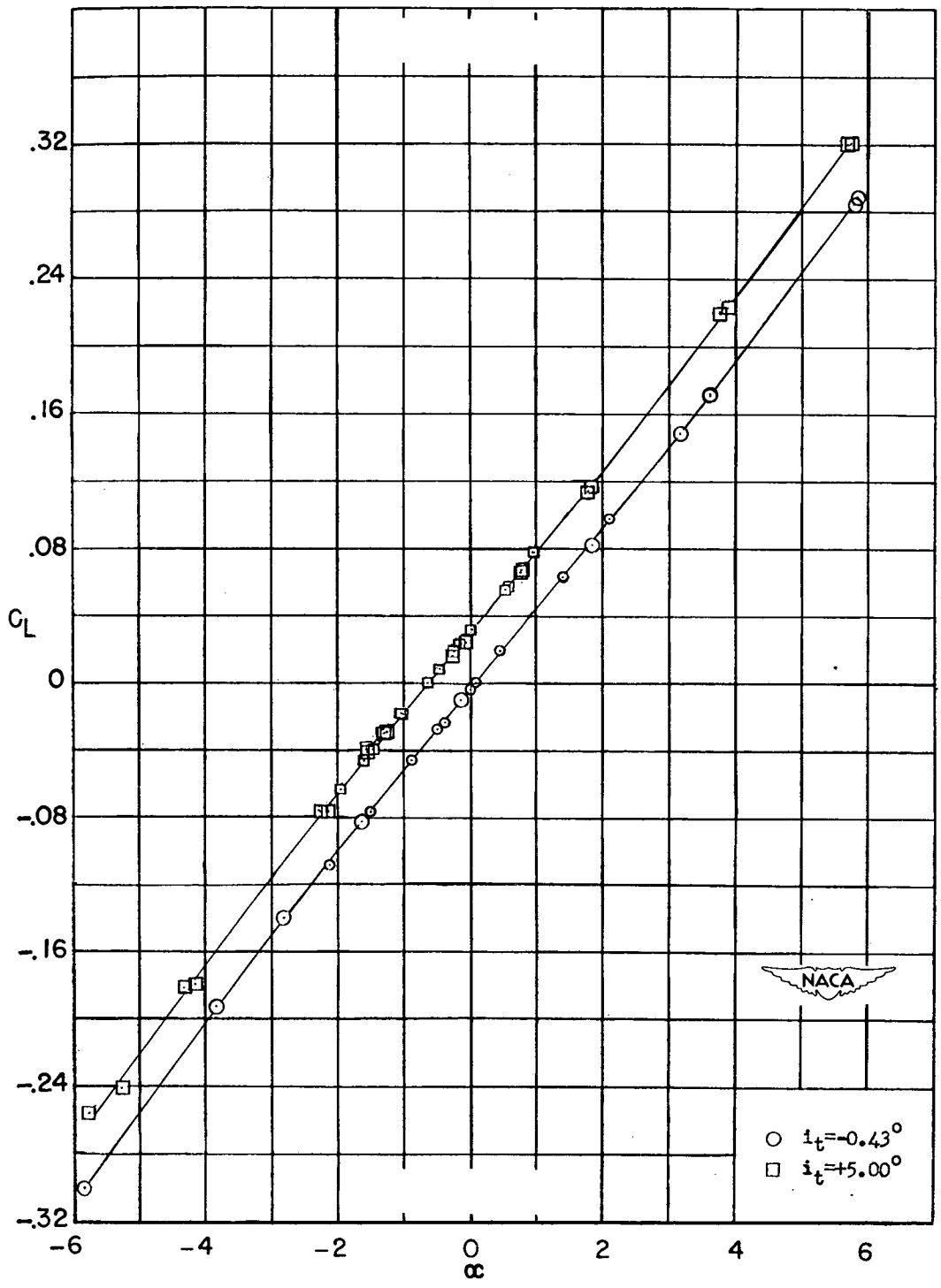
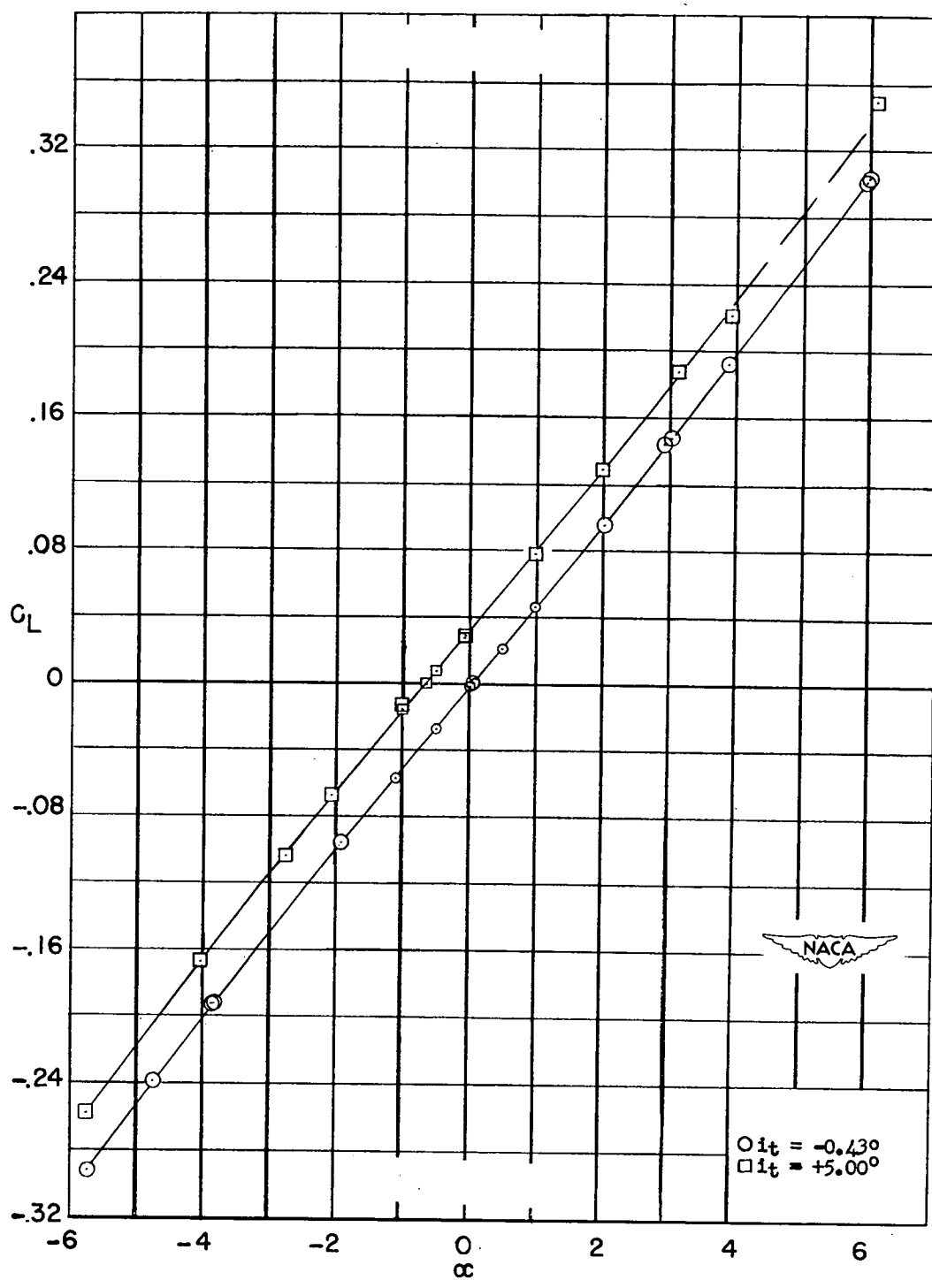


Figure 2.- Model dimensions.



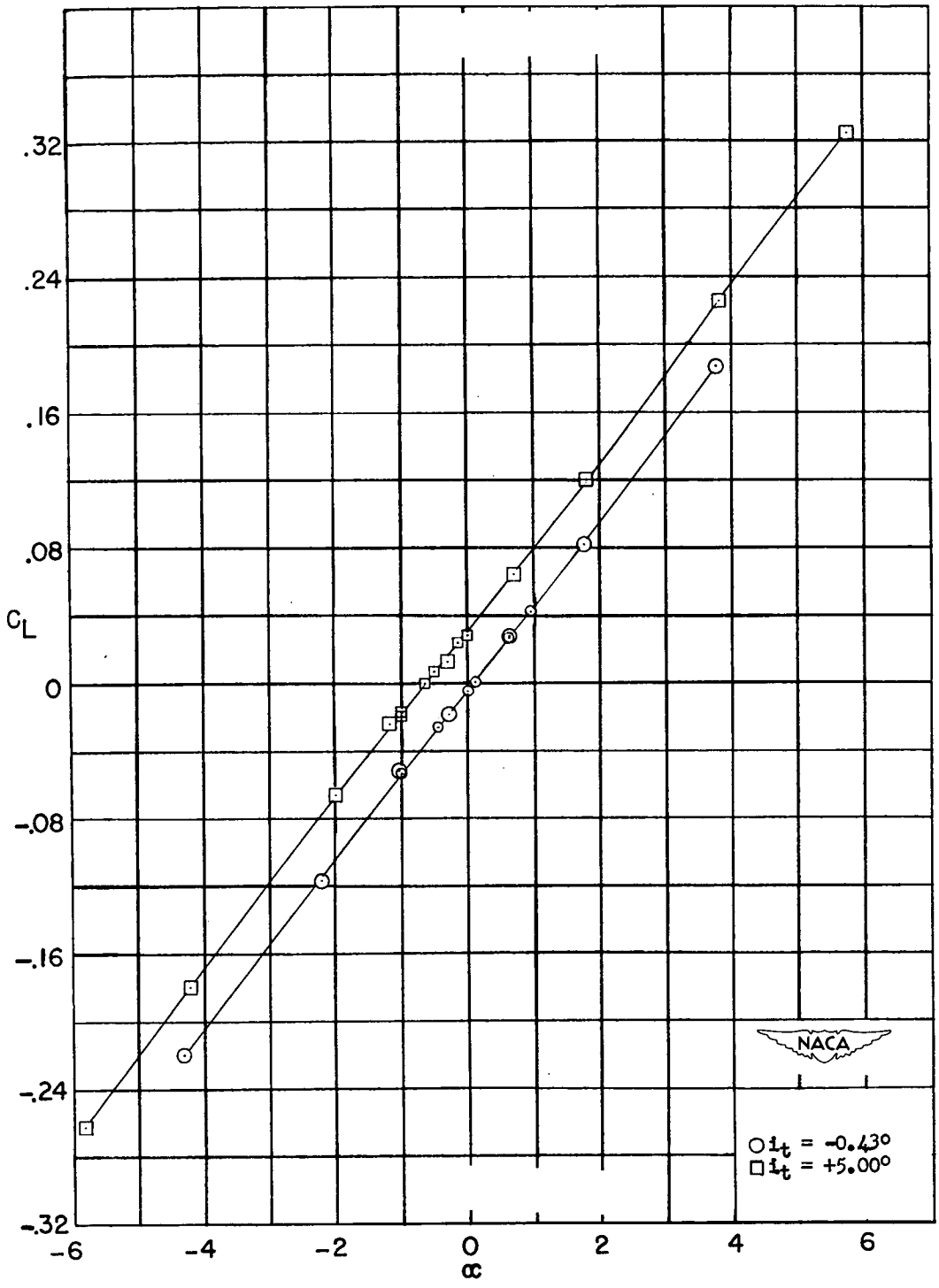
(a) BWT; $\frac{h}{c} = 0$; $\frac{l}{c} = 3.34$.

Figure 3.- Variation of lift coefficient with angle of attack for BWT, BT, and B.



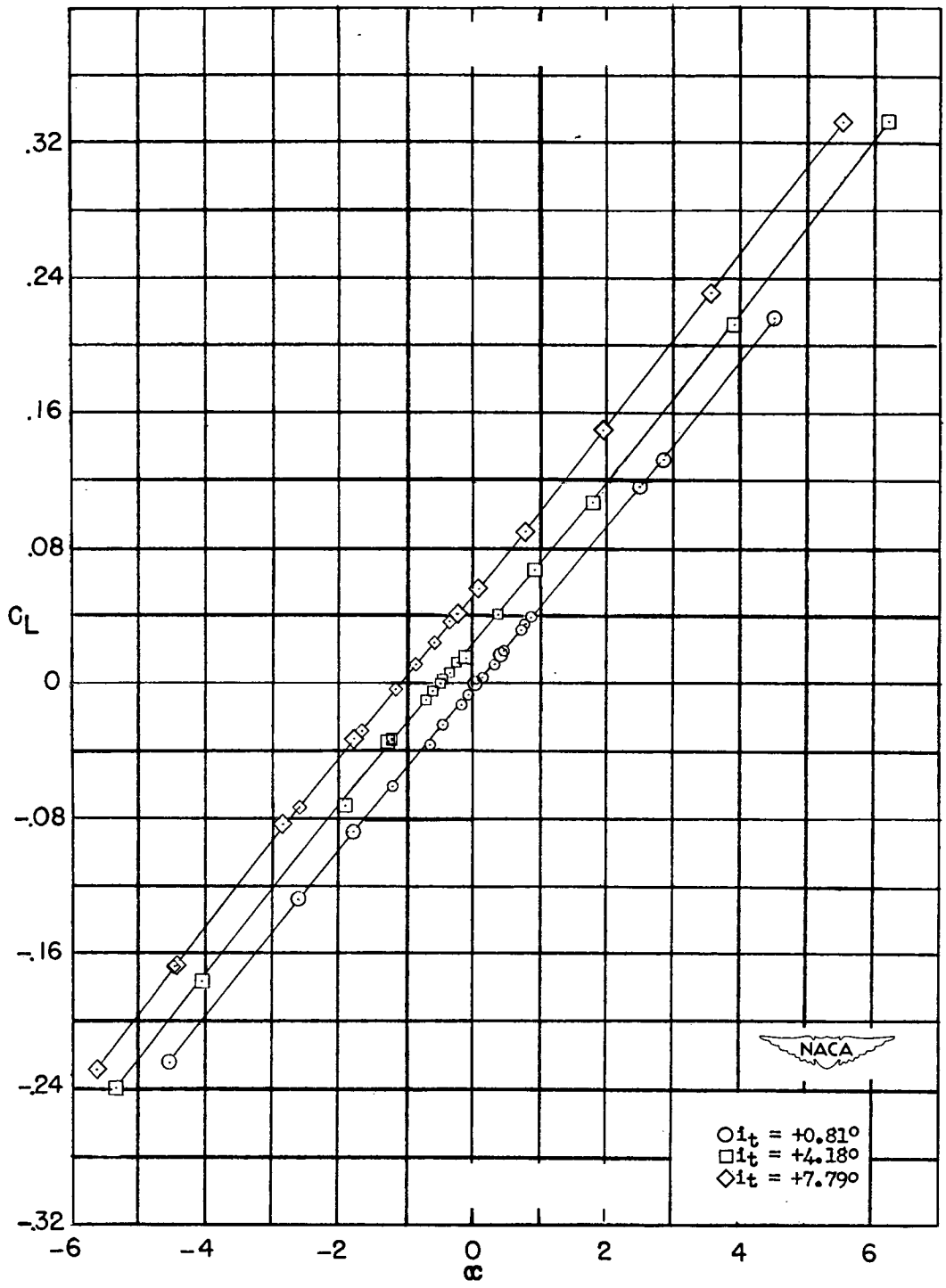
(b) BWT; $\frac{h}{c} = 0$; $\frac{l}{c} = 2.74$.

Figure 3.- Continued.



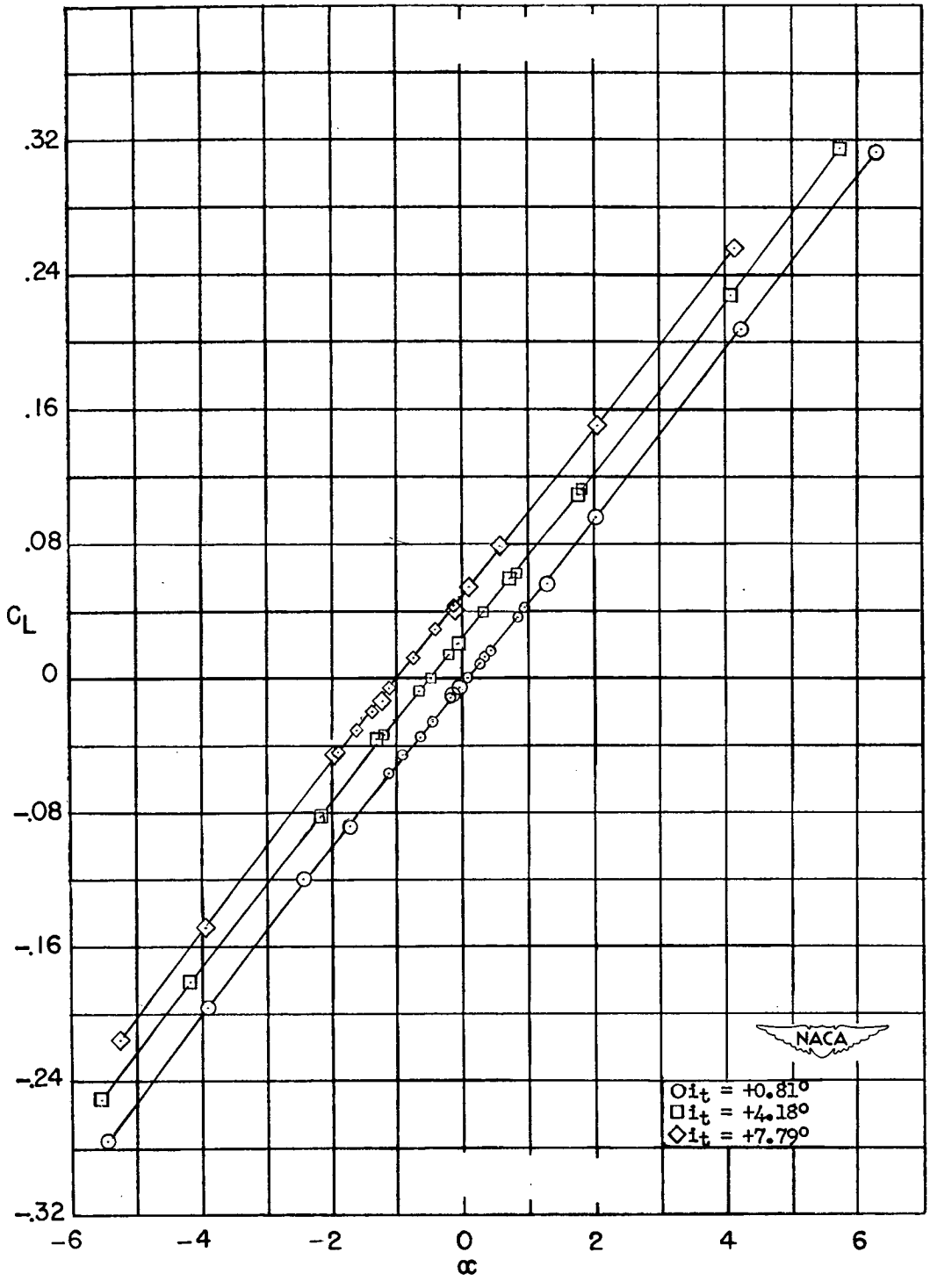
(c) BWT; $\frac{h}{c} = 0$; $\frac{l}{c} = 2.14$.

Figure 3.- Continued.



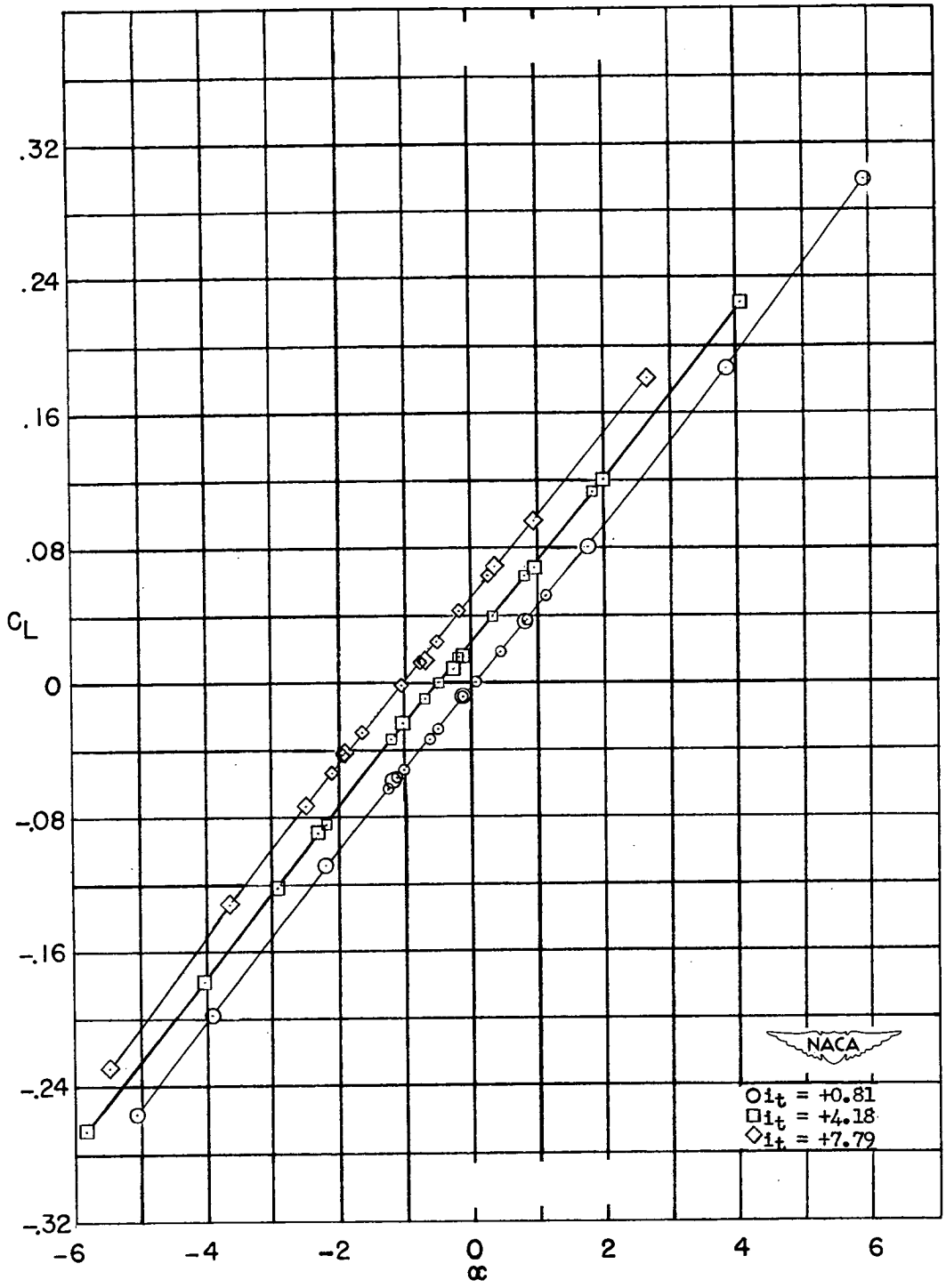
(d) BWT; $\frac{h}{c} = 0.35$; $\frac{l}{c} = 3.34$.

Figure 3.- Continued.



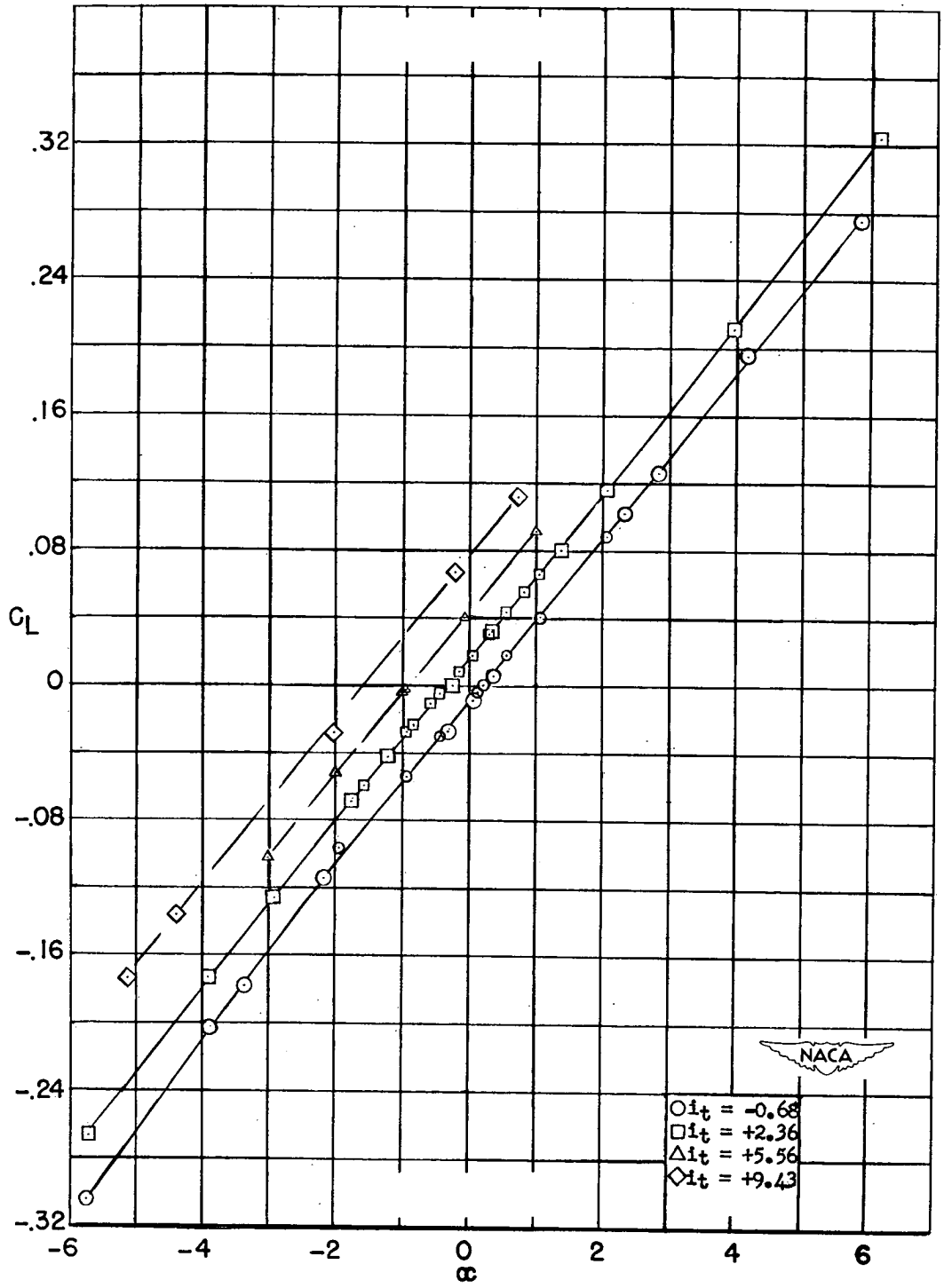
(e) BWT; $\frac{h}{c} = 0.35$; $\frac{l}{c} = 2.74$.

Figure 3.- Continued.



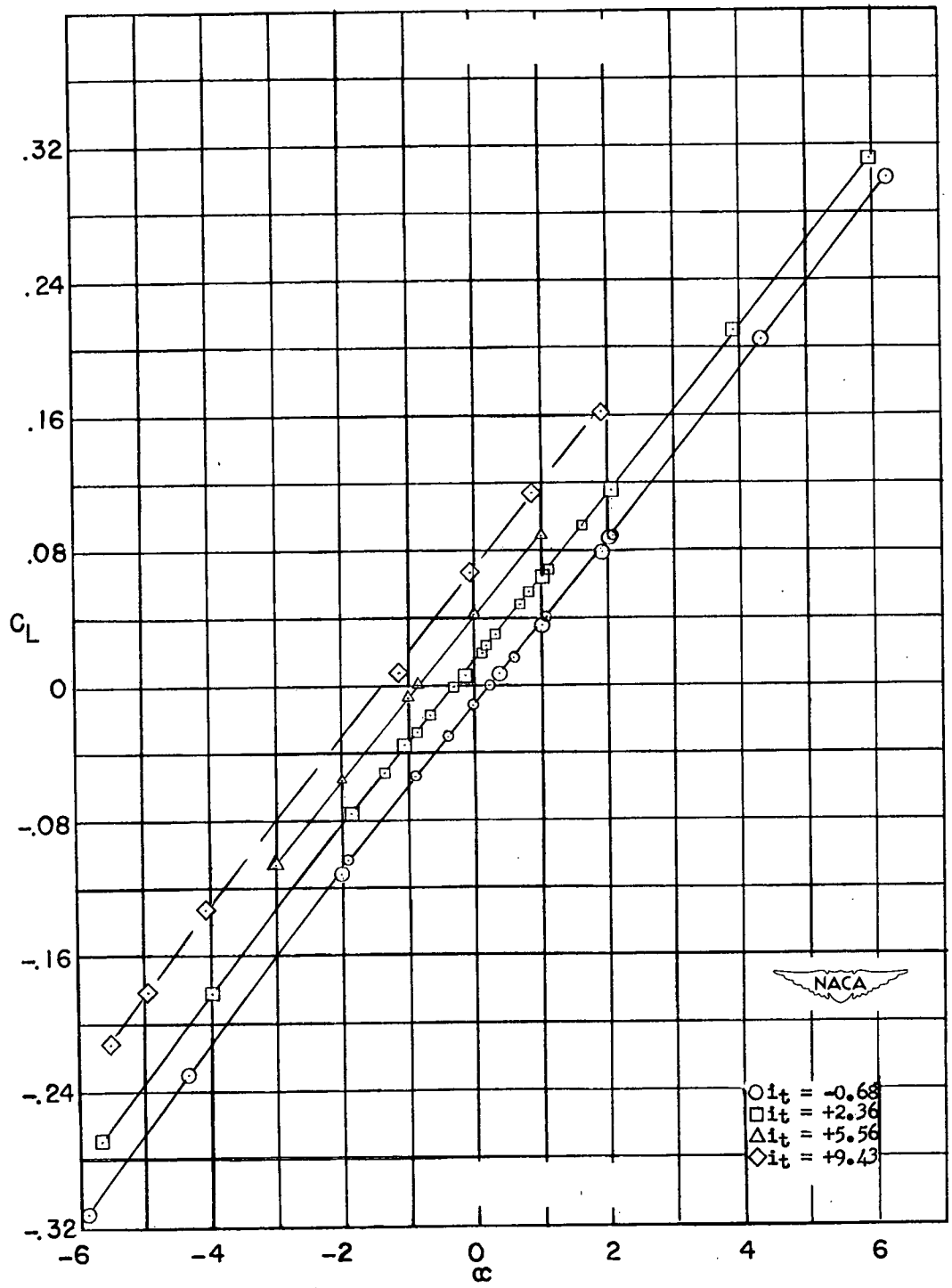
(f) BWT; $\frac{h}{c} = 0.35$; $\frac{l}{c} = 2.14$.

Figure 3.- Continued.



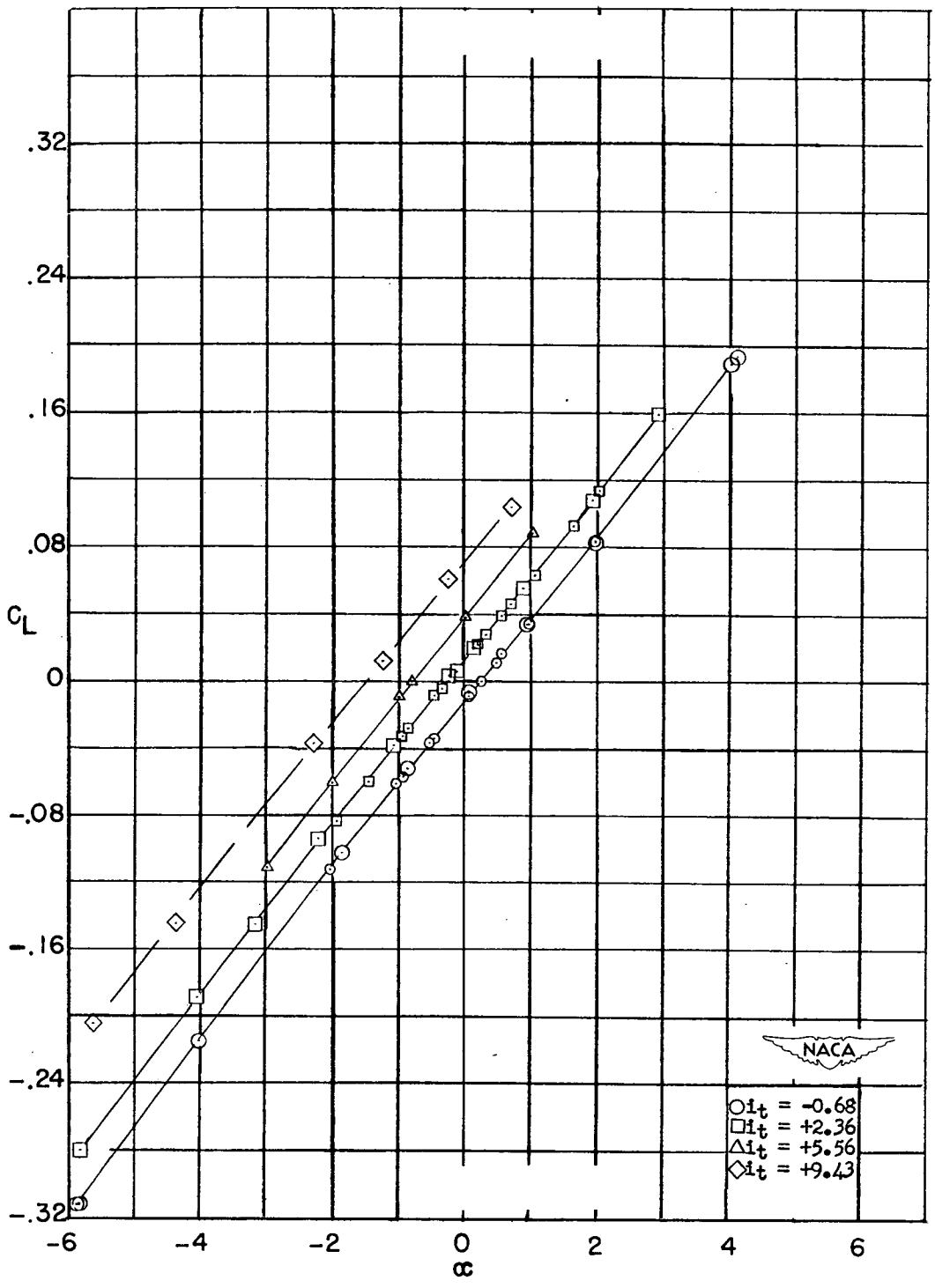
(g) BWT; $\frac{h}{c} = 0.70$; $\frac{l}{c} = 3.34$.

Figure 3.- Continued.



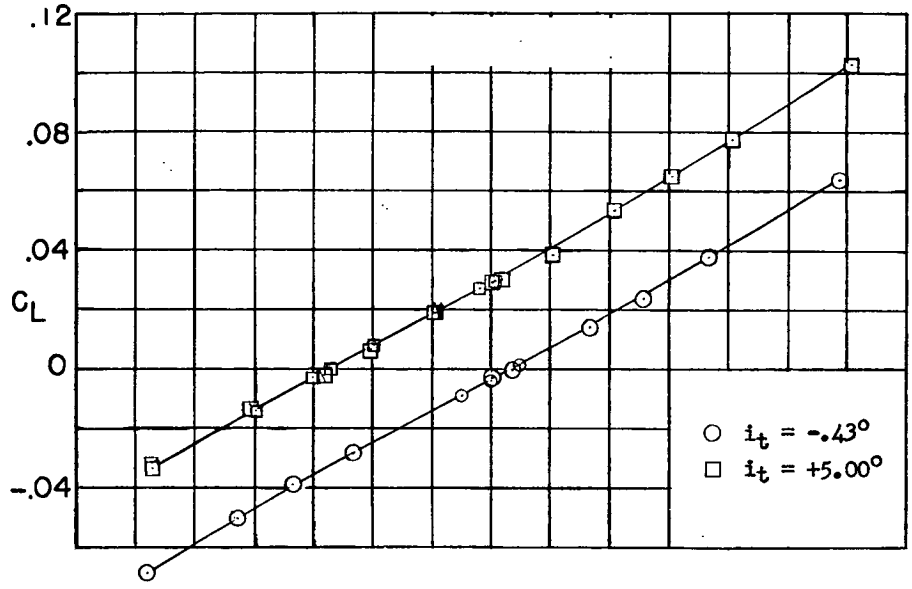
(h) BWT; $\frac{h}{c} = 0.70$; $\frac{l}{c} = 2.74$.

Figure 3.- Continued.

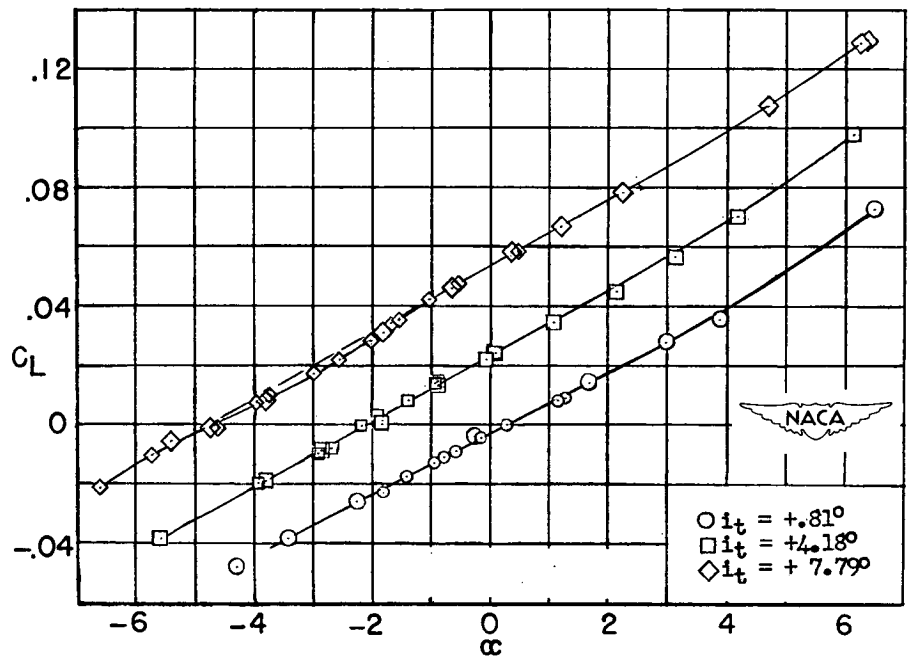


(i) BWT; $\frac{h}{c} = 0.70$; $\frac{l}{c} = 2.14$.

Figure 3.- Continued.

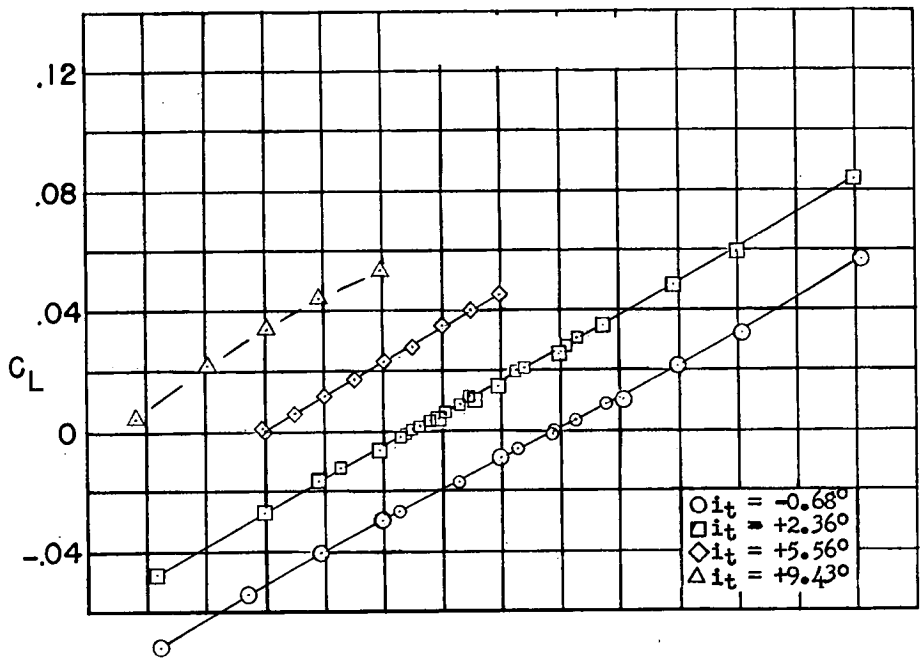


(j) BT; $\frac{h}{c} = 0.$

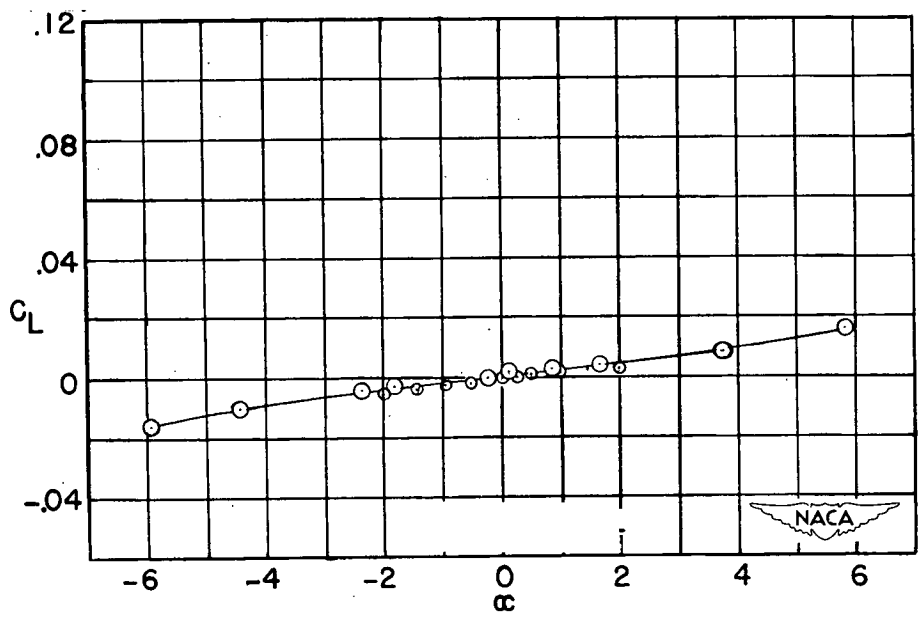


(k) BT; $\frac{h}{c} = 0.35.$

Figure 3.- Continued.

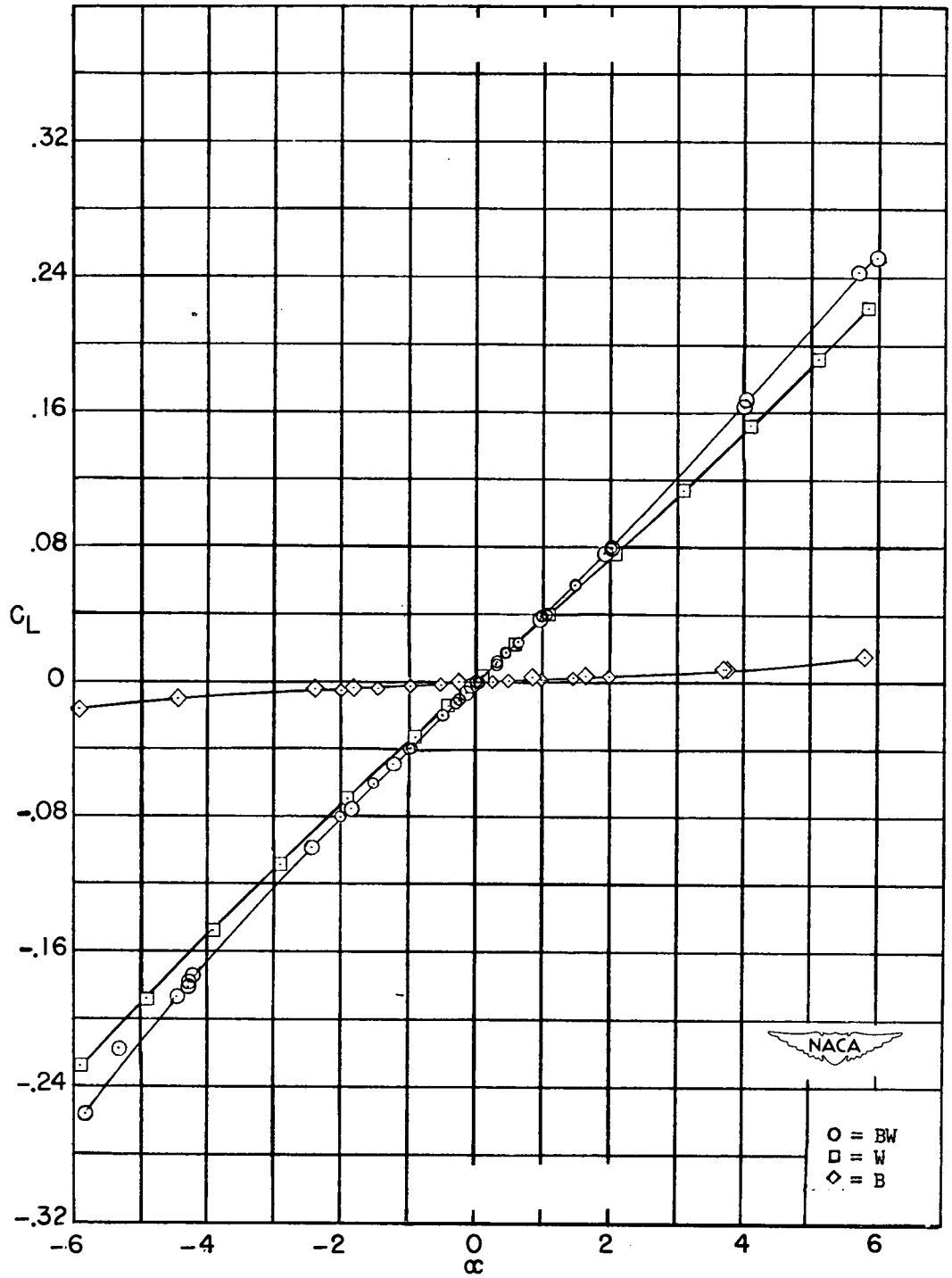


(l) BT; $\frac{h}{c}$ = 0.70.



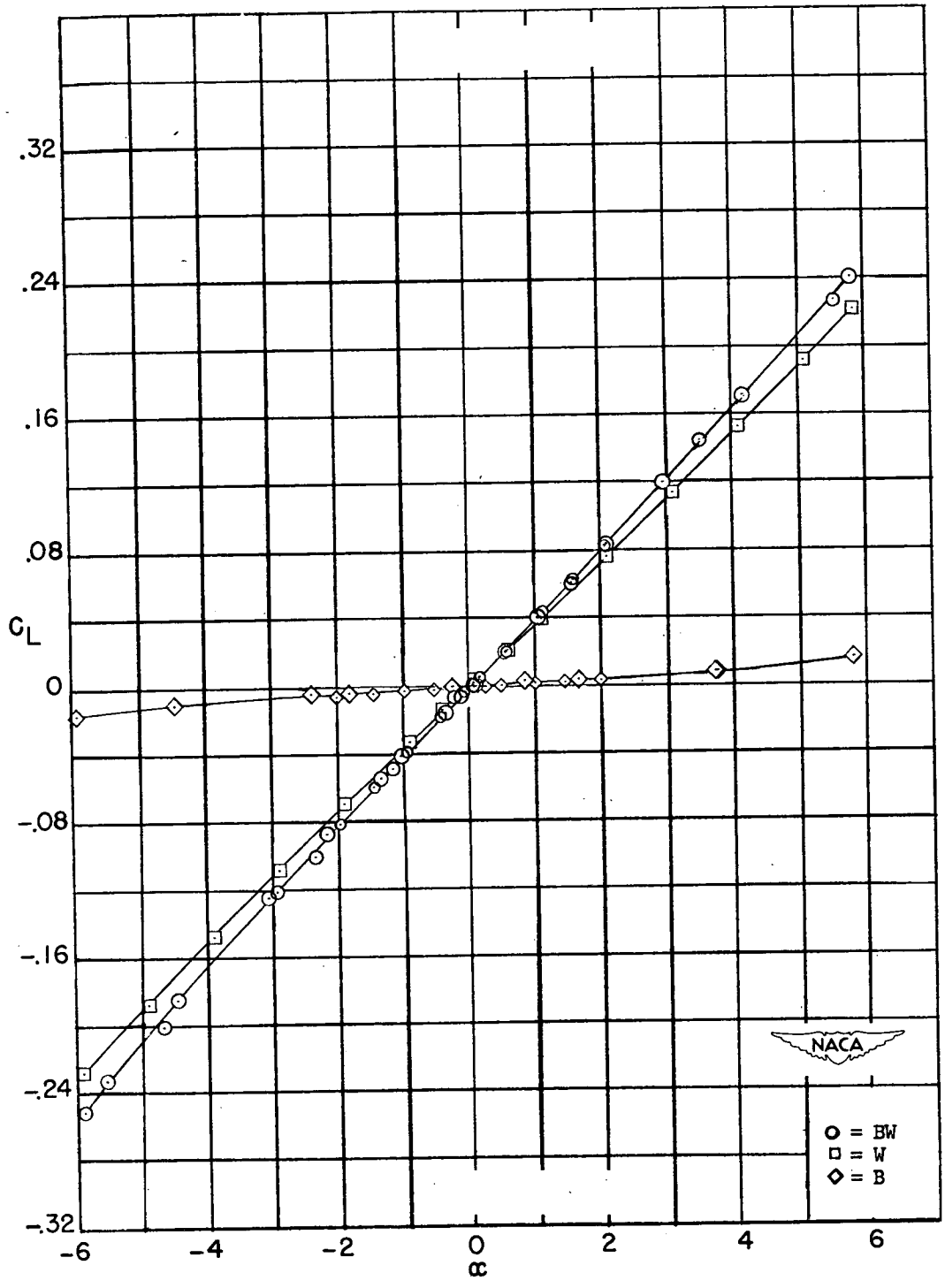
(m) B.

Figure 3.- Concluded.



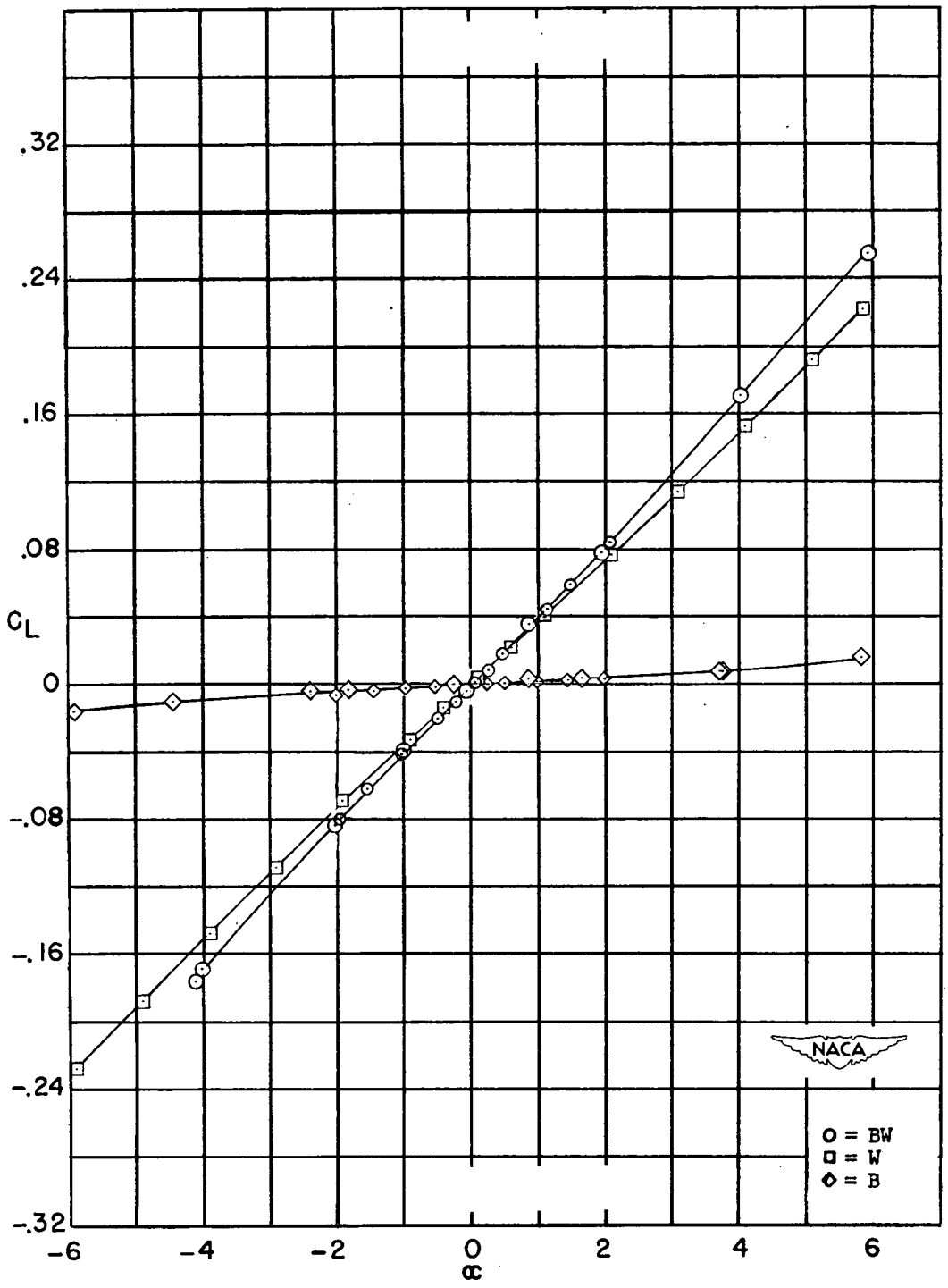
(a) BW with wing at $\frac{l}{c}$ = 3.34 location.

Figure 4.- Variation of lift coefficient with angle of attack for BW, W, and B.



(b) BW with wing at $\frac{l}{c} = 2.74$ location.

Figure 4.- Continued.



(c) BW with wing at $\frac{l}{c} = 2.14$ location.

Figure 4.- Concluded.

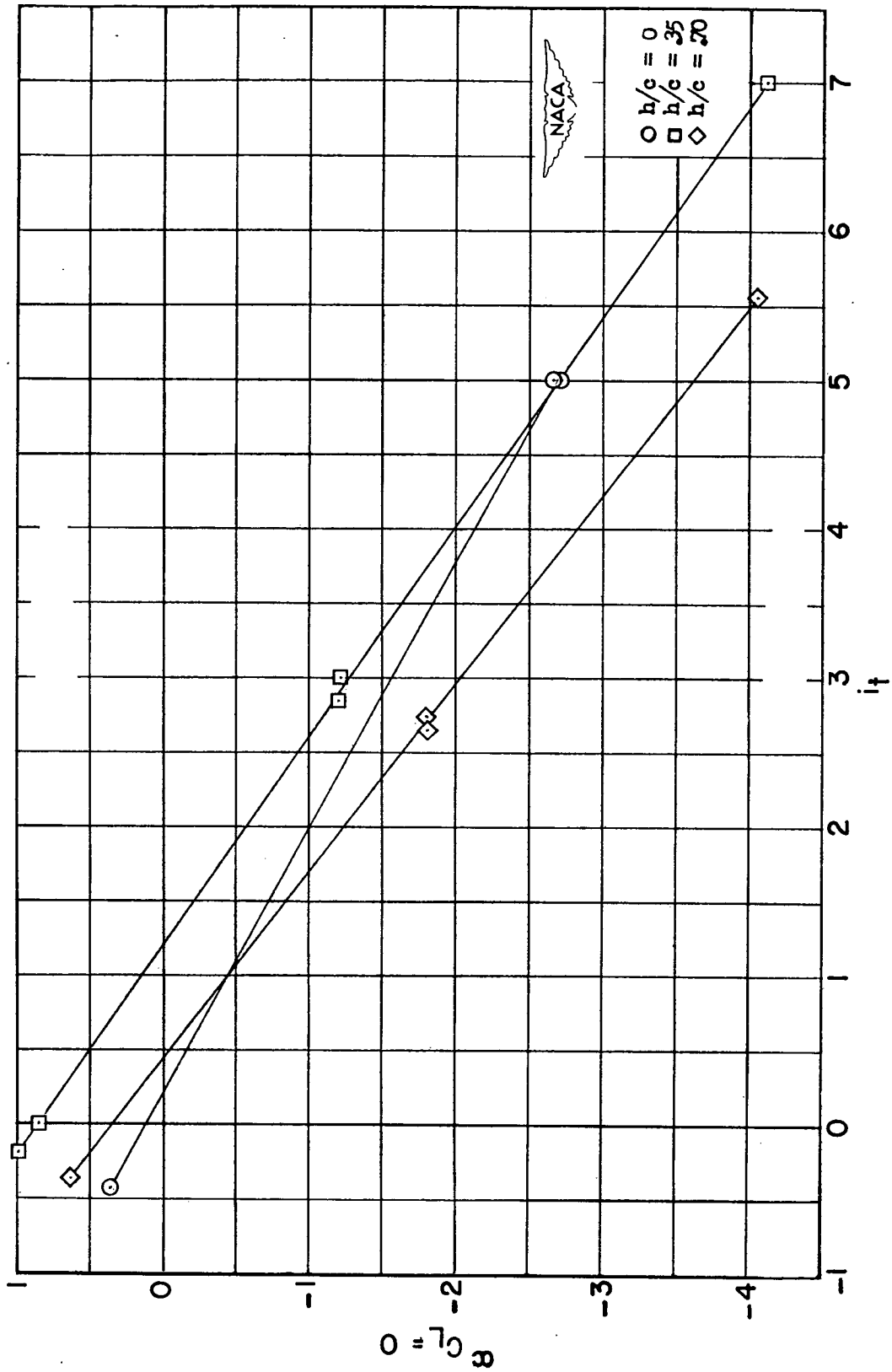
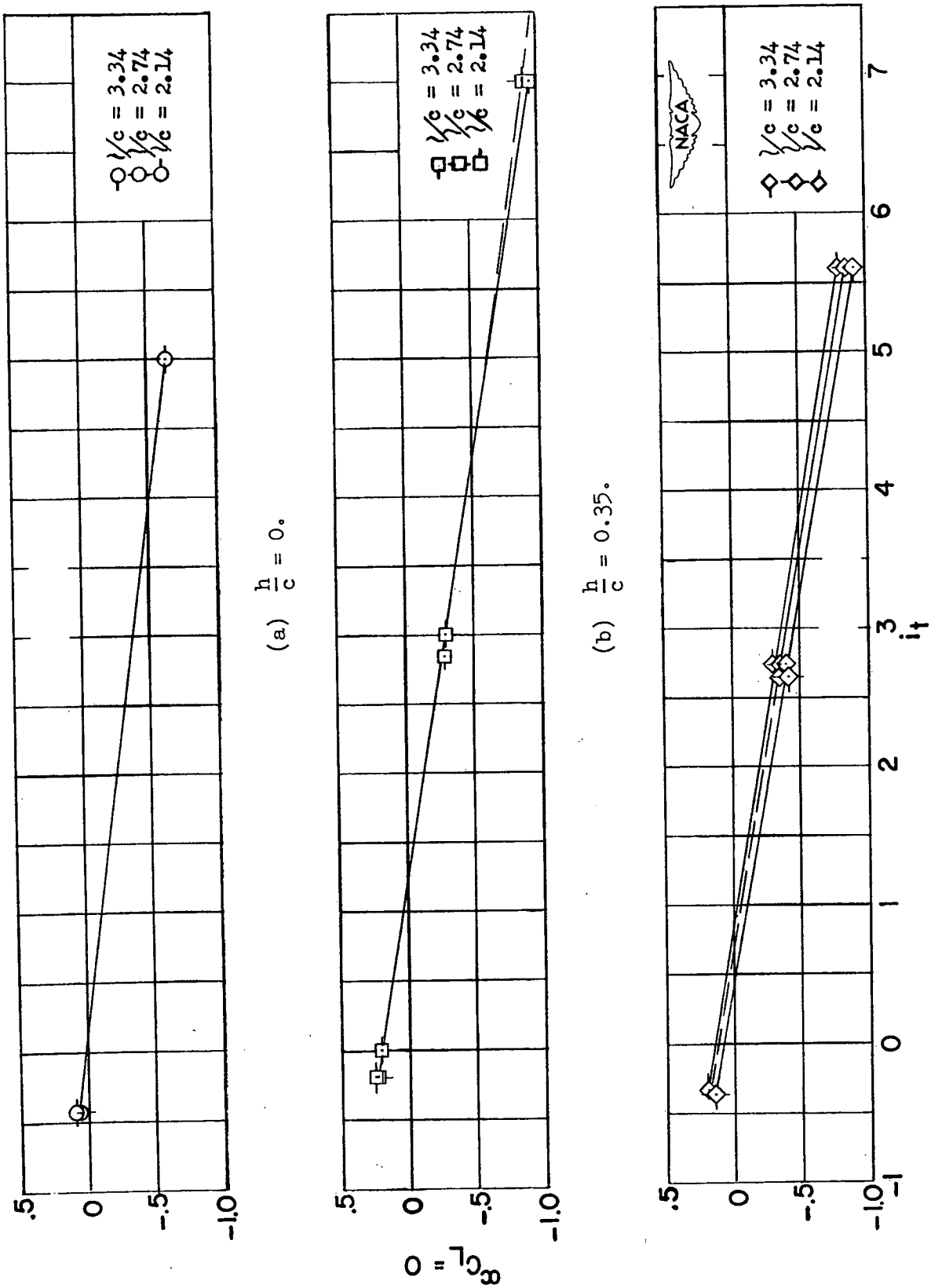


Figure 5.- Variation of angle of zero lift with tail incidence angle for BT.

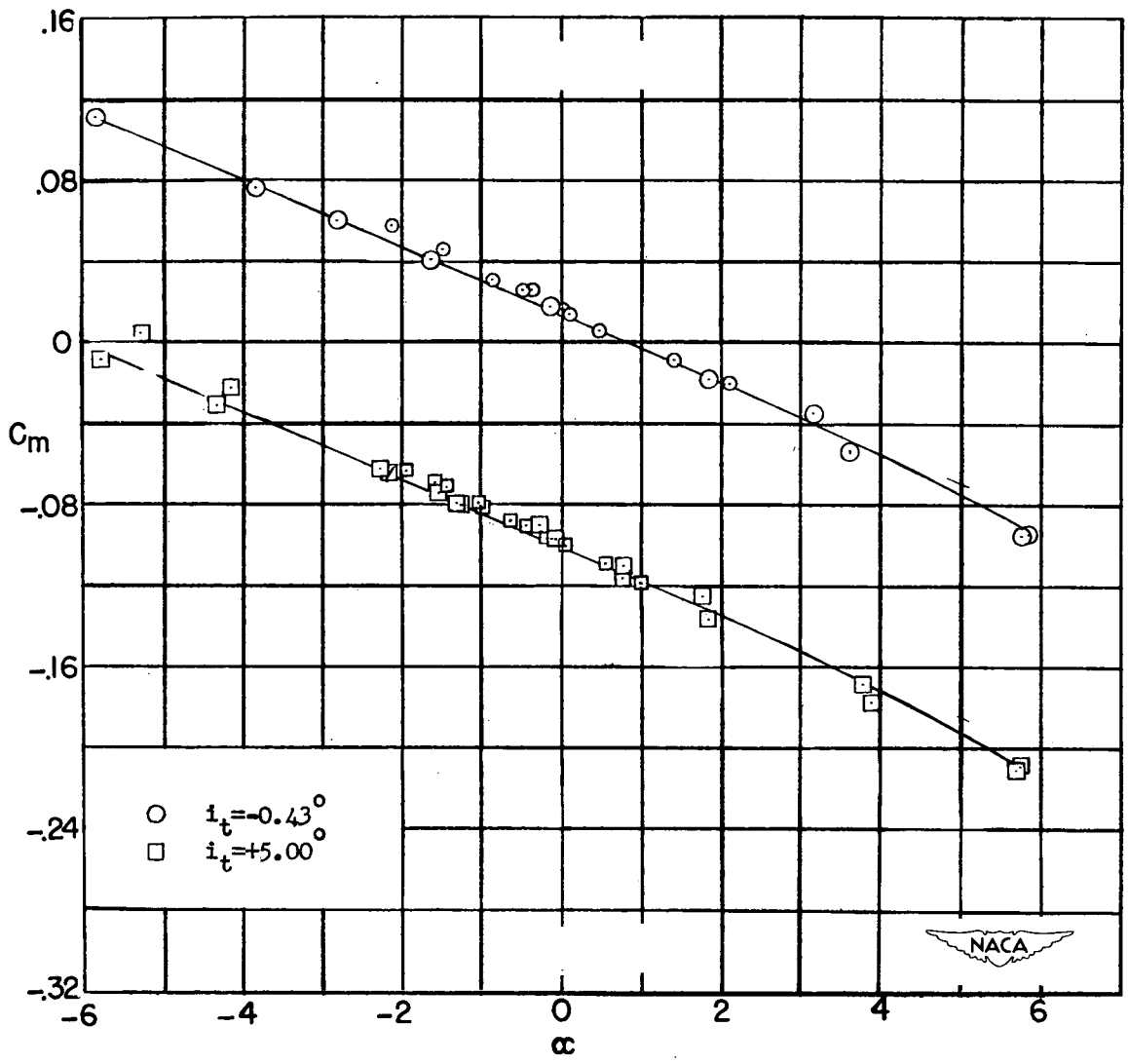


(a) $\frac{h}{c} = 0$.

(b) $\frac{h}{c} = 0.35$.

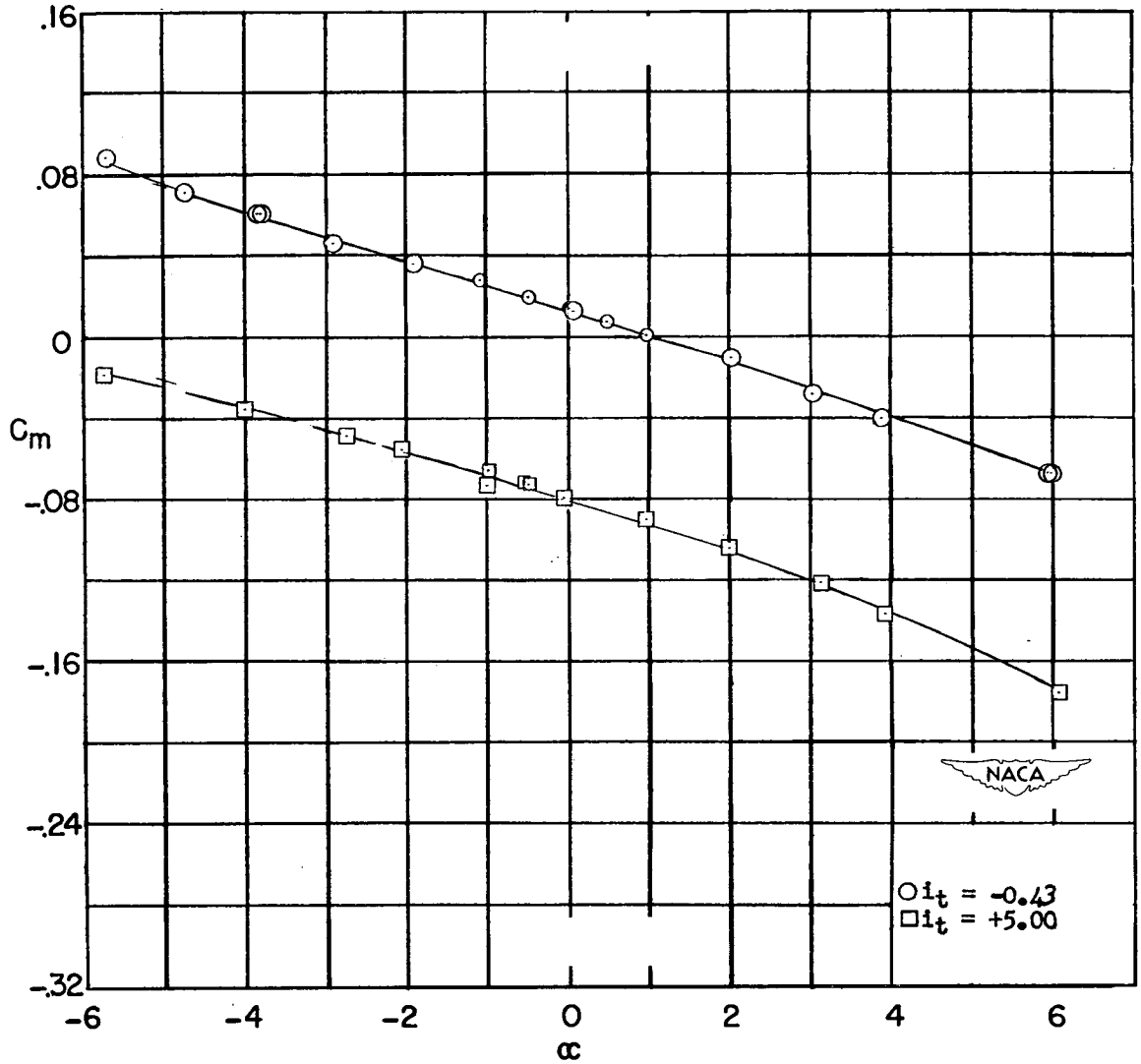
(c) $\frac{h}{c} = 0.70$.

Figure 6.- Variation of angle of zero lift with tail incidence angle for BWT.



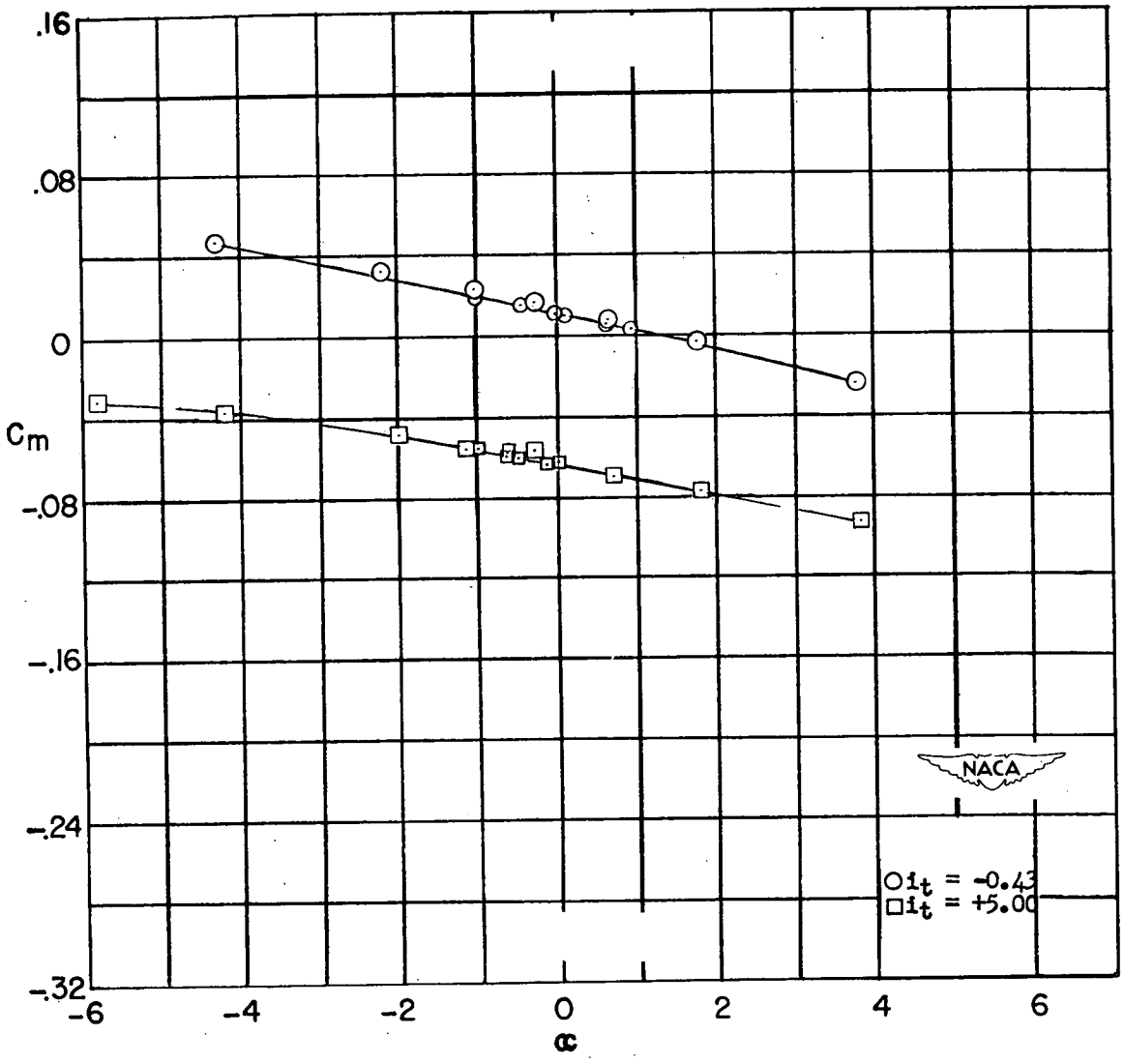
(a) BWT; $\frac{h}{c} = 0$; $\frac{l}{c} = 3.34$.

Figure 7.- Variation of pitching-moment coefficient with angle of attack for BWT and BT.



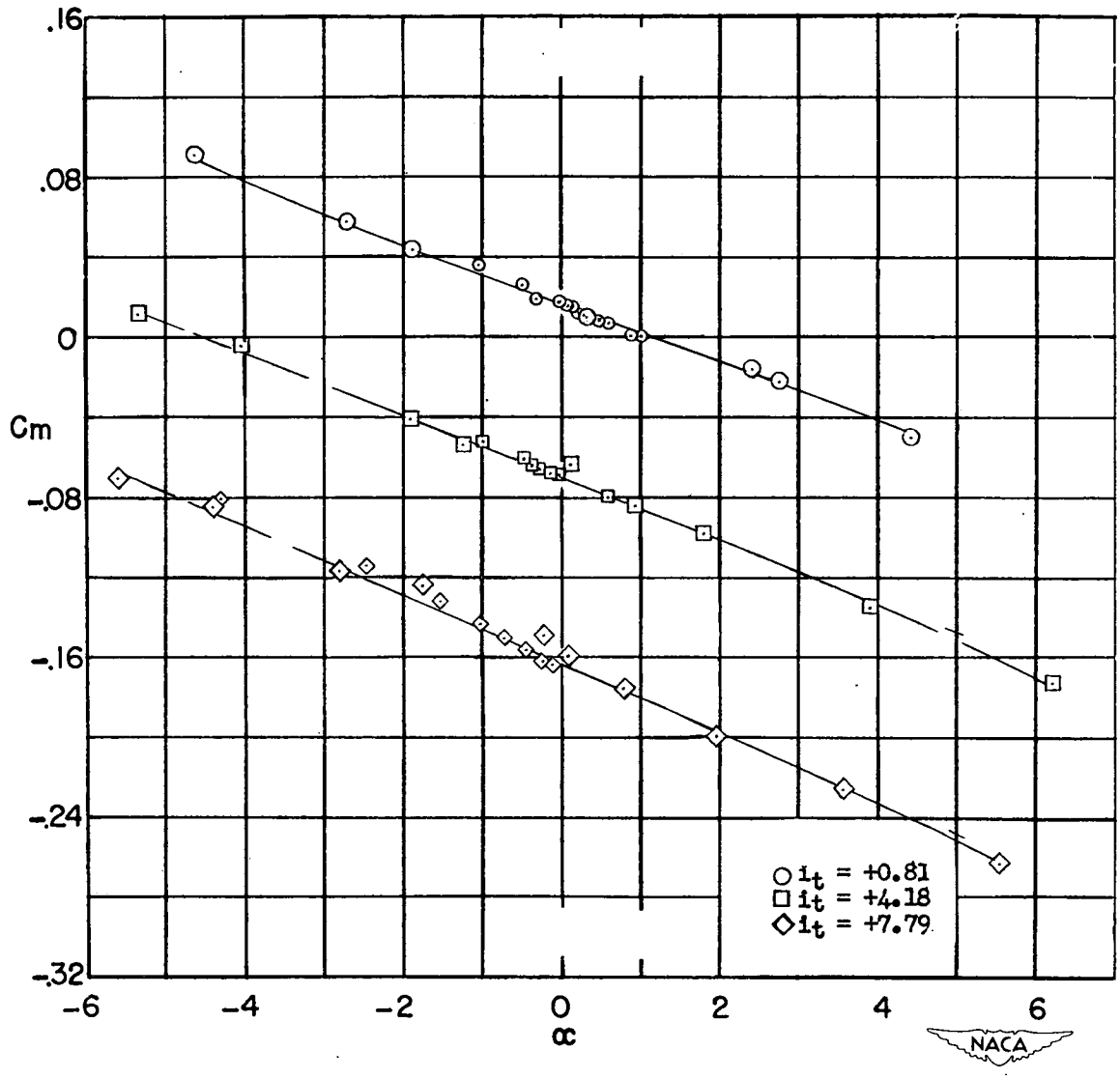
(b) BWT; $\frac{h}{c} = 0$; $\frac{l}{c} = 2.74$.

Figure 7.- Continued.



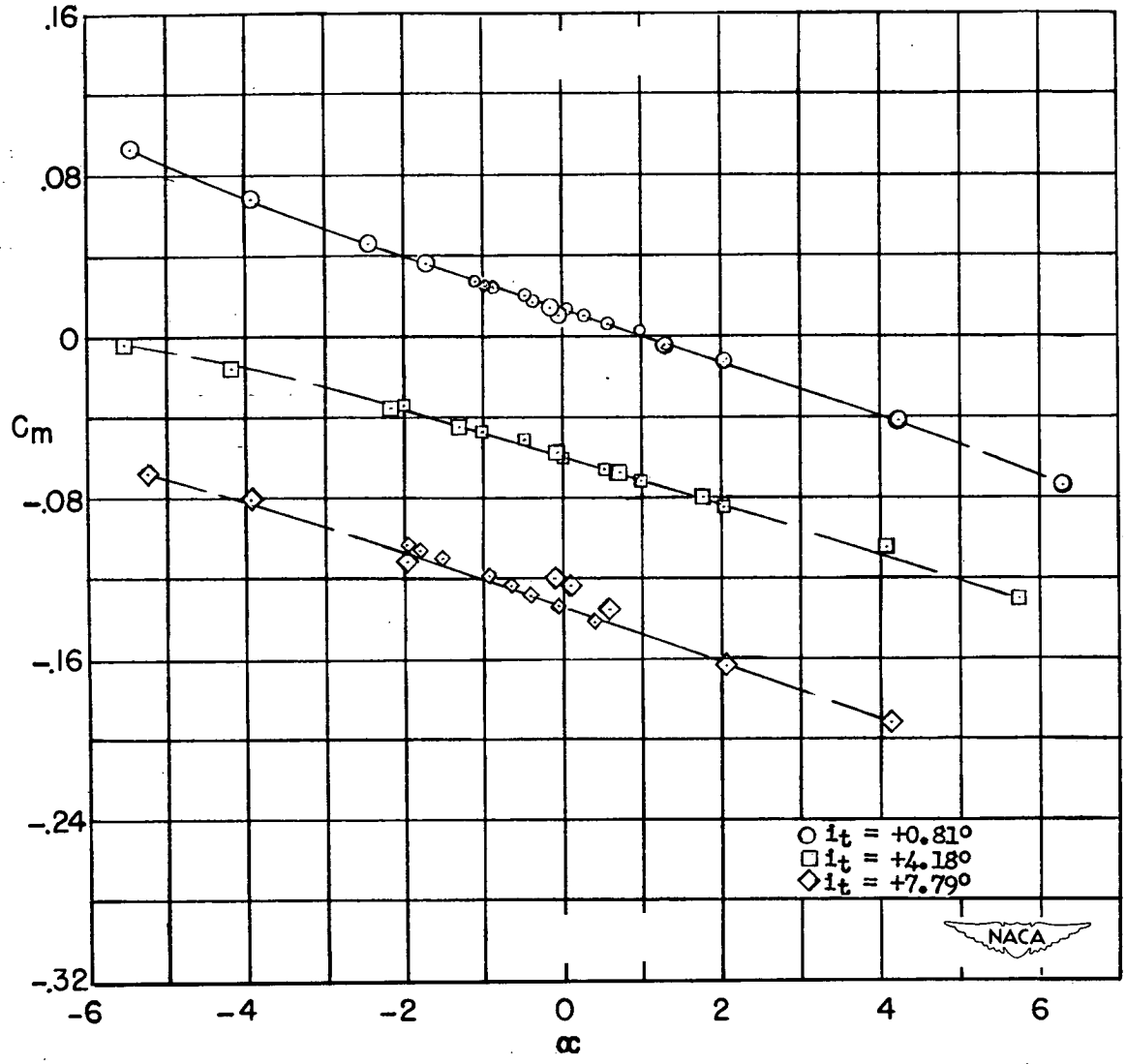
(c) BWT; $\frac{h}{c} = 0$; $\frac{l}{c} = 2.14$.

Figure 7.- Continued.



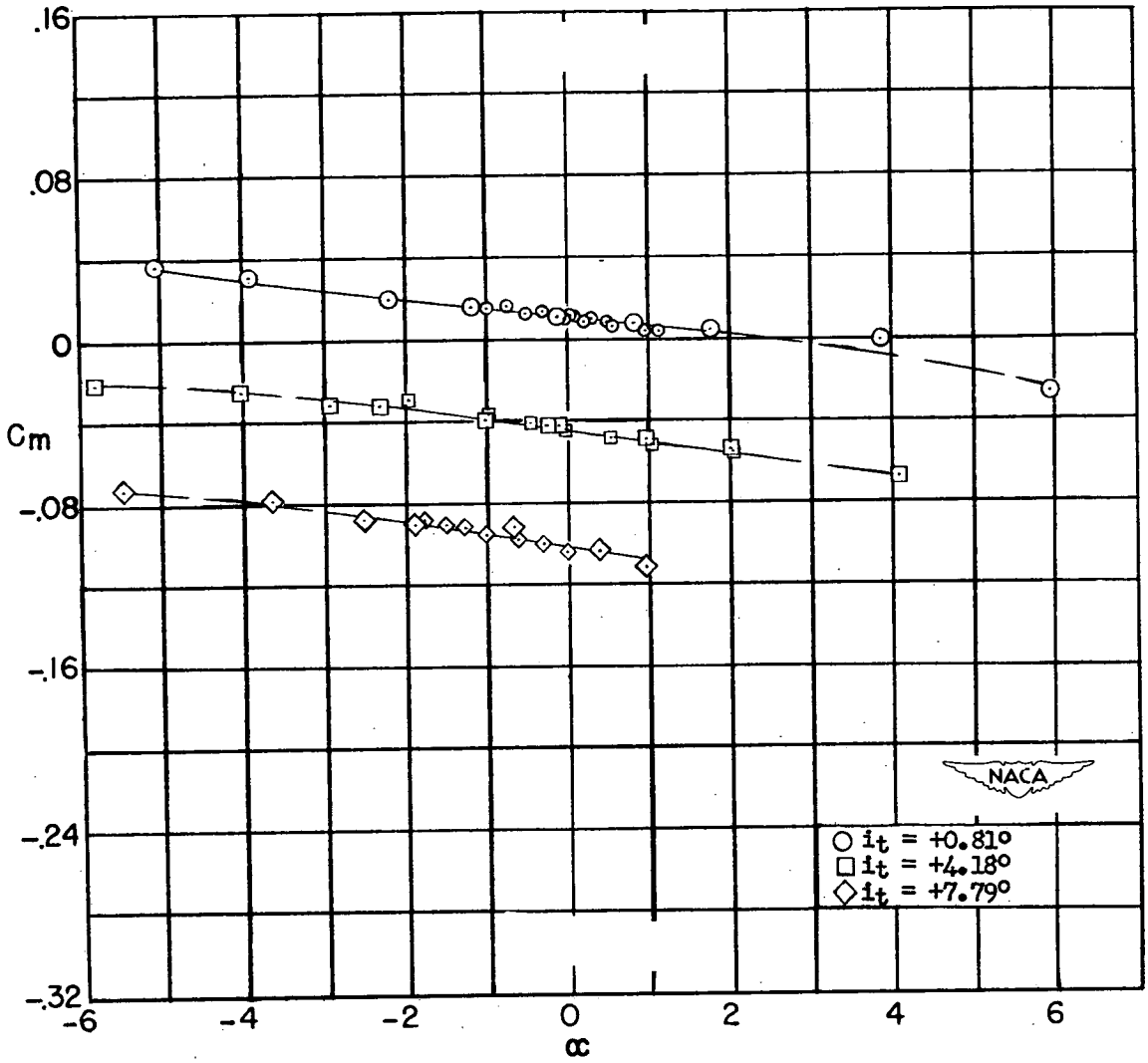
(d) BWT; $\frac{h}{c} = 0.35$; $\frac{l}{c} = 3.34$.

Figure 7.- Continued.



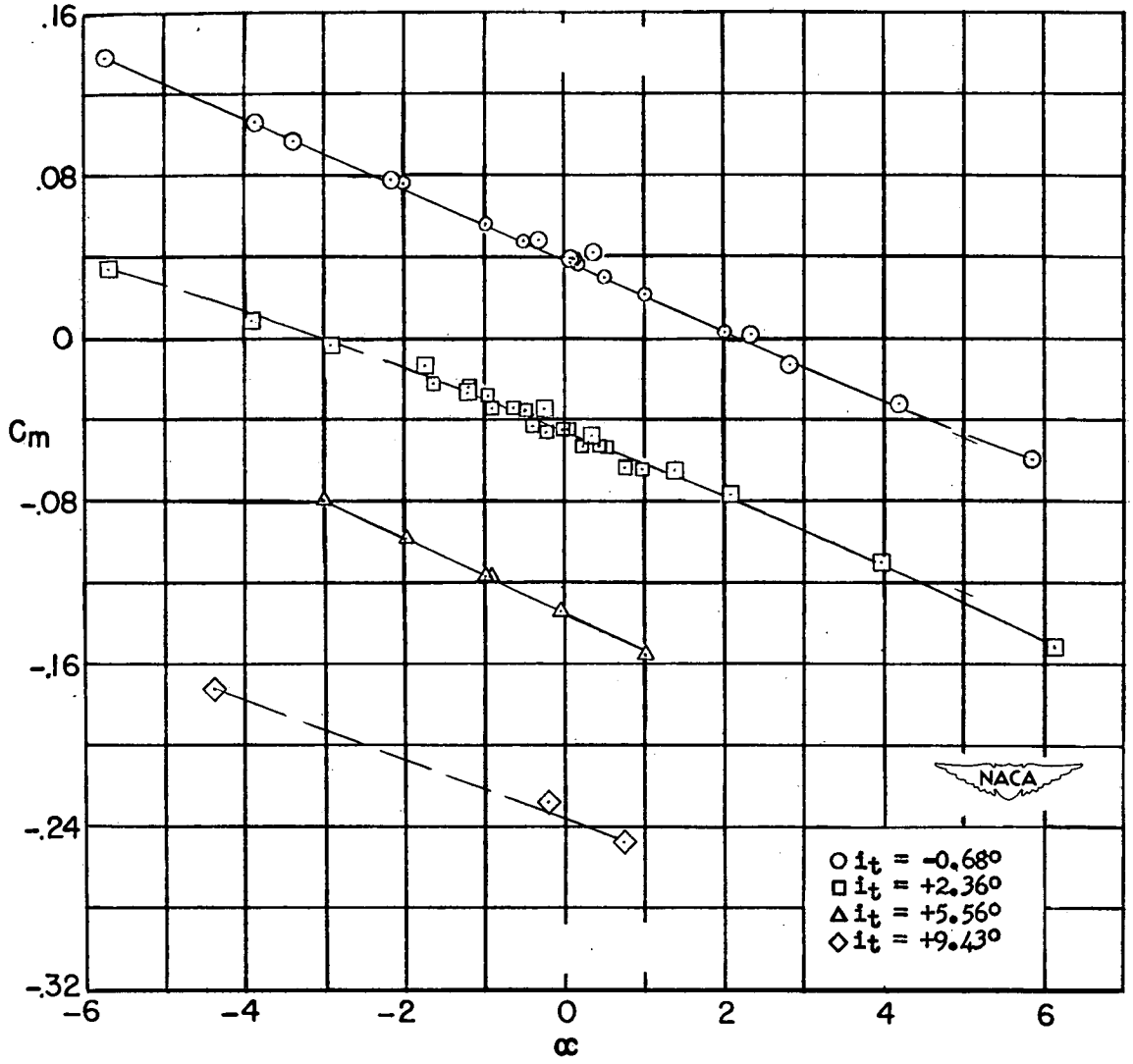
(e) BWT; $\frac{h}{c} = 0.35$; $\frac{l}{c} = 2.74$.

Figure 7.- Continued.



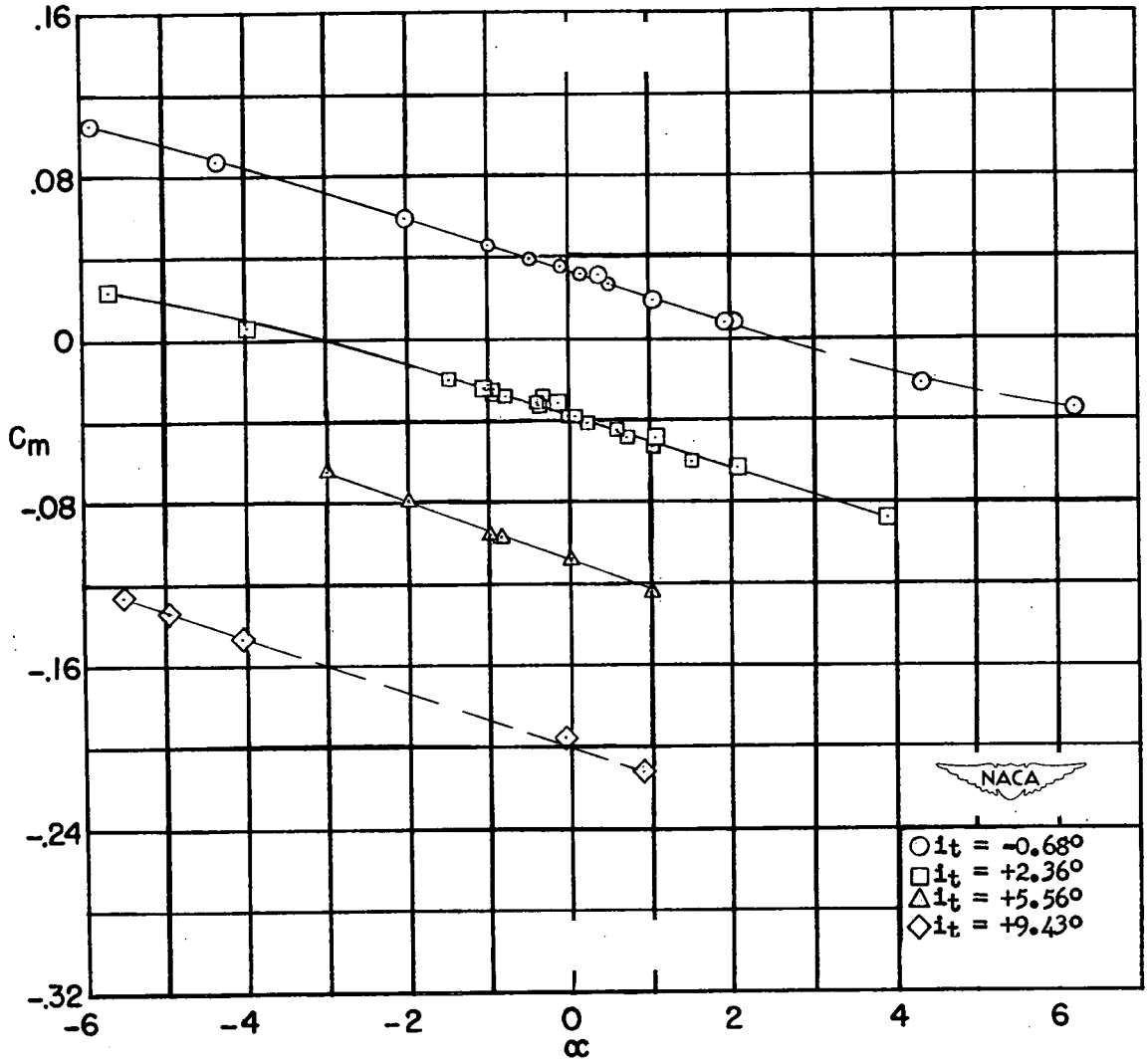
(f) BWT; $\frac{h}{c} = 0.35$; $\frac{l}{c} = 2.14$.

Figure 7.- Continued.



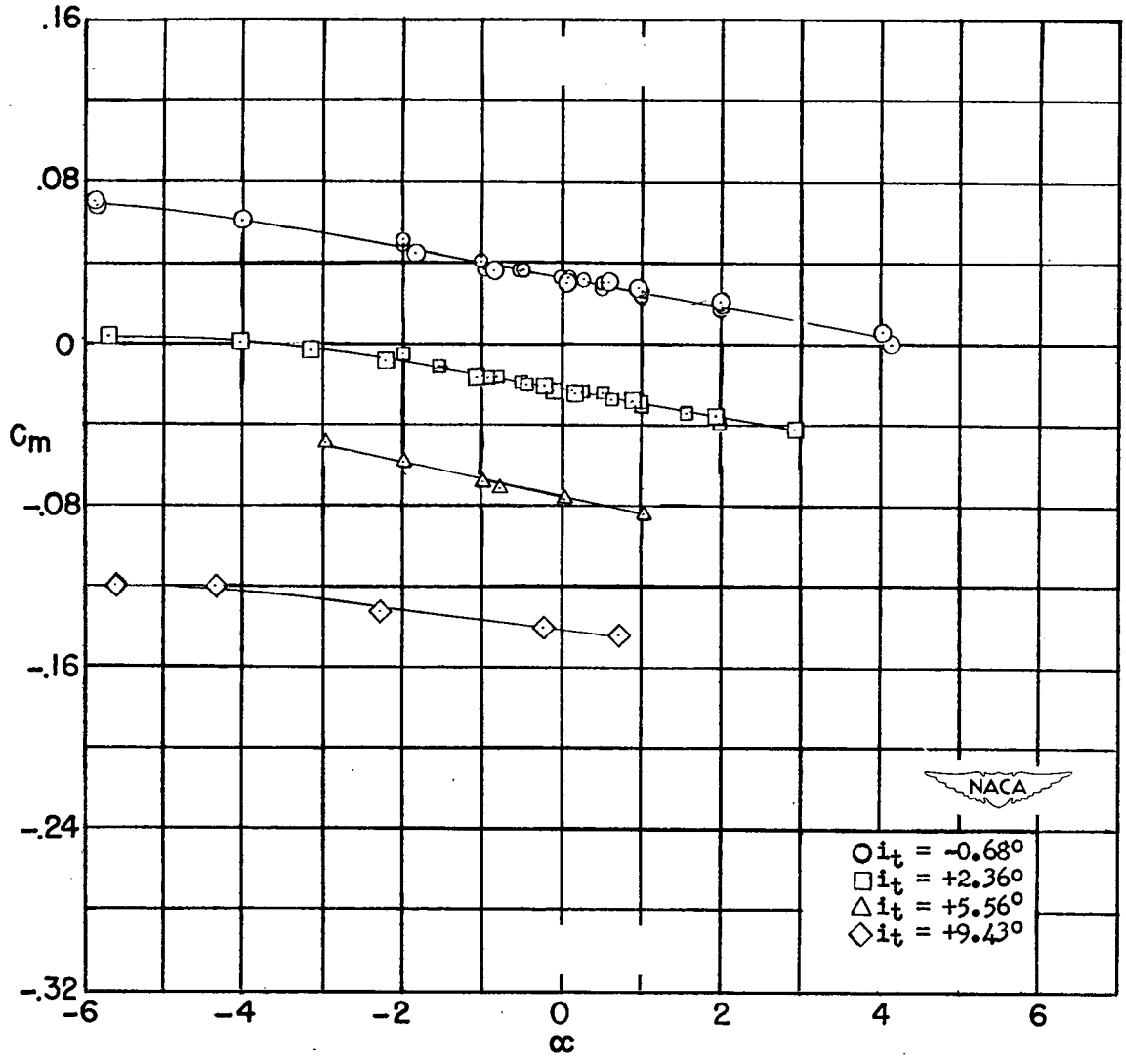
(g) BWT; $\frac{h}{c} = 0.70$; $\frac{l}{c} = 3.34$.

Figure 7.- Continued.



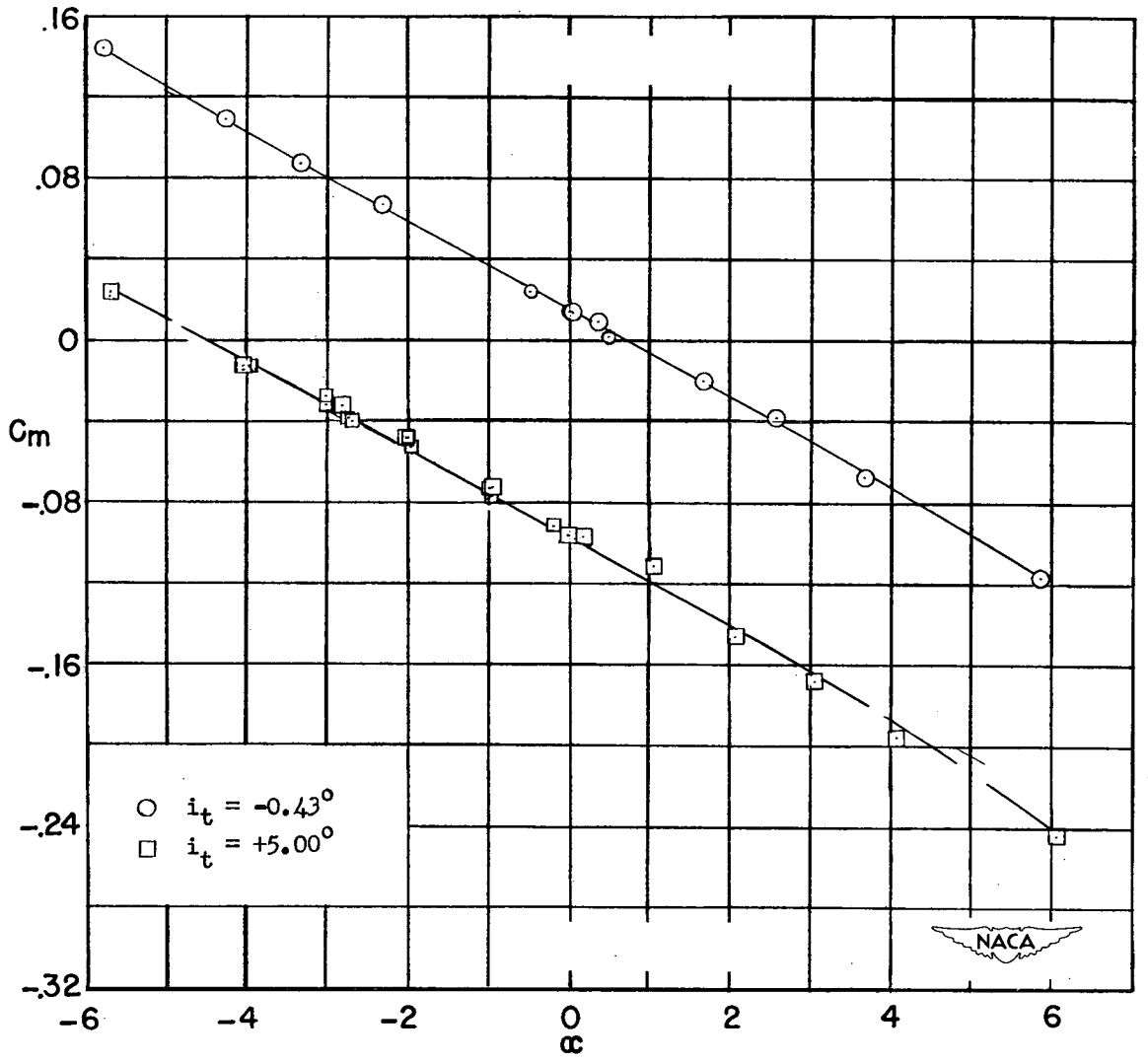
(h) BWT; $\frac{h}{c} = 0.70$; $\frac{l}{c} = 2.74$.

Figure 7.- Continued.



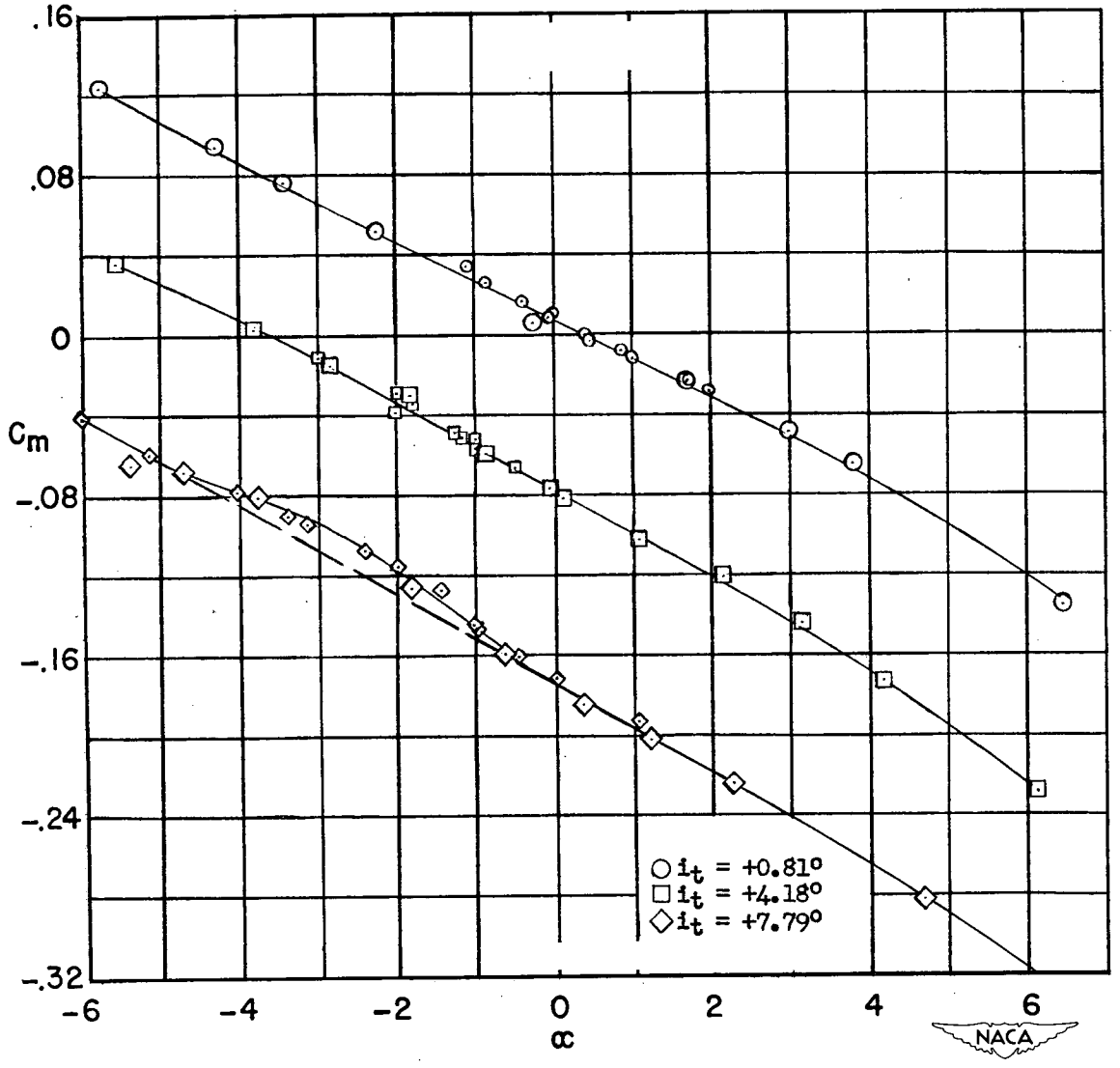
(i) BWT; $\frac{h}{c} = 0.70$; $\frac{l}{c} = 2.14$.

Figure 7.- Continued.



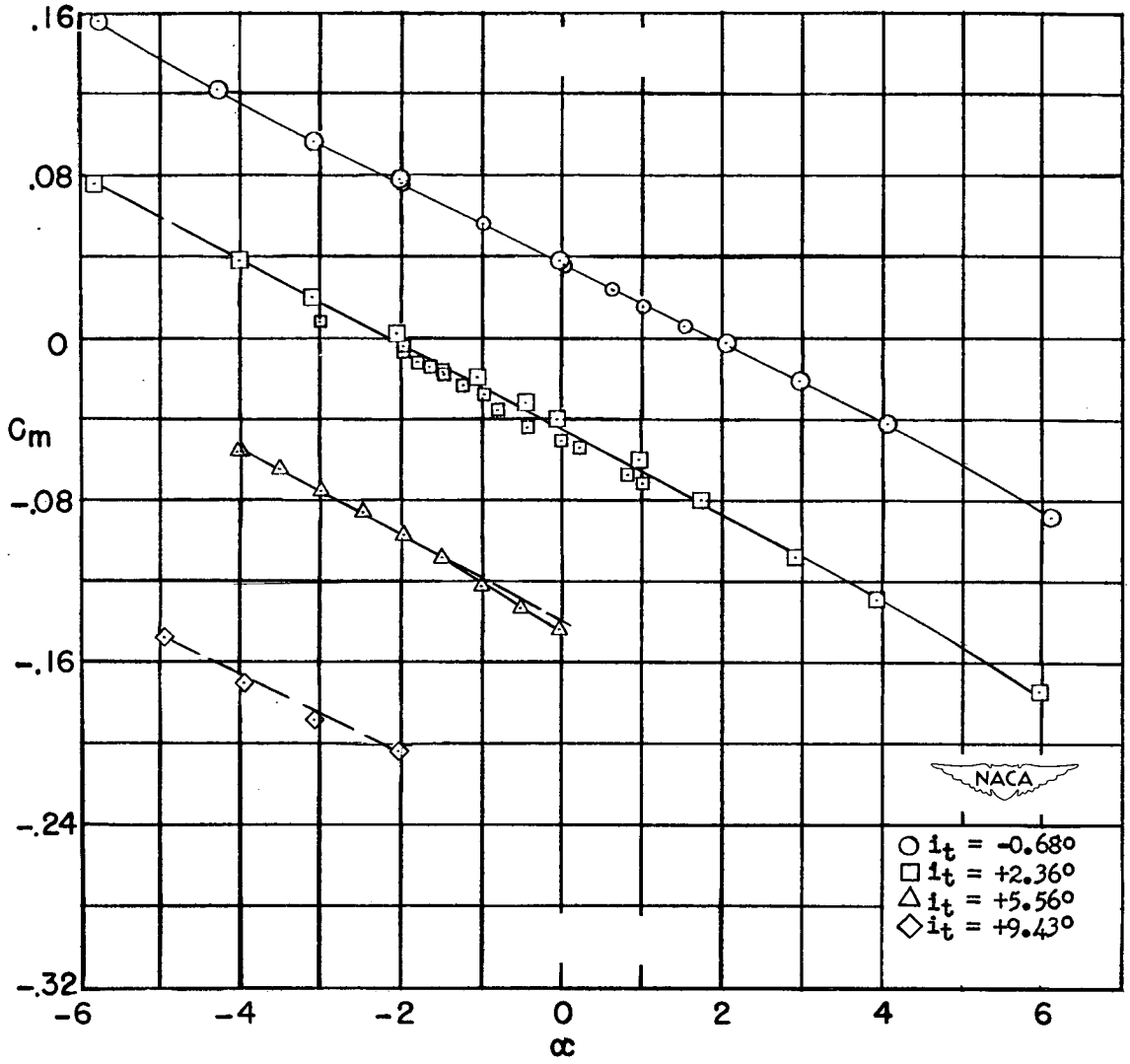
(j) BT; $\frac{h}{c} = 0$ $\left(\text{moment reference for } \frac{l}{c} = 3.34\right)$.

Figure 7.- Continued.



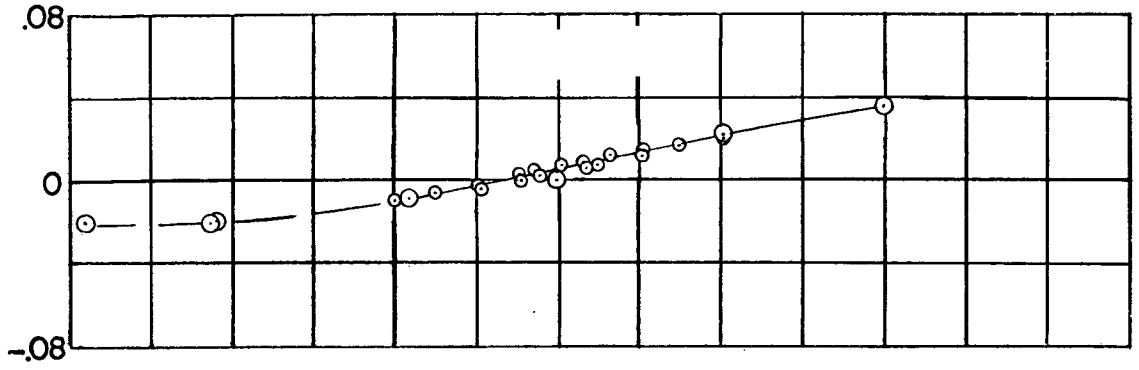
(k) BT; $\frac{h}{c} = 0.35$ $\left(\text{moment reference for } \frac{l}{c} = 3.34\right)$.

Figure 7.- Continued.

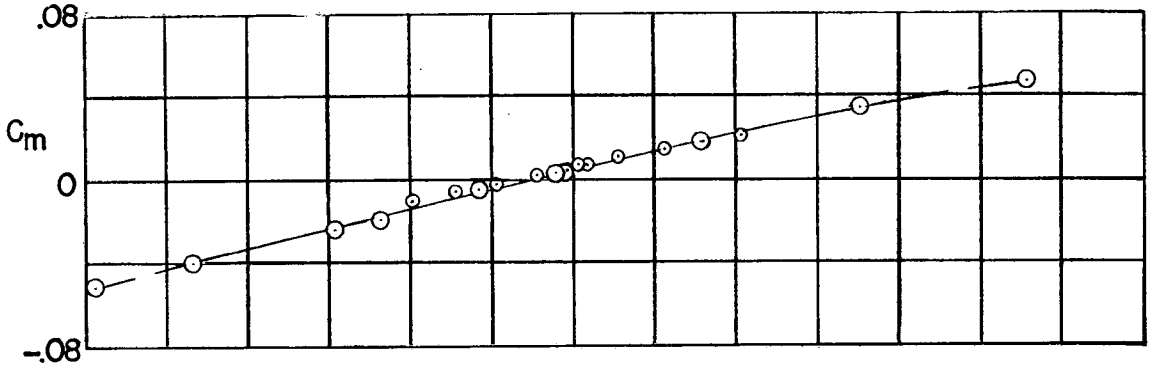


(l) BT; $\frac{h}{c} = 0.70$ $\left(\text{moment reference for } \frac{l}{c} = 3.34\right)$.

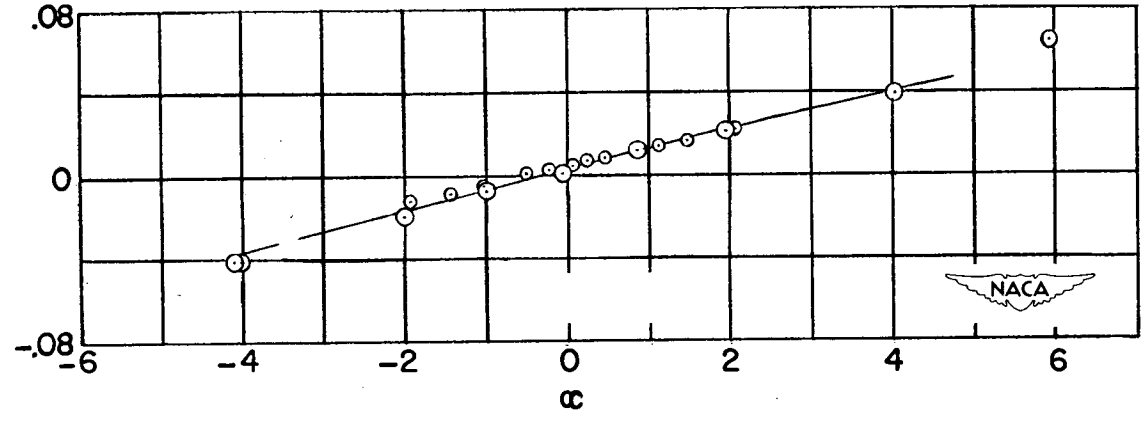
Figure 7.- Concluded.



(a) BW with wing at $\frac{l}{c}$ = 3.34 location.

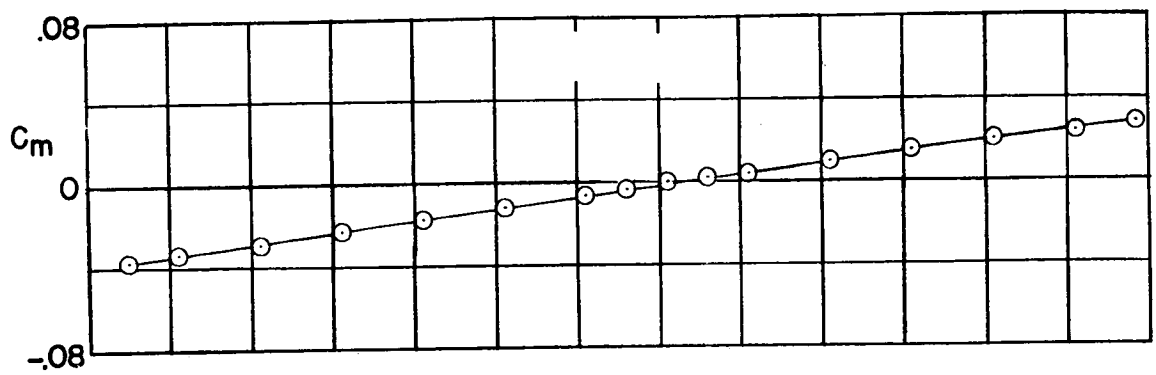


(b) BW with wing at $\frac{l}{c}$ = 2.74 location.

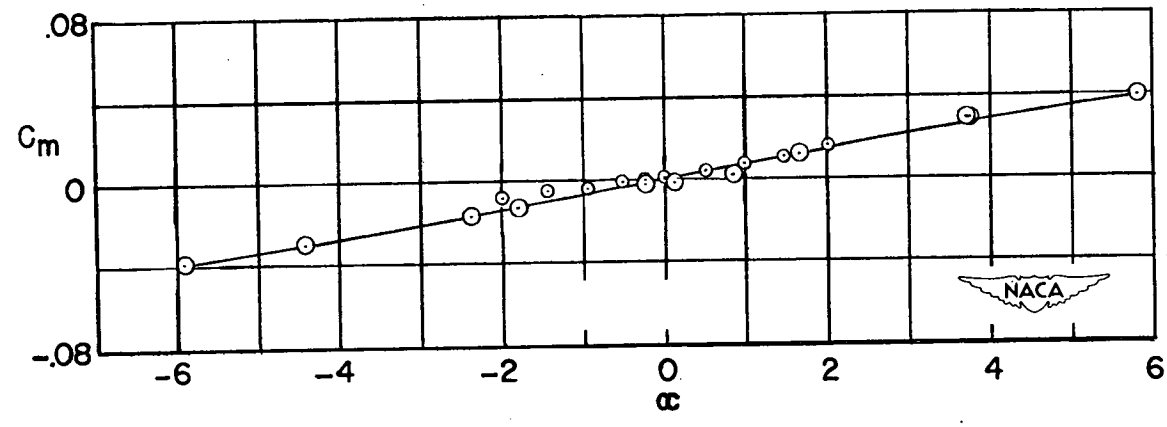


(c) BW with wing at $\frac{l}{c}$ = 2.14 location.

Figure 8.- Variation of pitching-moment coefficient with angle of attack for BW, W, and B.

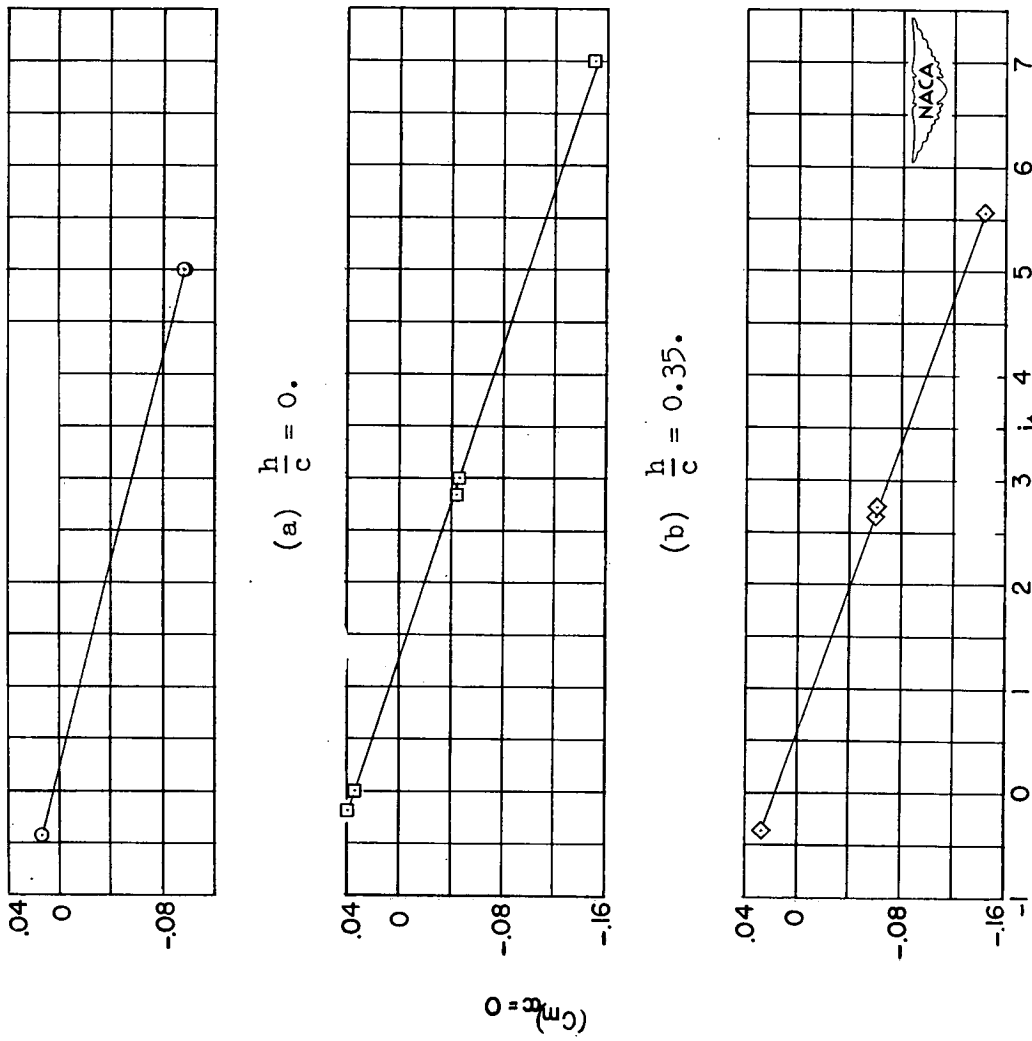


(d) W.



(e) B $\left(\text{moment reference for } \frac{l}{c} = 3.34\right)$.

Figure 8.- Concluded.

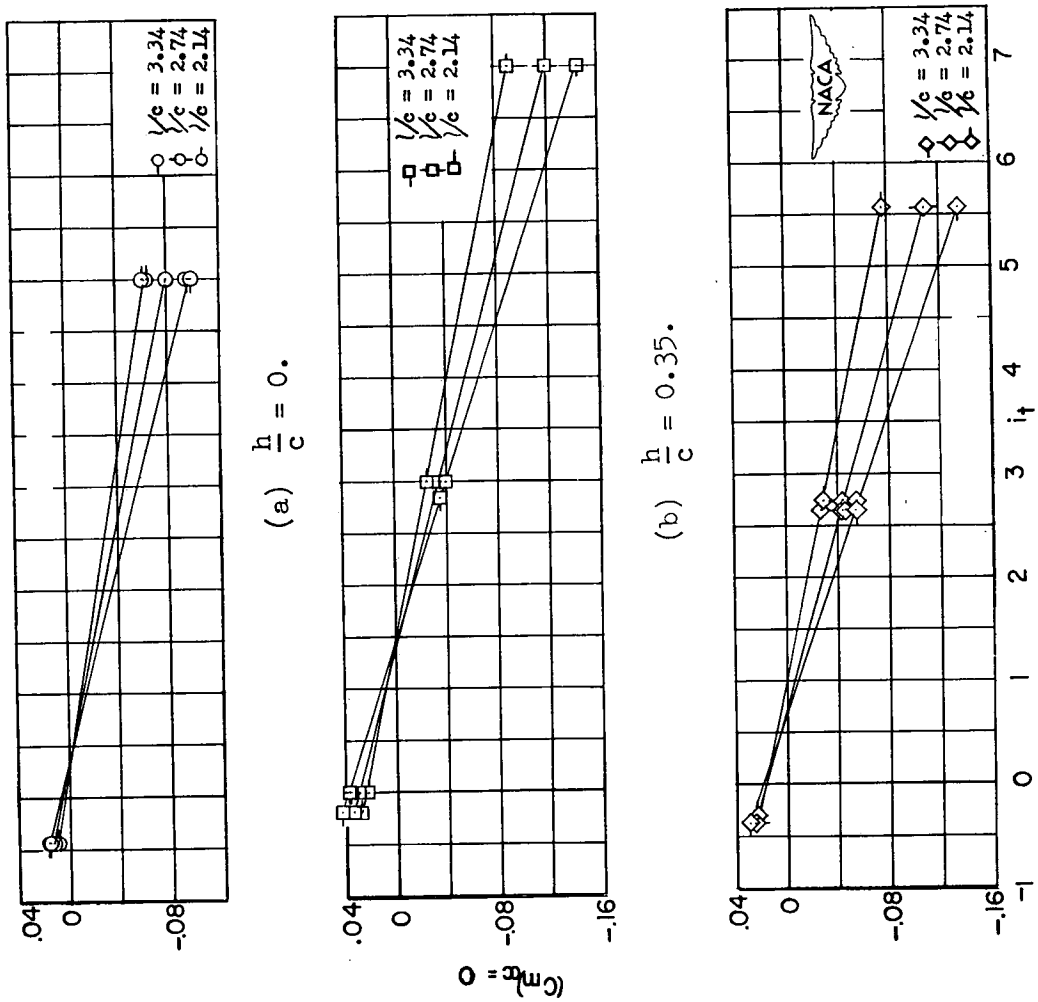


(a) $\frac{h}{c} = 0.$

(b) $\frac{h}{c} = 0.35.$

(c) $\frac{h}{c} = 0.70.$

Figure 9.- Variation of pitching-moment coefficient at zero angle of attack with tail incidence angle for BT. (Moment reference for $\frac{l}{c} = 3.34.$)

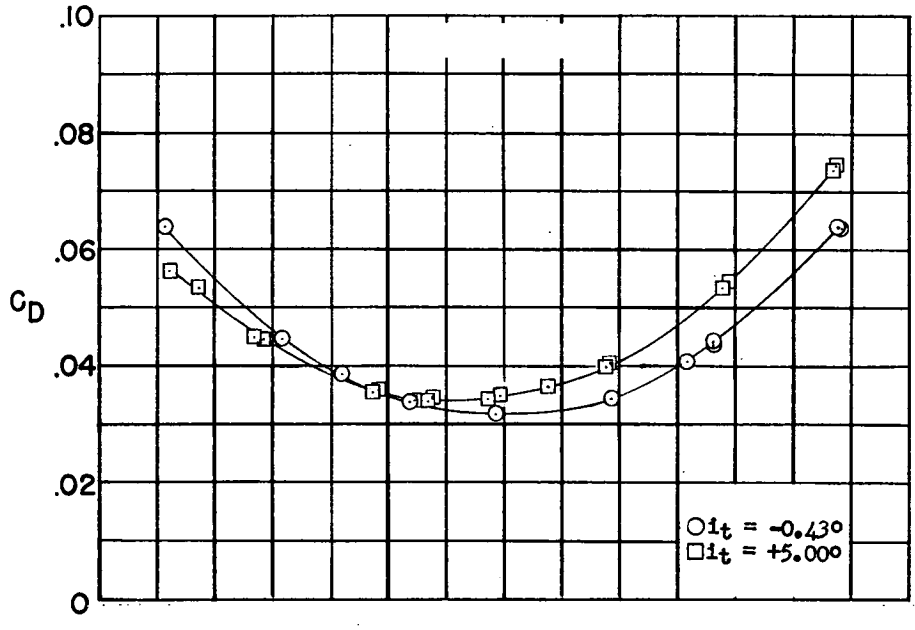


(a) $\frac{h}{c} = 0.$

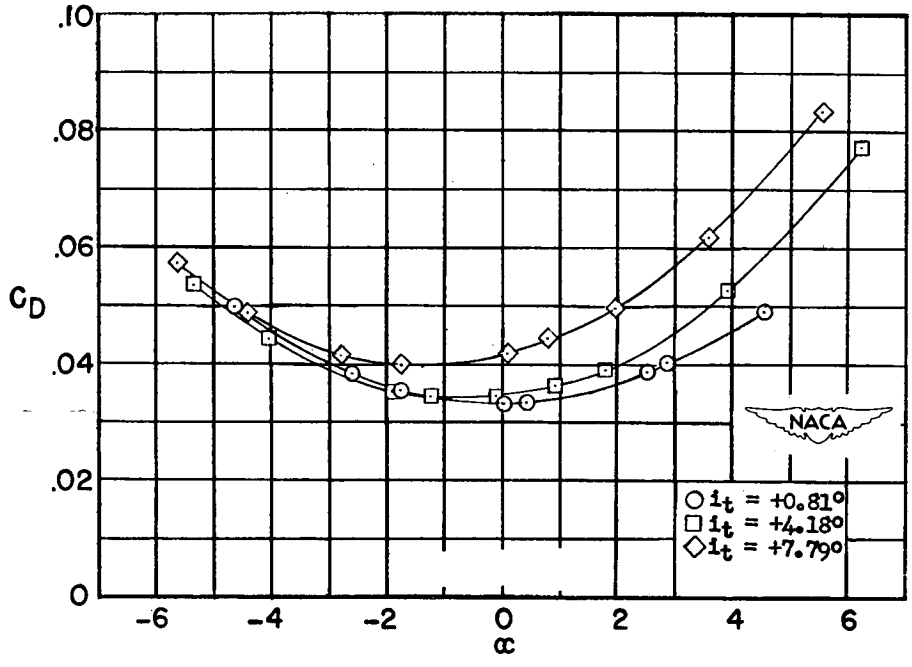
(b) $\frac{h}{c} = 0.35.$

(c) $\frac{h}{c} = 0.70.$

Figure 10.- Variation of pitching-moment coefficient at zero angle of attack with tail incidence angle for BWT.

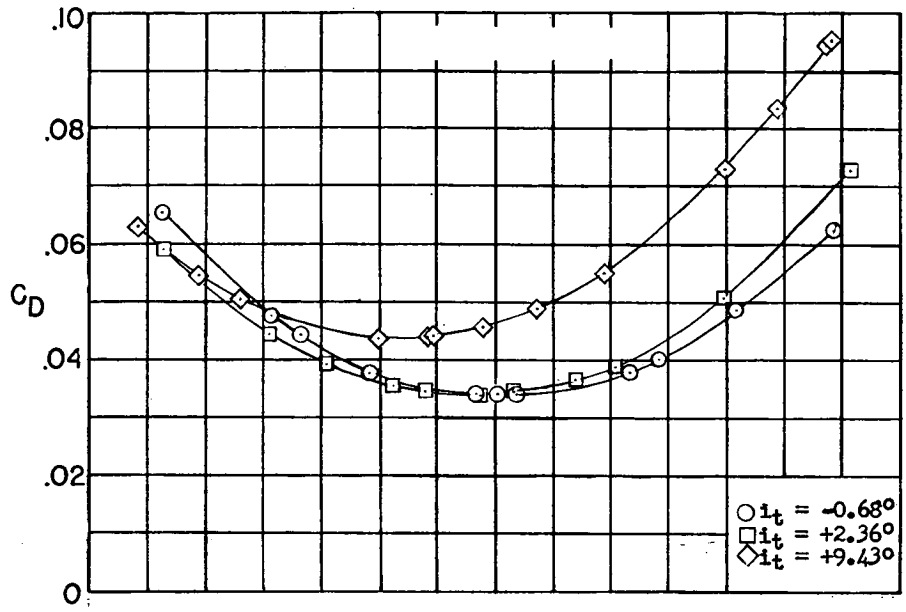


(a) BWT; $\frac{h}{c} = 0.$

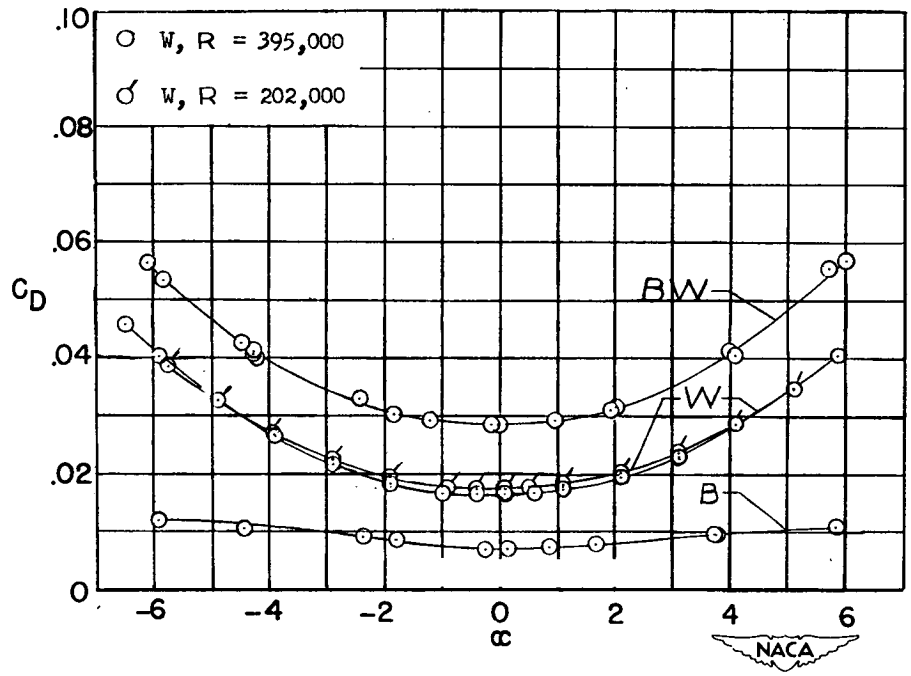


(b) BWT; $\frac{h}{c} = 0.35.$

Figure 11.- Variation of drag coefficient with angle of attack for BWT, BW, and W; $\frac{l}{c} = 3.34.$

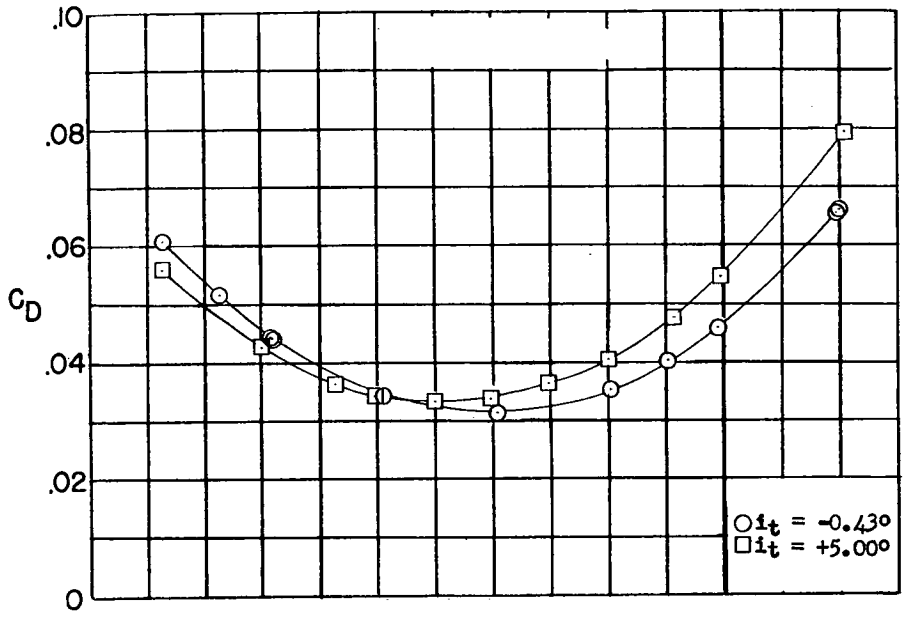


(c) BWT; $\frac{h}{c}$ = 0.70.

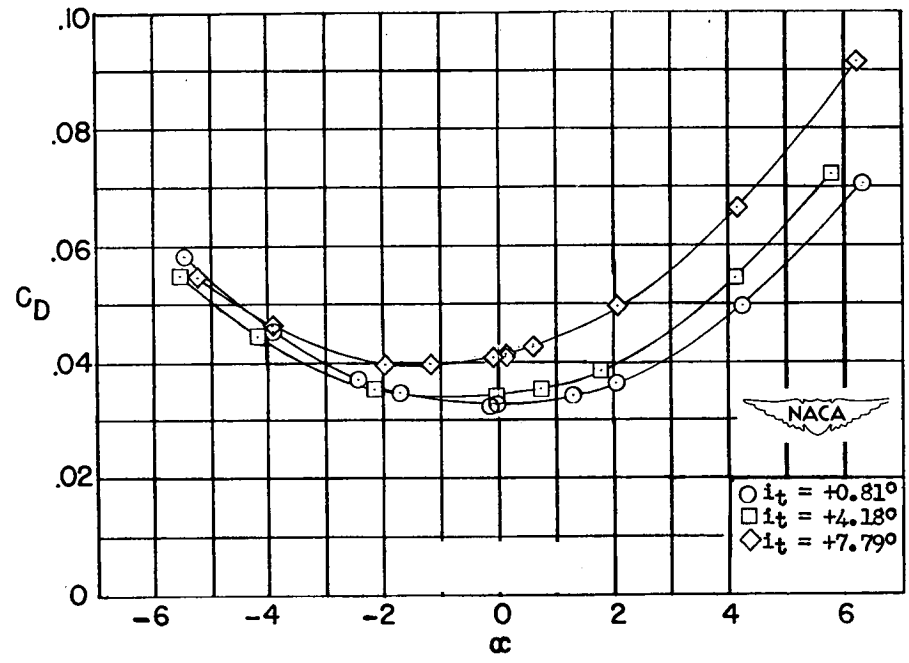


(d) BW, W, and B.

Figure 11.- Concluded.

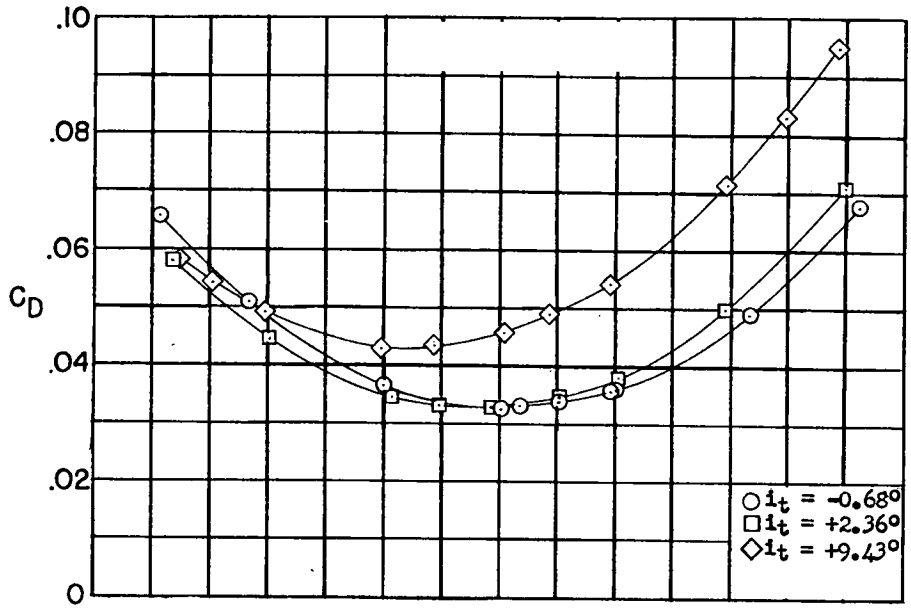


(a) BWT; $\frac{h}{c} = 0.$

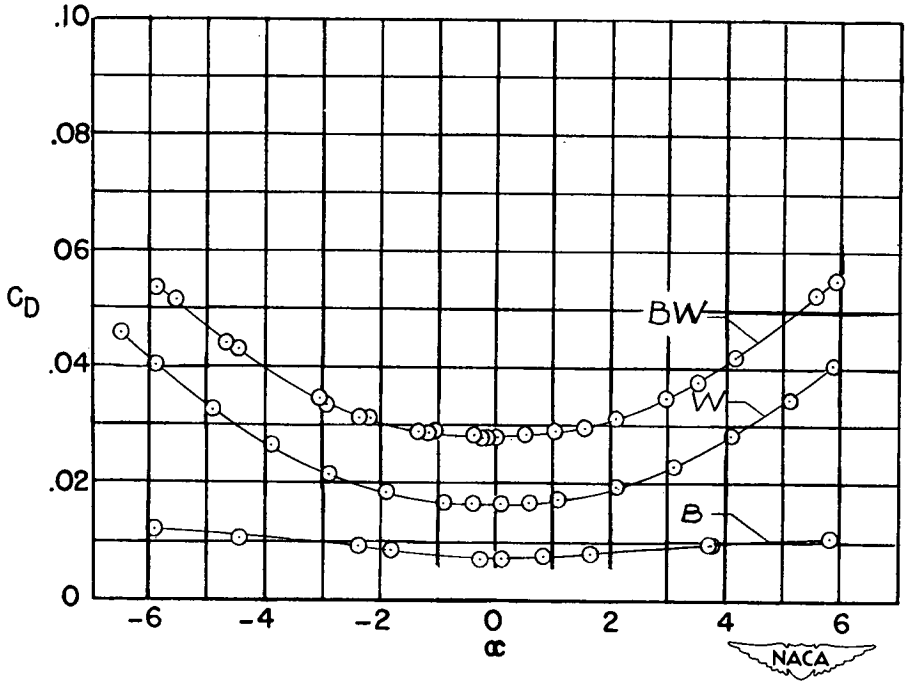


(b) BWT; $\frac{h}{c} = 0.35.$

Figure 12.- Variation of drag coefficient with angle of attack for BWT, BW, B, and W; $\frac{l}{c} = 2.74.$

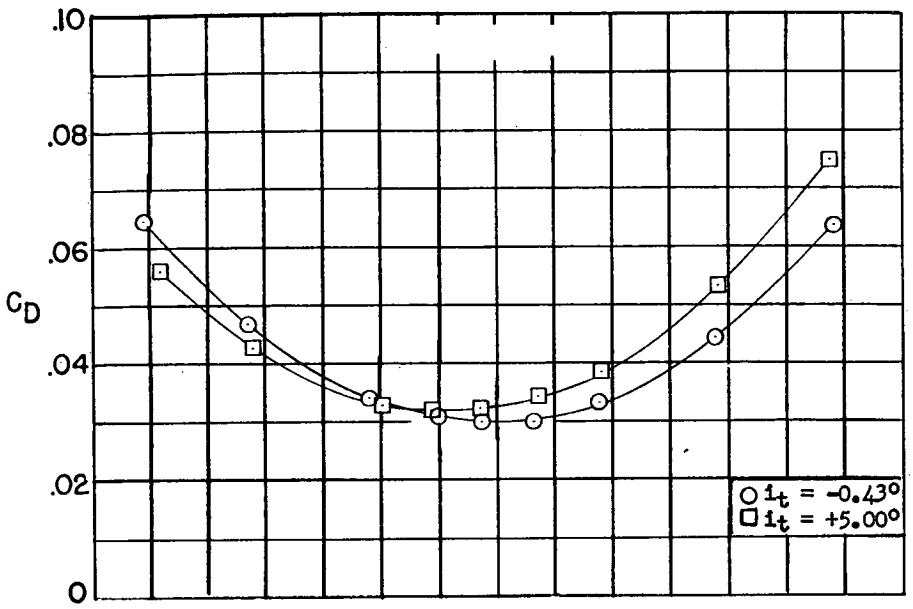


(c) BWT; $\frac{h}{c} = 0.70$.

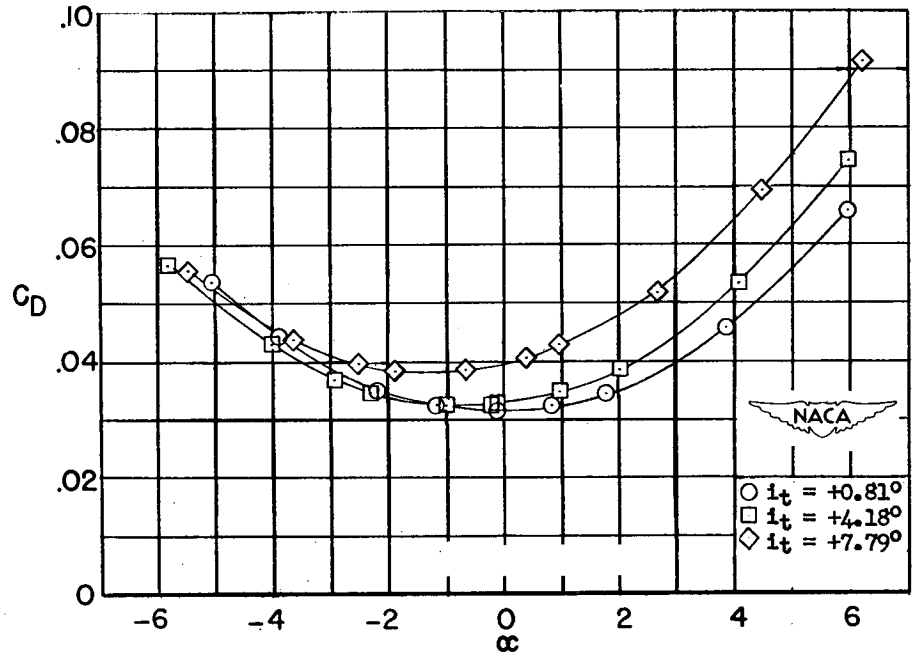


(d) BW, W, and B.

Figure 12.- Concluded.

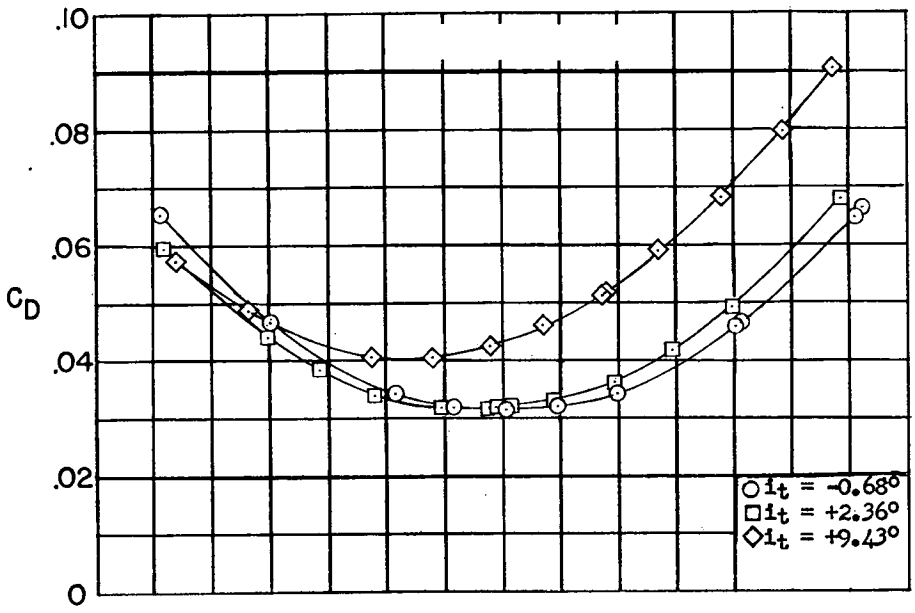


(a) BWT; $\frac{h}{c} = 0.$

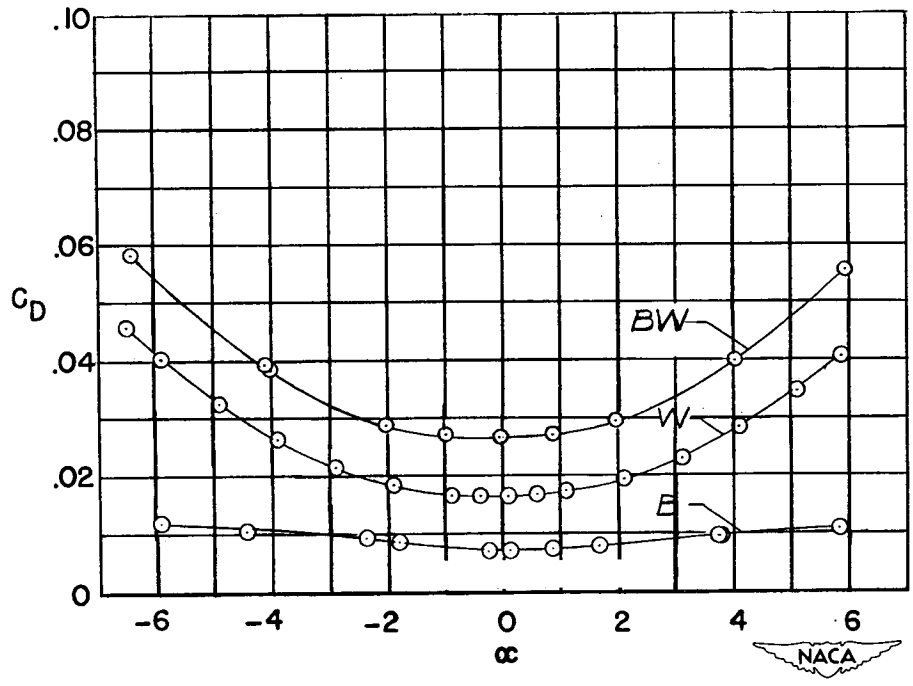


(b) BWT; $\frac{h}{c} = 0.35.$

Figure 13.- Variation of drag coefficient with angle of attack for BWT, BW, B, and W; $\frac{l}{c} = 2.14.$

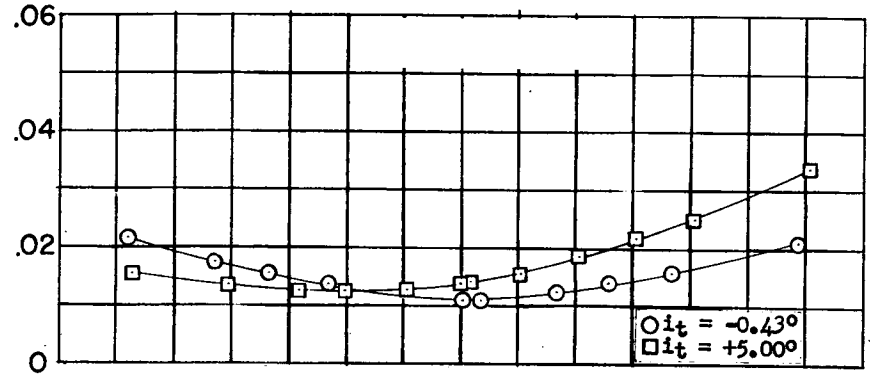


(c) BWT; $\frac{h}{c} = 0.70$.

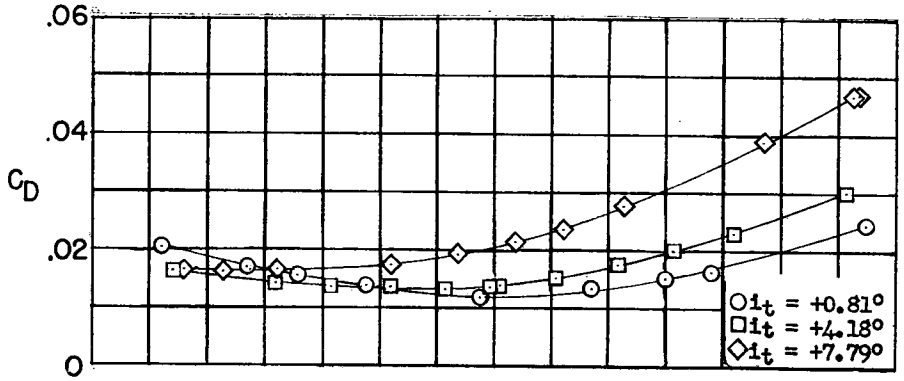


(d) BW, W, and B.

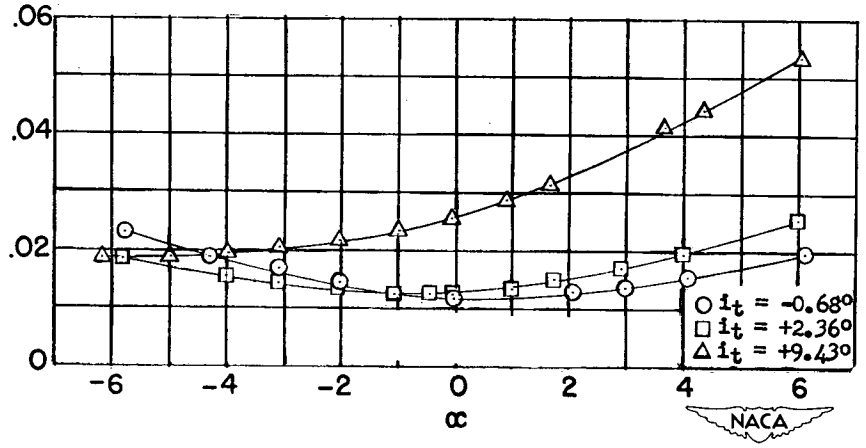
Figure 13.- Concluded.



(a) $\frac{h}{c} = 0.$

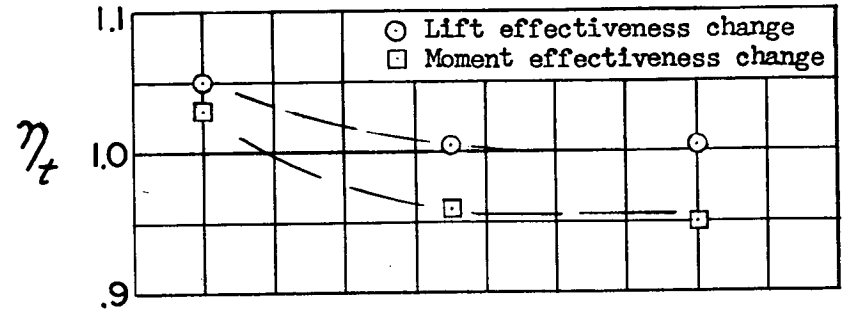


(b) $\frac{h}{c} = 0.35.$

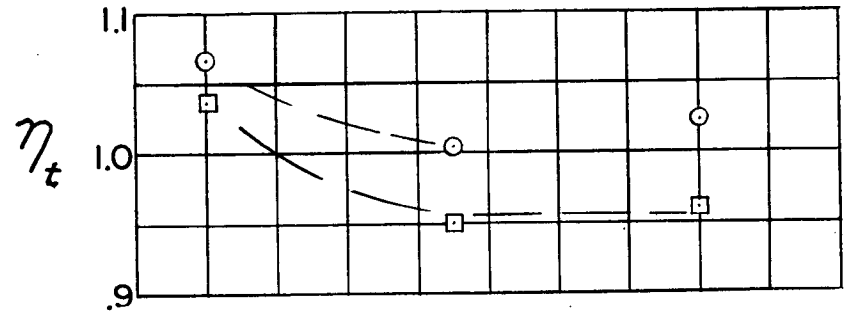


(c) $\frac{h}{c} = 0.70.$

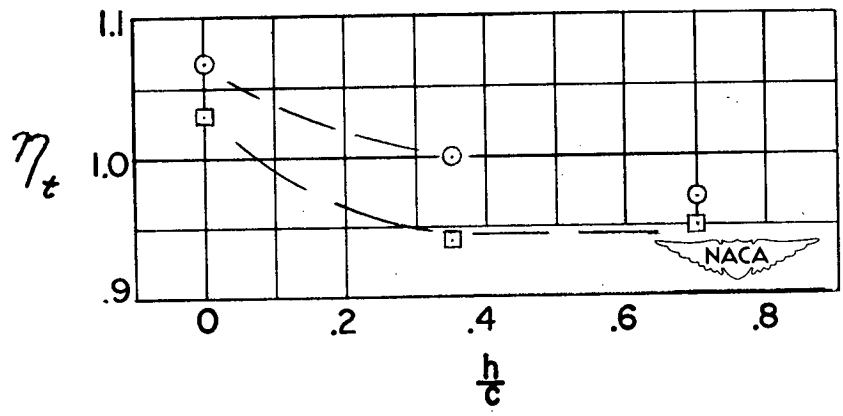
Figure 14.- Variation of drag coefficient with angle of attack for BT.



(a) $\frac{l}{c} = 3.34$.

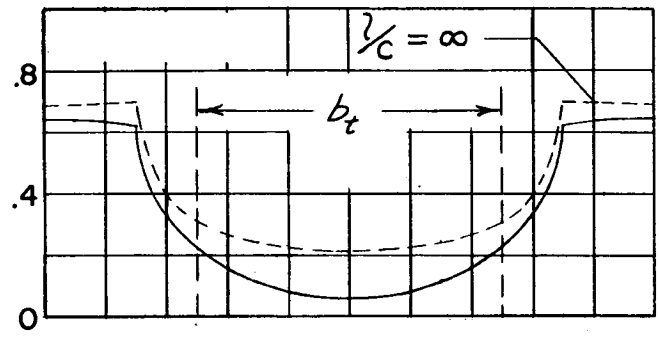


(b) $\frac{l}{c} = 2.74$.

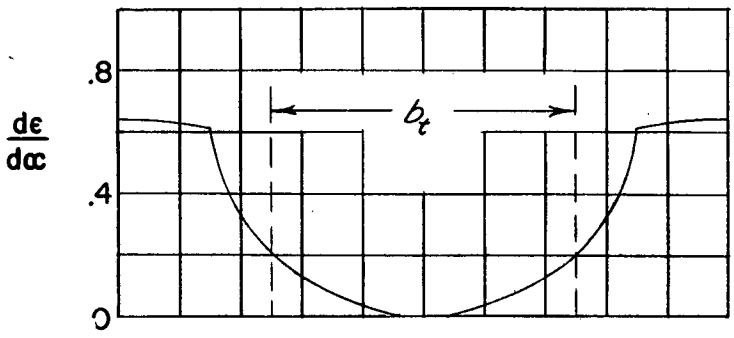


(c) $\frac{l}{c} = 2.14$.

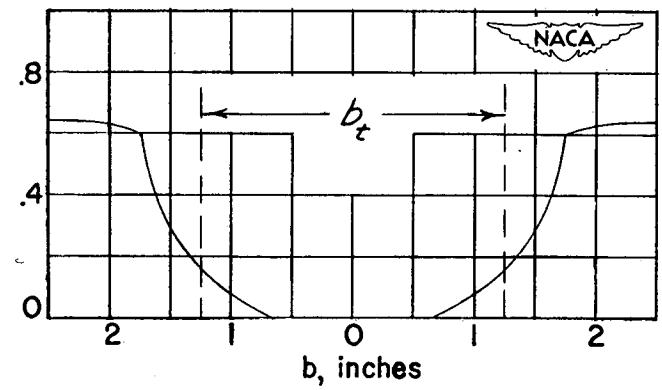
Figure 15.- Variation of wing-wake parameter with tail height.



(a) $\frac{l}{c} = 3.34$.

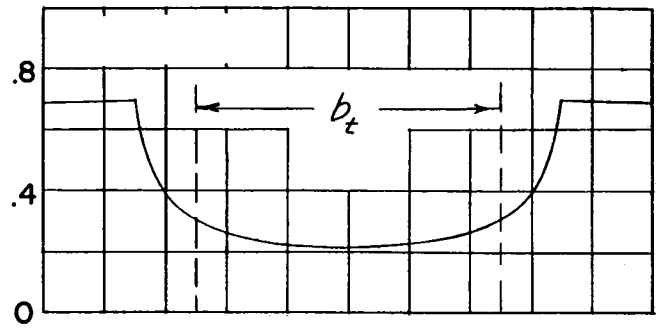


(b) $\frac{l}{c} = 2.74$.

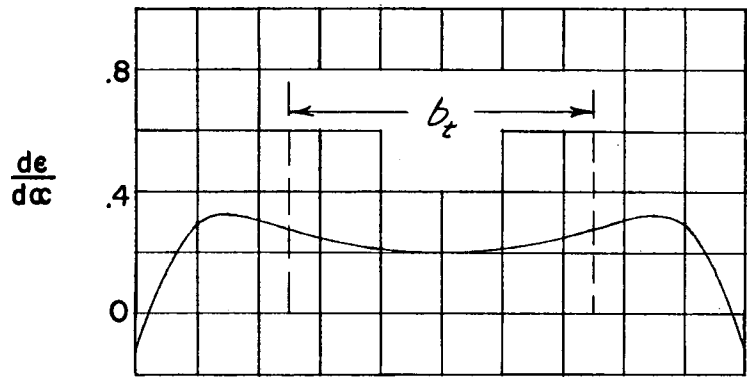


(c) $\frac{l}{c} = 2.14$.

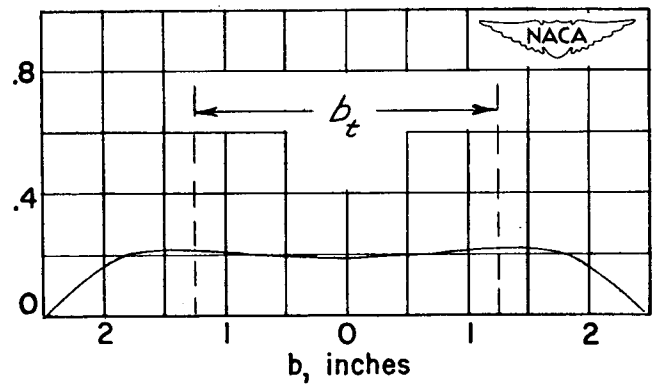
Figure 16.- Theoretical downwash angle distribution behind wing for $\frac{h}{c} = 0$.



(a) $\frac{h}{c} = 0.$

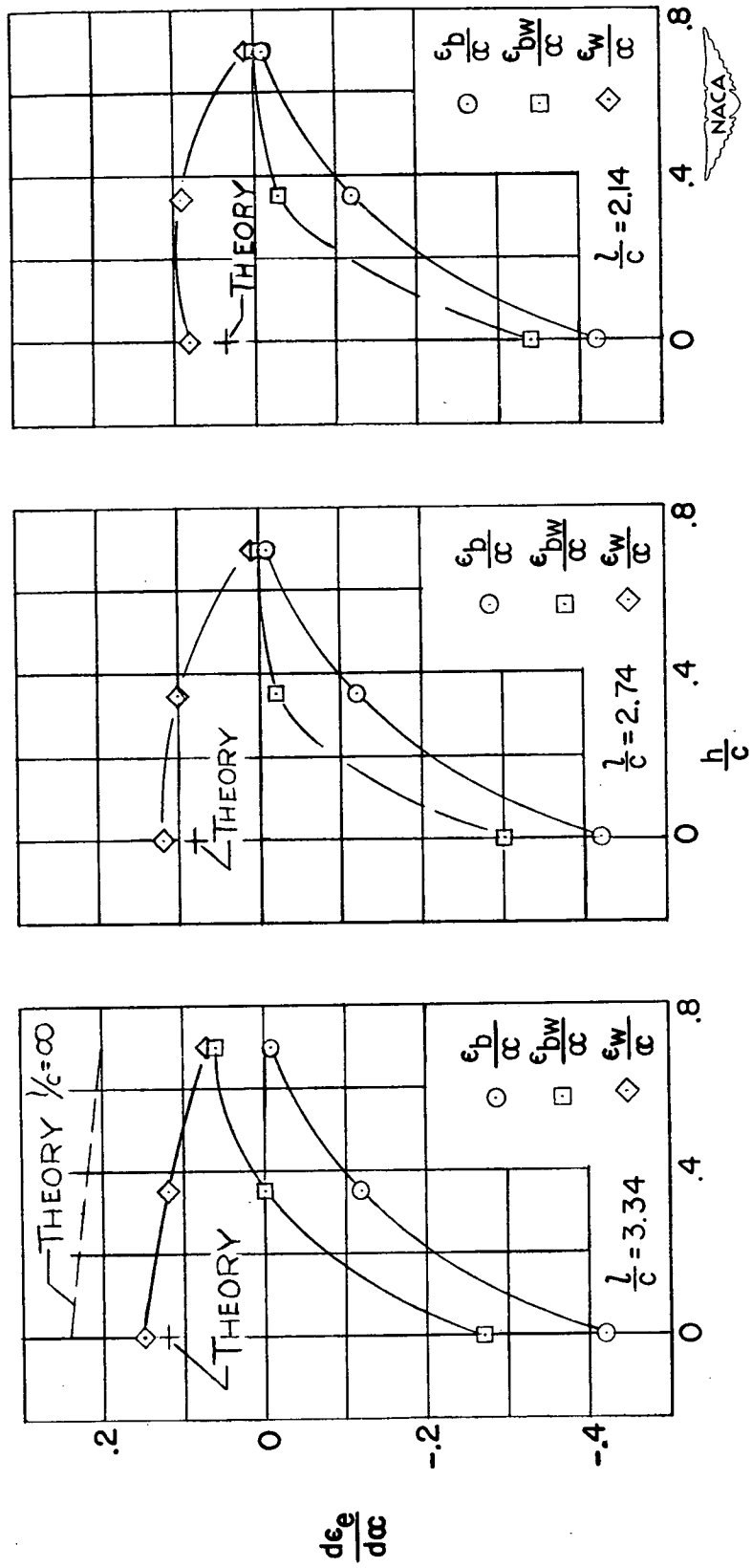


(b) $\frac{h}{c} = 0.30.$



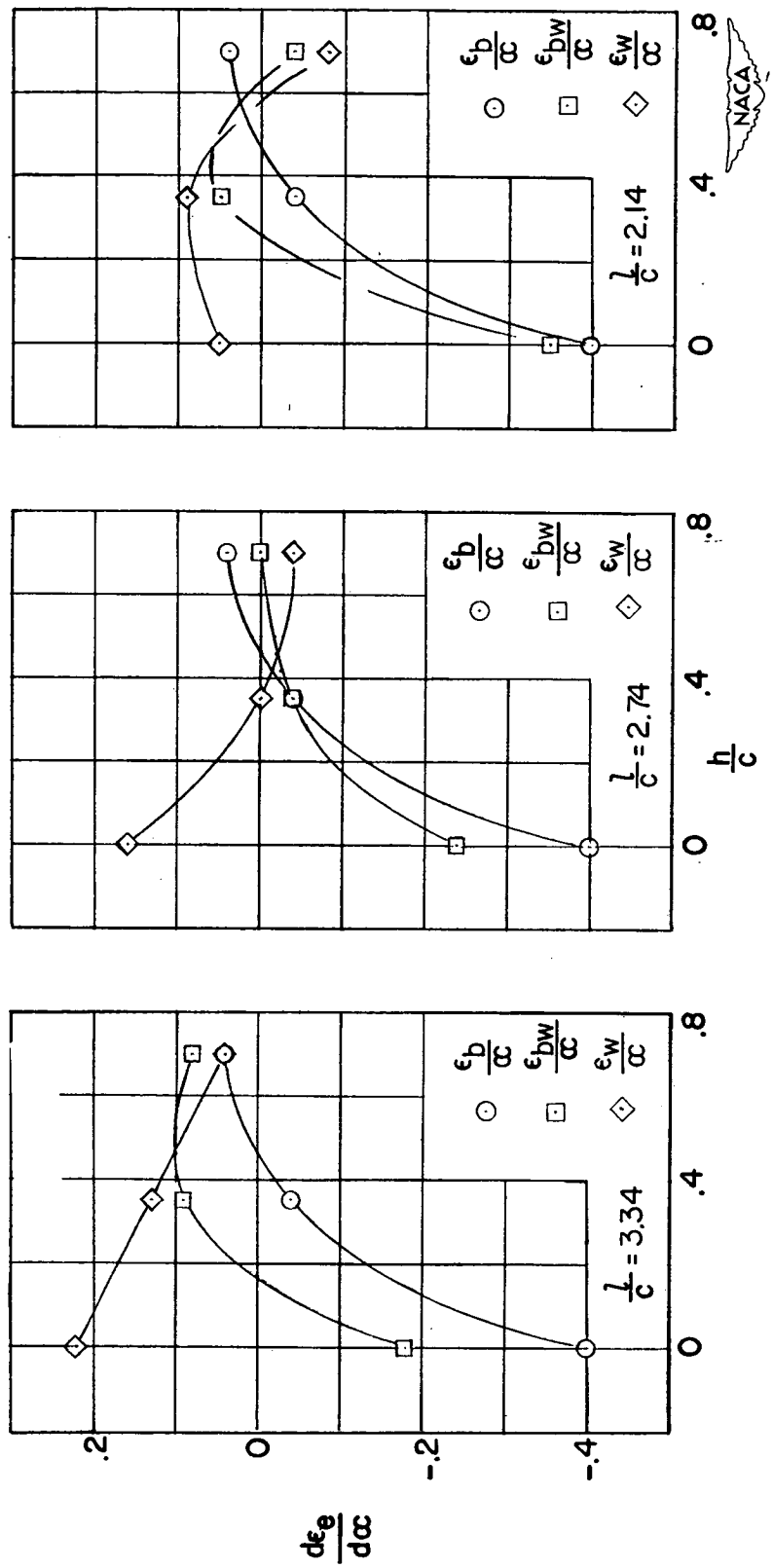
(c) $\frac{h}{c} = 0.61.$

Figure 17.- Theoretical downwash angle distribution behind wing for $\frac{l}{c} = \infty$.



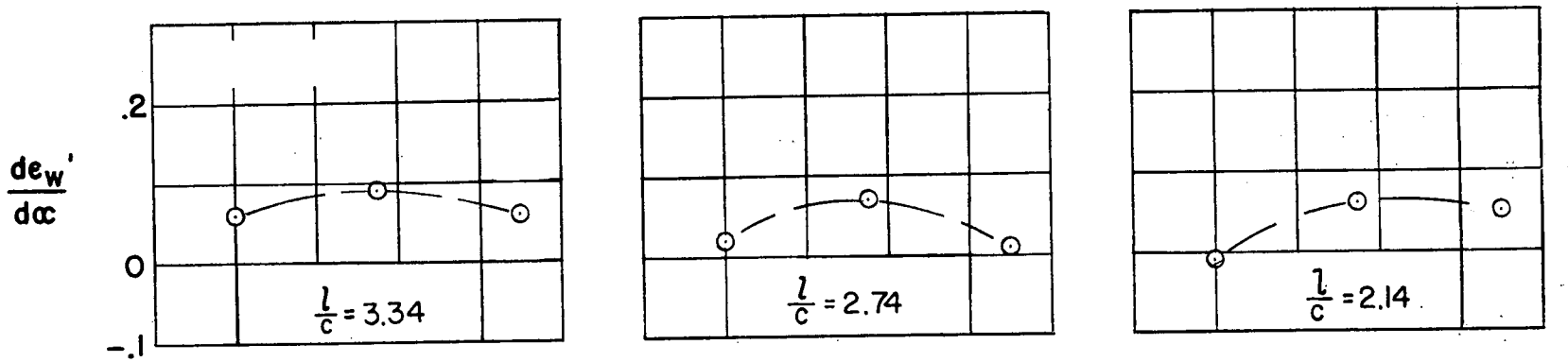
(a) Computed from experimental lift-curve slopes, equation (6).

Figure 18.- Variation of rate of change of downwash angle with angle of attack with tail height.

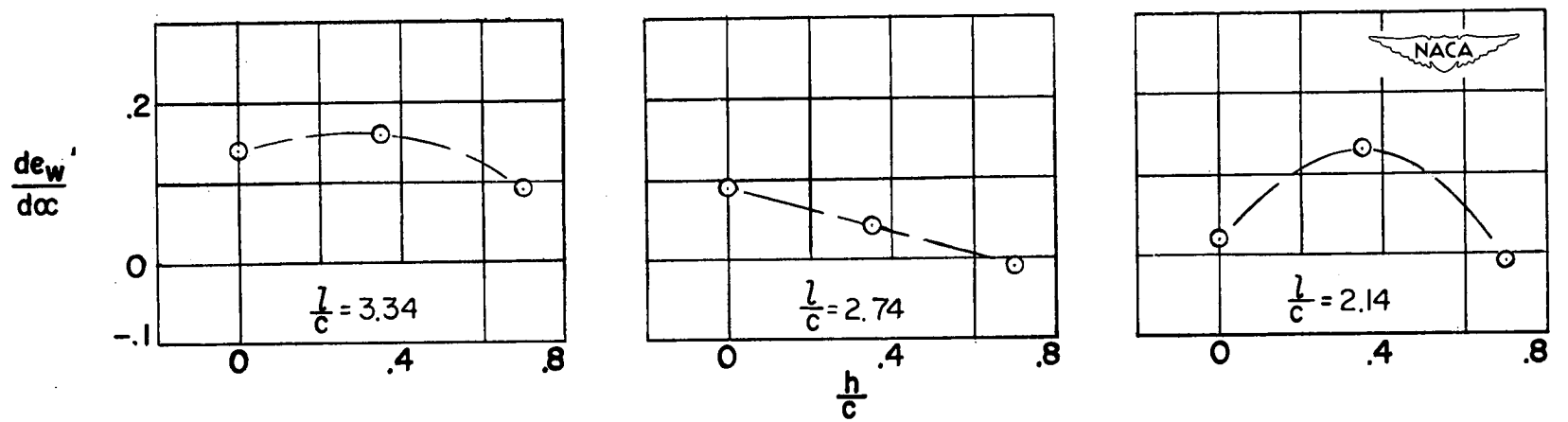


(b) Computed using experimental pitching-moment-curve slopes in equation (6).

Figure 18.- Continued.

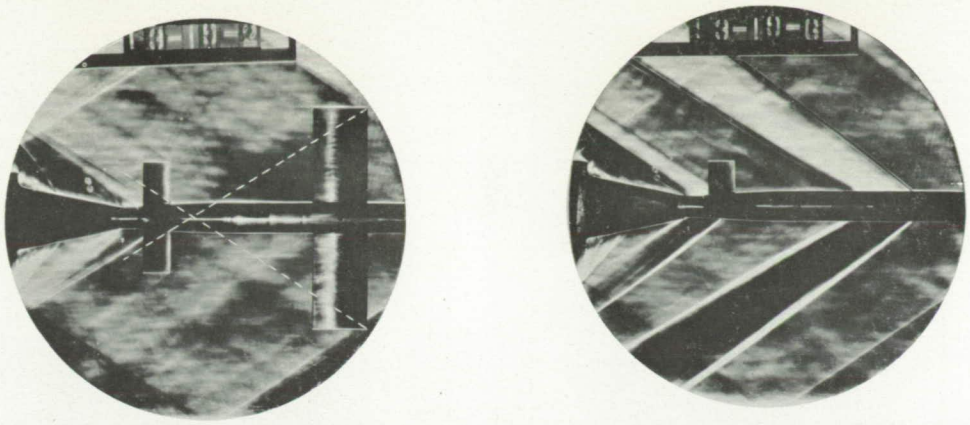


(c) Computed using experimental lift-curve slopes in equation (7).

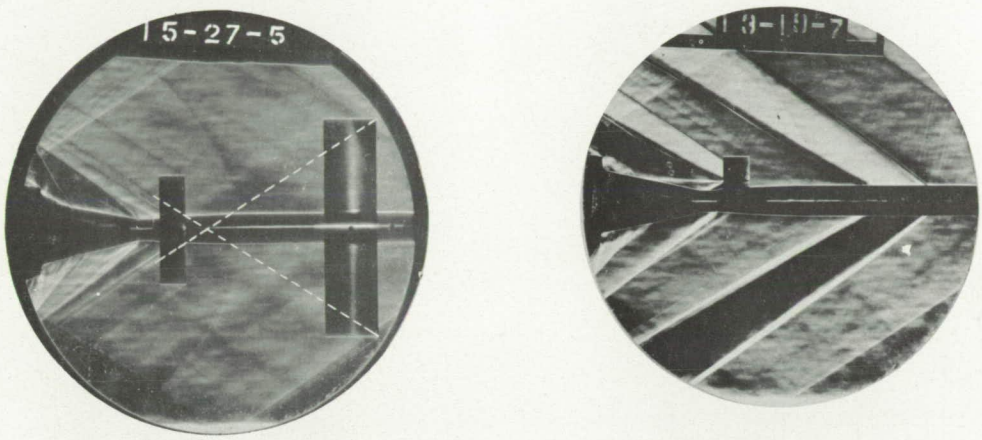


(d) Computed using experimental moment-curve slopes in equation (7).

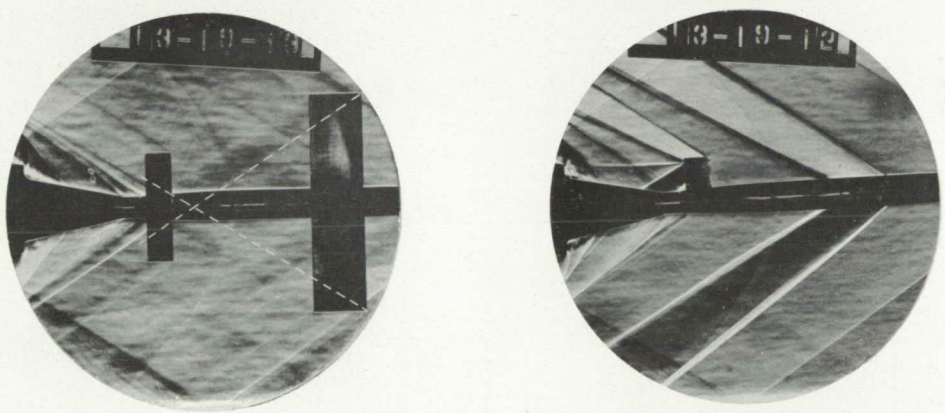
Figure 18.- Concluded.



(a) $\frac{h}{c} = 0$, $i_t = -0.43^\circ$, $\alpha \approx 0^\circ$.



(b) $\frac{h}{c} = 0.35$, $i_t = 4.18^\circ$, $\alpha \approx 0^\circ$.

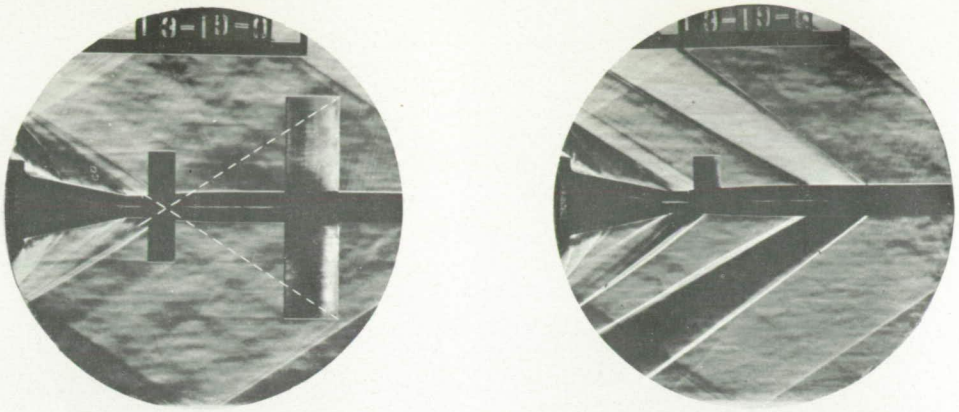


(c) $\frac{h}{c} = 0.70$, $i_t = 2.36^\circ$, $\alpha \approx 0^\circ$.

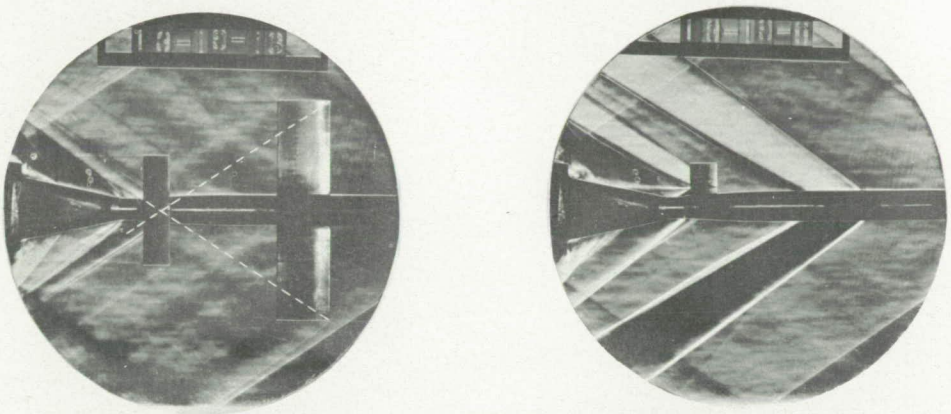
NACA

L-63575

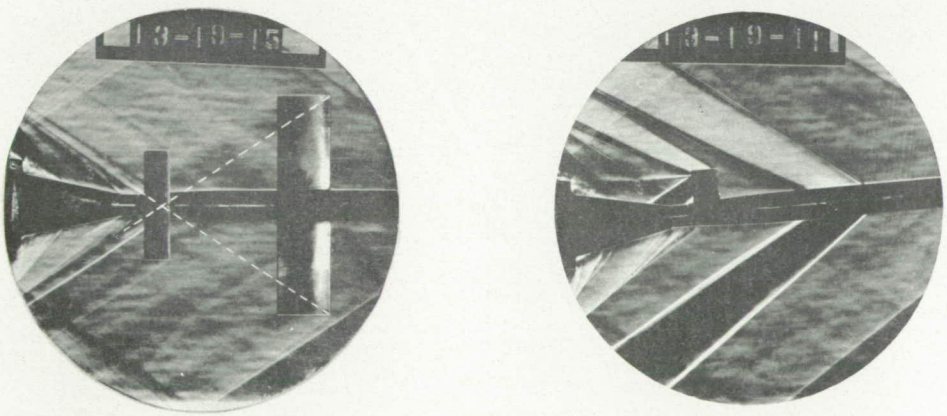
Figure 19.- Schlieren photographs of BWT, $\frac{l}{c} = 3.34$. M = 1.92; knife edge horizontal.



(a) $\frac{h}{c} = 0$, $i_t = -0.43^\circ$, $\alpha \approx 0^\circ$.



(b) $\frac{h}{c} = 0.35$, $i_t = 4.18^\circ$, $\alpha \approx 0^\circ$.

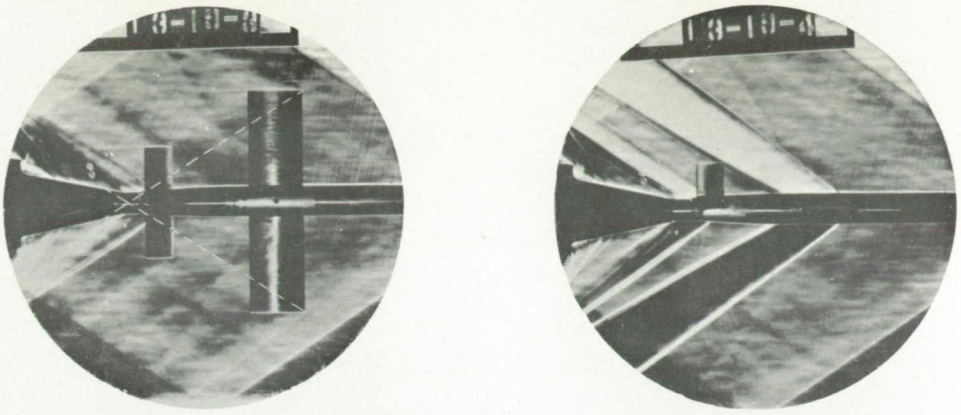


(c) $\frac{h}{c} = 0.70$, $i_t = 2.36^\circ$, $\alpha \approx 0^\circ$.

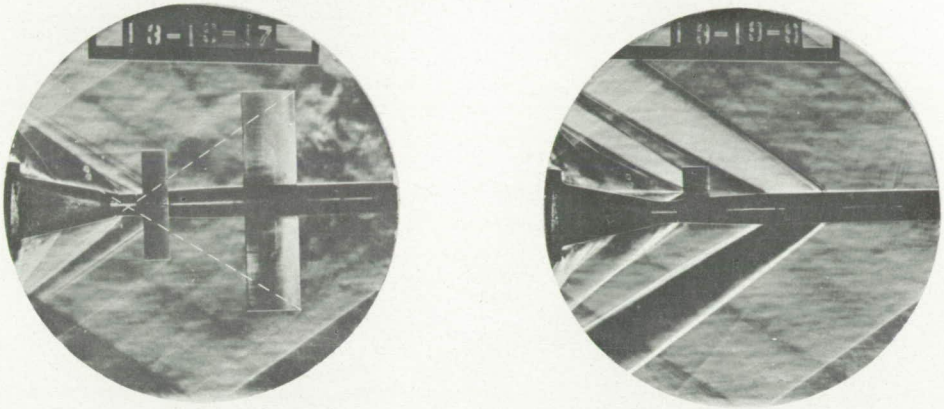
NACA

L-63576

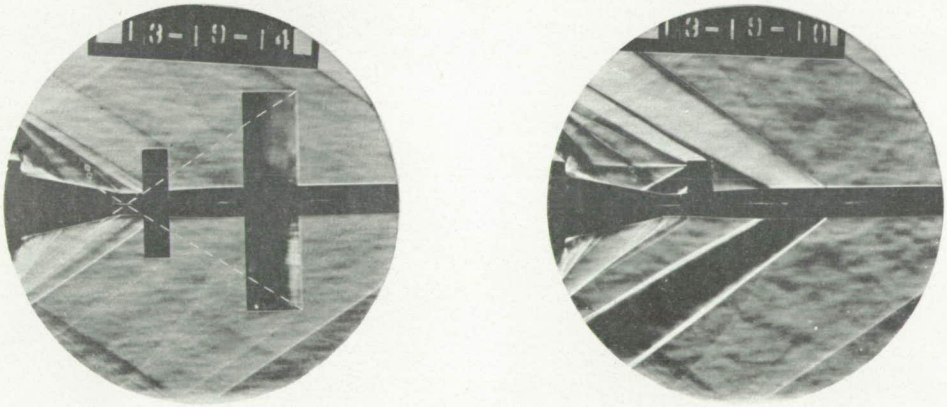
Figure 20.- Schlieren photographs of BWT, $\frac{l}{c} = 2.74$. M = 1.92; knife edge horizontal.



(a) $\frac{h}{c} = 0$, $i_t = -0.43^\circ$, $\alpha \approx 0^\circ$.



(b) $\frac{h}{c} = 0.35$, $i_t = 4.18^\circ$, $\alpha \approx 0^\circ$.

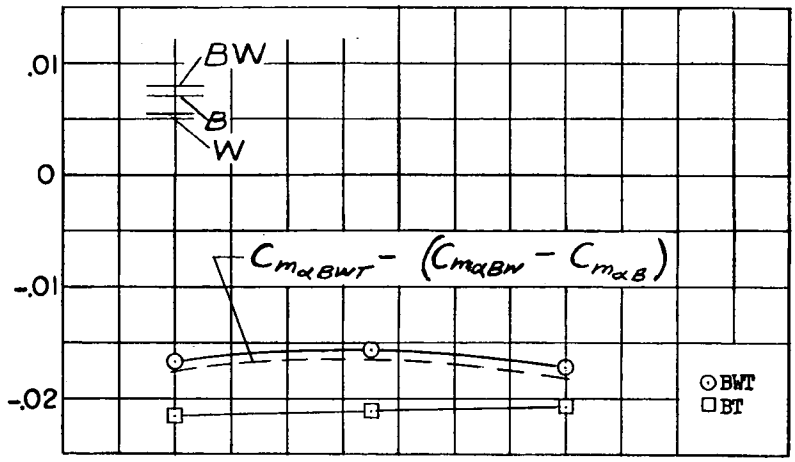


(c) $\frac{h}{c} = 0.70$, $i_t = 2.36^\circ$, $\alpha \approx 0^\circ$.

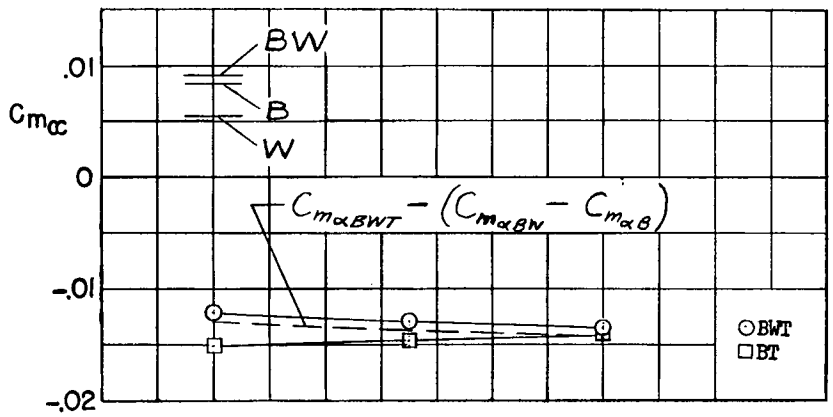
NACA

L-63577

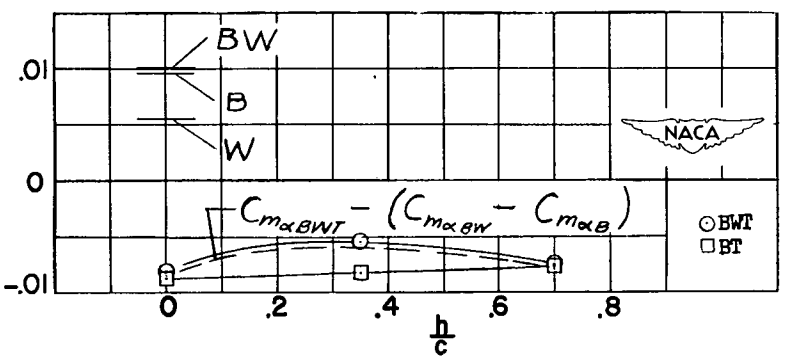
Figure 21.- Schlieren photographs of BWT, $\frac{l}{c} = 2.14$. M = 1.92; knife edge horizontal.



(a) $\frac{l}{c} = 3.34.$

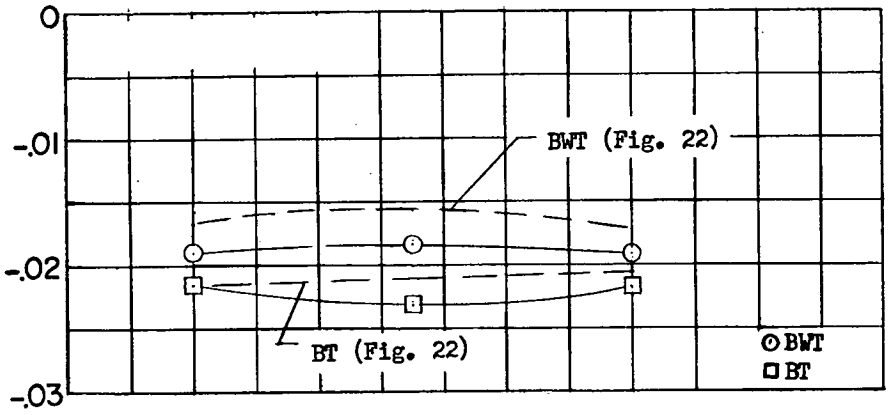


(b) $\frac{l}{c} = 2.74.$

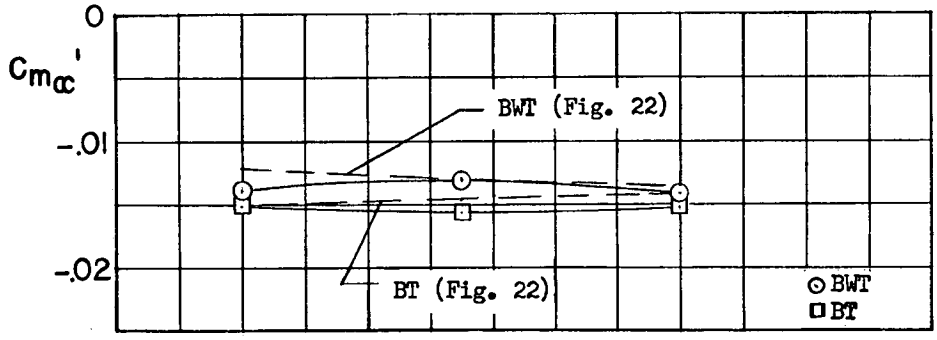


(c) $\frac{l}{c} = 2.14.$

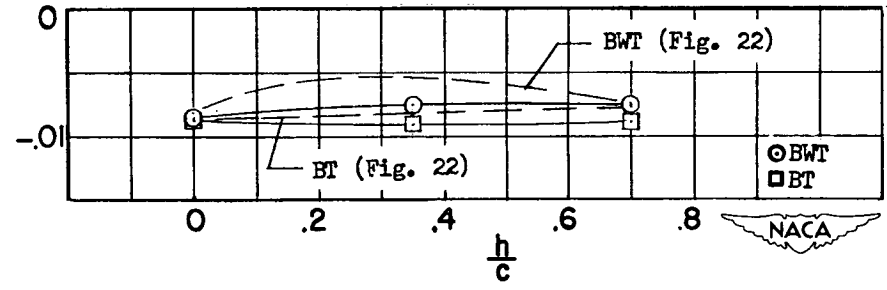
Figure 22.- Variation of pitching-moment-curve slope with tail height for BWT and BT. (BW, W, and B values are also shown.)



(a) $\frac{l}{c} = 3.34$.



(b) $\frac{l}{c} = 2.74$.



(c) $\frac{l}{c} = 2.14$.

Figure 23.- Variation of pitching-moment-curve slope computed from incremental tail-lift values with tail height for BWT and BT.